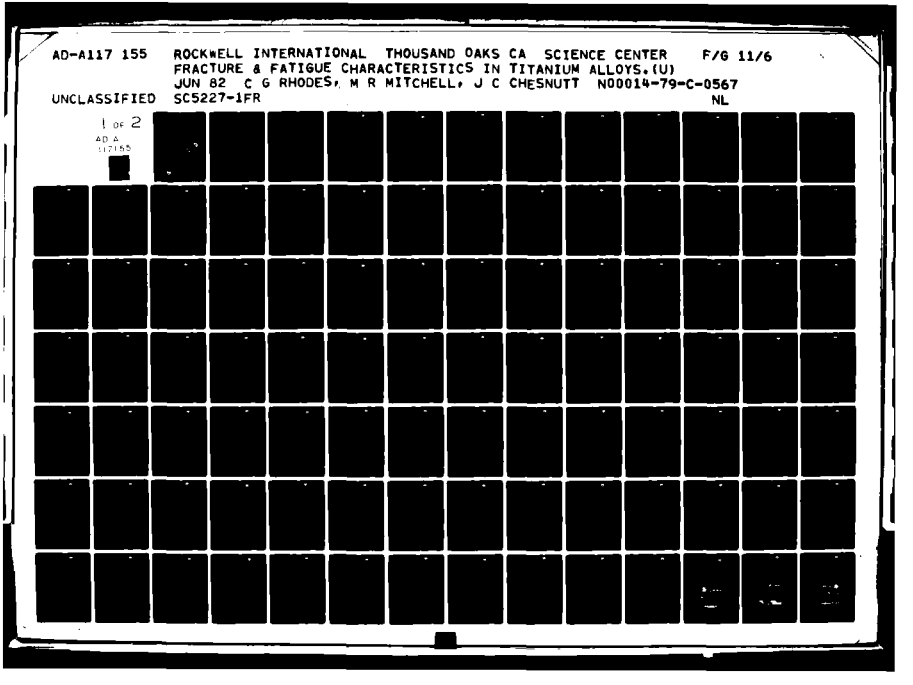
AD-A117 155
ROCKWELL INTERNATIONAL THOUSAND OAKS CA SCIENCE CENTER F/G 11/6
FRACTURE & FATIGUE CHARACTERISTICS IN TITANIUM ALLOYS.(U)
JUN 82 C G RHODES, M R MITCHELL, J C CHESNUTT N00014-79-C-0567
UNCLASSIFIED SC5227-1FR NL
1 OF 2
AD A
117155

(12)

SC5227.1FR

Copy No. 21

FRACTURE & FATIGUE CHARACTERISTICS IN TITANIUM ALLOYS

FINAL REPORT FOR THE PERIOD
July 1, 1979 through September 30, 1981

CONTRACT NO. N00014-79-C-0567

Prepared for

Office of Naval Research
800 North Quincy Street
Arlington, VA 22217

C.G. Rhodes
M.R. Mitchell
J.C. Chesnutt

JUNE 1982

Rockwell International
Science Center

UNCLASSIFIED

SECURITY CLASSIFICATION OF THIS PAGE (When Data Entered)

REPORT DOCUMENTATION PAGE		READ INSTRUCTIONS BEFORE COMPLETING FORM
1. REPORT NUMBER	2. GOVT ACCESSION NO. AD-A117155	3. RECIPIENT'S CATALOG NUMBER
4. TITLE (and Subtitle) Fracture and Fatigue Characteristics in Titanium Alloys		5. TYPE OF REPORT & PERIOD COVERED Final Report 7/1/79 - 9/30/81
		6. PERFORMING ORG. REPORT NUMBER SC5227.1FR
7. AUTHOR(s) C. G. Rhodes M. R. Mitchell J. C. Chesnutt		8. CONTRACT OR GRANT NUMBER(s) N00014-79-C-0567
9. PERFORMING ORGANIZATION NAME AND ADDRESS Rockwell International Science Center 1049 Camino Dos Rios Thousand Oaks, CA 91360		10. PROGRAM ELEMENT, PROJECT, TASK AREA & WORK UNIT NUMBERS NR 031-824 Project No. 471
11. CONTROLLING OFFICE NAME AND ADDRESS Dr. Bruce MacDonald Office of Naval Research, 800 N. Quincy Arlington, VA 22217		12. REPORT DATE June, 1982
		13. NUMBER OF PAGES 122
14. MONITORING AGENCY NAME & ADDRESS(if different from Controlling Office)		15. SECURITY CLASS. (of this report) Unclassified
		15a. DECLASSIFICATION DOWNGRADING SCHEDULE

16. DISTRIBUTION STATEMENT (of this Report)

Approved for public release; distribution unlimited

17. DISTRIBUTION STATEMENT (of the abstract entered in Block 20, if different from Report)

18. SUPPLEMENTARY NOTES

19. KEY WORDS (Continue on reverse side if necessary and identify by block number)

Titanium alloys, fracture toughness, fatigue crack growth rate, tensile properties, quantitative microstructural analysis, fatigue crack initiation, surface condition effects, hydrogen effects

20. ABSTRACT (Continue on reverse side if necessary and identify by block number)

The influence of sub-transus solution treatment on room temperature fracture toughness of Ti-6Al-4V (6-4) and Ti-4.5Al-5Mo-1.5Cr (CORONA-5) has been studied as a function of elemental partitioning and volume fraction of alpha and beta phases. Scanning/transmission electron microscopy was used to analyze quantitatively the microstructural components of the two alloys. It was found that, for as-solution treated condition, fracture toughness of 6-4 (cont.)

DD FORM 1 JAN 73 1473

UNCLASSIFIED

SECURITY CLASSIFICATION OF THIS PAGE (When Data Entered)

20. ABSTRACT (cont.)

increased as volume fraction of primary alpha, aluminum content of primary alpha, aluminum content of beta phase, or vanadium content of beta phase decreased. Similarly, for as-solution treated CORONA-5, increases in volume fraction of primary alpha, aluminum and molybdenum contents of primary alpha, or chromium content of beta phase led to a decrease in toughness. In the case of solution-treated and aged 6-4, the analysis indicated that toughness was improved by increasing the vanadium content of the beta phase, increasing the size of secondary alpha plates, reducing the aluminum content of primary alpha, or by reducing the volume fraction of retained beta. Aging CORONA-5 after solution treatment resulted in a very fine secondary alpha structure within transformed beta regions. For this alloy, toughness was improved by increasing the chromium contents of primary alpha and beta phases, increasing the volume fraction of beta phase, reducing the aluminum contents of primary alpha and beta phases, or by reducing the size of secondary alpha plates. The differences between Ti-6Al-4V and Ti-4.5Al-5Mo-1.5Cr can be attributed to the volume fractions of primary alpha (~90 pct. in 6-4, ~50 pct. in CORONA-5) and the average size of secondary alpha plates. In the Second Part of this program, Ti-6Al-4V processed from pre-alloyed powder was analyzed for microstructural anomalies and elemental partitioning. The inferior mechanical properties of the as hot-isostatically pressed material could be related to the presence of voids and bubbles in the microstructure, as well as the non-equilibrium partitioning of aluminum and vanadium between the alpha and beta phases. In the Third Part of the program, the effects of surface condition, microstructure, and internal hydrogen on fatigue crack initiation in Ti-6Al-4V were studied. Neither surface residual stresses nor internal hydrogen promoted internal fatigue crack initiation in beta treated, recrystallization annealed, or solution treated and overaged 6-4. Surface residual stresses were apparently relieved as a result of cyclic softening during fatigue testing and were thus rendered ineffectual in promoting internal crack initiation. Internal hydrogen was found to enhance ductility in the localized region of the crack tip and made no contribution to internal crack initiation.

TABLE OF CONTENTS

TABLE OF CONTENTS (Continued)

LIST OF FIGURES

LIST OF FIGURES (Continued)

LIST OF FIGURES (Continued)

LIST OF FIGURES (Continued)

LIST OF TABLES

LIST OF TABLES (Continued)

PREFACE

This document is the final report on Contract N00014-79-C-0567 sponsored by the Office of Naval Research entitled "Fracture and Fatigue Characteristics in Titanium Alloys." This report describes results of research conducted during the period July 1979 through September 1981. The program was monitored by Dr. Bruce MacDonald of ONR and was conducted at the Rockwell International Science Center by Mr. C. C. Rhodes, Mr. J. C. Chesnutt, Dr. M. R. Mitchell, and Dr. N. E. Paton. Experimental assistance was provided by Messrs. R. A. Spurling, P. Q. Sauers, M. Calabrese, L. F. Nevarez, A. R. Murphy and Mrs. M. V. Spriggs. Regression analysis was performed by Mr. Jack Gysbers. Ti-4.5Al-5Mo-1.5Cr was kindly supplied by Prof. Harold Margolin of the Polytechnic Institute of New York. Powder processed Ti-6Al-4V was made available to us by Drs. J. E. Magnuson and R. R. Boyer of the Boeing Airplane Company.

1.0 INTRODUCTION

Titanium alloys offer excellent strength to density ratios and are used in a wide variety of vehicle structures, ranging from moderately to severely loaded parts. Consequently, a detailed understanding of the fracture characteristics of these alloys is of great importance. Although there has been a continuing advancement in recent years in our understanding of fracture behavior, there are still several areas in which further study is needed. This three-part report describes the results of a study in three such areas. Part I is concerned with the effects of heat treatment and microstructure on fracture toughness, fatigue crack propagation, and tensile properties in α/β titanium alloys, Part II involves microstructural studies of powder processed titanium alloy, and Part III is directed at characterizing internal fatigue crack initiation sites in an α/β alloy.

Part I includes a systematic study of the effect of sub-transus heat treatments on microstructure and mechanical properties in Ti-6Al-4V and Ti-4.5Al-5Mo-1.5Cr (CORONA 5). Very little is known about the mechanisms by which variations in sub-transus treatment temperature produce changes in fracture toughness, fatigue crack propagation, and tensile properties in α/β alloys, hence Part I was aimed at exploring this area. The wide variety of annealing treatments used in industry points out the importance of understanding the mechanism by which sub-transus treatments can alter mechanical properties.

It has been reported that fracture toughness in α/β titanium alloys decreases with increasing sub-transus solution temperature[1-3] and a similar effect has been observed for fatigue life of Ti-6Al-4V.[4] Although there is speculation that the influence of sub-transus treatment arises from 1) the amount of grain boundary alpha[5] or 2) the size and spacing of fine α-phase particles in the transformed β regions,[2] neither has been established. Indeed, some workers who have observed the effect have declined to speculate on its origin.[1,3] It is quite likely there are other factors contributing to

this phenomenon. For instance, the strength and toughness of each of the two phases in the microstructure are dependent on the composition of each phase, hence partitioning of alloying elements and impurities between the alpha and beta phases is an important variable contributing to fracture toughness. Volume fractions of alpha and beta phases are also likely factors influencing toughness, fatigue crack resistance and tensile properties.

Ti-6Al-4V was selected in this study because it has extensive applications, and CORONA 5 was selected to compare the findings of 6-4 with those in an α/β alloy having the more slowly diffusing Mo added as a β-stabilizer. The primary objective of this part of the program was to ascertain which microstructural features and compositional variations are instrumental in affecting fracture toughness, fatigue crack propagation values and tensile properties. With these parameters defined, it will be easier to devise heat treatments to produce desired mechanical properties in an α/β alloy.

Part II is an investigation into the microstructure of Ti-6Al-4V made by powder metallurgy (PM) techniques. The fabrication of titanium alloy parts (near net shapes) by PM techniques has received considerable attention recently,[6-9] primarily as a cost saving approach to the manufacture of finished products. Processing techniques are still in the evolutionary stages, and at this juncture, the use of pre-alloyed powder which is pressed, sintered and hot-isostatically pressed appears to offer the most promise. In general, it has been reported that mechanical properties such as tensile,[6] fracture toughness,[8] LCF,[8] and HCF[8] in PM Ti-6Al-4V are inferior to those in the wrought alloy.

The degradation of mechanical properties in PM titanium alloys has been attributed to foreign contaminants introduced during the processing of the powders. However, there has been no characterization of the microstructure developed in PM products in terms of alloying element partitioning and α and β phase distributions. It is quite possible that properties of PM products can be accounted for by microstructural considerations and that additional processing that develops structures present in wrought material will

restore properties. The objective of this task was to assess the microstructures developed in PM products and compare them to conventional wrought material microstructures.

Part III is concerned with the influence of surface condition and internal hydrogen on fatigue crack initiation. Advanced manufacturing techniques for Ti-6Al-4V utilize many surface finishing techniques. For example, chemical machining, grinding, polishing, and in some instances, where enhanced fatigue resistance is required in the long-life regime (i.e., approximately 10^6 cycles and greater), shot or strain peening are employed. Each process results in a surface residual stress that may be tensile or compressive and which will affect not only the fatigue life but also the location (surface or subsurface) of crack initiation.[10]

It is well established that residual stress patterns and the relaxation rate of residual surface stresses are markedly affected by the strength and microstructure of a material, as well as the stress or strain history of a service environment.[11] For example, a lower rate of residual stress relaxation is associated with lower stress amplitudes and higher yield strength. Thus, in a fatigue situation, "soft" materials will not, generally, sustain residual stresses as a result of cyclic plasticity generated even at low cycle stress amplitudes.[12,13]

Hydrogen effects on both fatigue crack initiation and propagation in α/β alloys involve a complex interaction of hydrogen solubility and diffusion in the beta phase and diffusion and hydride precipitation in the alpha phase. Hydrogen concentrations in the range of 3 to 1500 ppm are known to have a pronounced effect on crack initiation and propagation.[14-16] Specific combinations of temperature and stress can enhance hydride precipitation[17], localized cracking and early initiation.

Therefore, this portion of the research on Ti-6Al-4V was focused on the potential for subsurface crack initiation due to the combined effects of surface preparation techniques, internal hydrogen contents, and microstructure.

2.0 EXPERIMENTAL

The alloys used in Part I had nominal compositions of Ti-6Al-4V and Ti-4.5Al-5Mo-1.5Cr (CORONA 5); chemical analyses are given in Table I. Each of the alloys was α/β processed, resulting in a microstructure consisting of equiaxed primary alpha in a beta matrix. The Part II alloy, Table I, was Ti-6Al-4V supplied to Rockwell International by Boeing where mechanical tests were performed.[6] Heat treatments were carried out with samples either in a flowing inert gas atmosphere, encapsulated in evacuated ampules or, for low temperature aging, in salt bath.

Table I. Compositions of Alloys Used in Parts I, II, and III

Program Part	Alloy Designation	Al	V	Mo	Cr	Fe	O	Ti
I	6-4	6.10	4.00	-	-	0.19	0.122	Bal
I	CORONA 5	4.75	-	4.73	1.43	0.07	0.133	Bal
II	6-4	6.60	4.25	-	-	0.05	0.204	Bal
III	6-4	6.20	4.10	-	-	0.22	0.122	Bal

Fracture toughness was measured by notched, pre-cracked Charpy bars tested in slow bend. The slow bend tests produced a value of W/A which was converted to K_Q through the expression $K_Q = [(W/A)E/2(1-\nu^2]^{1/2}$, where W is energy required to fracture the specimen, A is the fracture area of the specimen, E is Young's modulus, and ν is Poisson's ratio. Compact tension specimens were used for fatigue crack growth rate measurements, which were carried out in laboratory air at room temperature at 30 Hz and R = 0.1. Crack length was measured optically with the specimens removed from the testing machine. Tensile tests were performed on round bars at $\dot{\varepsilon} = 2.6 \times 10^{-4}\ s^{-1}$.

Thin foils for transmission electron microscopy were prepared by conventional electropolishing techniques[18] or by ion milling.[19] The foils were examined in a Philips EM 400 electron microscope, equipped with double tilt goniometer stage, scanning/transmission, and x-ray energy dispersive analysis accessories. Fractography was carried out using an ETEC Autoscan scanning electron microscope (SEM).

Quantitative x-ray energy dispersive microanalysis of the individual phases in the microstructure was accomplished by means of the technique described in the Appendix and in Ref. 20. Volume fraction measurements of alpha and beta phases were made by the point count method[21] directly on the SEM CRT image.

Specimen blanks for Part III of the program were cut from uniformly and weakly textured pancake forgings of well documented Ti-6Al-4V,[16] Table I. The blanks were heat treated to produce the microstructures βF, RA and STOA using the schedule outlined in Table II. Internal hydrogen charging to nominally 3, 100 and 300 wppm was then accomplished in a Sievert's apparatus. Specimens were machined to the finished dimensions shown in Fig. 1 after hydrogen charging. Several specimens of each microstructure in the as-machined condition* were set aside for subsequent testing. Other specimen lots were either electrochemically polished or shot peened. Prior to fatigue testing, the surface residual stresses were measured in the longitudinal direction using x-ray analysis. Testing was concentrated between fatigue lives of 10^5-10^7 cycles since surface treatment effects[22-24] and internal hydrogen contents[25] are most pronounced in this regime. Also, longer life testing should promote subsurface crack initiation since nominally elastic behavior prevails, as opposed to the shorter life regime where plasticity effects eradicate residual stresses.[26]

*As-machined surfaces were produced by single point machining to near-final dimensions followed by mechanical polishing in steps using 250, 400 and 600 grit carborundum paper on a rotating mandrel at 45° to the specimen axis.

Table II. Heat Treatments for Ti-6Al-4V Used in Part III

Condition	Fabrication	Heat Treatment
β-Forge (βF)	β Forge/AC β Finish/AC	704°C(1300°F)/2 hours/AC
Recrystallization Anneal (RA)	α-β Forge/AC α-β Finish/AC	927°C(1700°F)/4 hours cool at 50°C/hr to 760°C(1400°F)/AC
Solution treat and overage (STOA)	α-β Forge/AC α-β Finish/AC	954°C(1750°F)/1 hour/WQ + 593°C(1100°F)/24 hours/AC

3.0 RESULTS

3.1 Part I. A. Effect of Sub-Transus Solution Temperature on Mechanical Properties of α/β Ti Alloys

3.1.1 Ti-6Al-4V

3.1.1.1 Microstructure

a. Solution Temperature Effects

The starting microstructure of Ti-6Al-4V consisted of equiaxed primary alpha grains ~12 μm in diameter dispersed in a beta phase matrix. Solution treatments were carried out at 700°C to 975°C in 50°C intervals (the β transus of this heat of 6-4 was ~980°C); the samples were held at solution temperature for one hour and water quenched to room temperature to preserve the volume fractions and compositions of the alpha and beta phase which existed at temperature. When quenched from 850°C and above, the beta phase generally transformed martensitically to α'. However, it was noted that, where the beta phase was very narrow between two alpha grains, it did not transform to martensite. This phenomenon is discussed in more detail in Sections 3.1b and 4.1.4.

The results of composition and volume fraction measurements are presented in the form of pseudo-binary phase diagrams, Figs. 2 and 3. The phase boundaries are defined by the composition measurements with the error bars representing 95% confidence intervals for the multiple readings comprising each data point. The alloy composition lines in Figs. 2 and 3 are positioned experimentally from the volume fraction measurements using the lever rule. As such, the alloy composition lines act as independent checks on the accuracy of the composition measurements, and the fact that they fall at 6% Al and 4% V (the composition of the alloy) attests to the validity of the phase boundary positions.

The compositions of the beta phase in samples quenched from 850°C and above was assumed to be identical to the composition of the martensite observed at room temperature. The consistency of the results shown in Figs. 2 and 3 bears out this assumption.

b. Cooling Rate Effects, Ti-6Al-4V

Ti-6Al-4V was solution treated at 700, 800, 900, and 975°C for 1 hour and cooled at 5000°C/hr, 300°C/hr, and 50°C/hr to compare volume fraction and compositions of alpha and beta phases to those observed in the quenched material. The objective here was to ascertain if constant volume fractions of α and β phases could be produced with varying compositions or vice versa. The results are presented in Figs. 4-7 where compositions are plotted against volume fraction primary alpha. The slower cooled material has volume fractions of primary alpha phase ranging between 0.85 and 0.90 with composition variations ranging from small in the case of vanadium in alpha phase (Fig. 5) to large in the case of vanadium in beta phase (Fig. 7).

For the slow-cooled material, there was a concentration gradient in the beta phase. That is, vanadium concentration was highest and aluminum concentration lowest in beta phase near the α/β interface, Fig. 8. The absolute values of Al and V concentration appear to be relatively constant as a function of distance for a particular heat treatment, so that narrower strips of beta phase have a higher average vanadium content than the broader patches. A comparison of vanadium concentration in beta phase as a function of distance from the α/β interface for three different cooling rates from 900°C solution temperature is presented in Table III. The vanadium concentration reaches a minimum value at a distance of between 300 and 600 nm from the nearest interface.

Aluminum concentration in beta phase shows a distribution inverse to that for vanadium. That is, Al values of about 1.5 wt pct are observed near the α interface, increasing to approximately 2.5 wt pct in the center of the broad beta patch.

Table III. Composition Gradients in Beta Phase of Ti-6Al-4V Solution Treated at 900°C for 1 Hour

Cooling Rate From Solution Temperature	Wt Pct Vanadium in Beta Phase Distance from α Interface, nm 100	200	300	600	Vol Fraction β
5000°C/hr	22.1	21.6	20.7	17.7	0.10
300°C/hr	21.4	19.2	18.8	-	0.15
50°C/hr	25.0	22.0	20.0	18.5	0.11

Because the majority of the beta phase existed as narrow strips in the slow-cooled samples, the values of Al and V reported in Figs. 4-7 are taken from those regions. No attempt was made to calculate a weighted average to include the concentrations from the broader beta patches.

3.1.1.2 Fracture Toughness

Previous ONR research demonstrated that Ti-6Al-4V rolled plate may contain a banded microstructure that significantly affects fracture toughness.[27] That is, when the banded structure is normal to the propagating crack direction, toughness is considerably greater than when the crack progresses parallel to the banding. The material used in this study exhibited a slight degree of banding, and only specimens having crack direction normal to the banding have been included in the correlations of toughness and microstructure.

Test specimens were subjected to three different cooling rates following solution treatment at various sub-transus temperatures, thus providing a variety of volume fractions and compositions of alpha and beta phases for correlation with toughness. The cooling rates were water quench (~3×10^4°C/hr), air cool (~3×10^3°C/hr), and furnace cool (3×10^2°C/hr).

Toughness values for the water quenched conditions are given in Fig. 9. The M_s temperature for 6-4 depends on the beta phase composition,

and, therefore, on the sub-transus solution temperature. For the specimen sizes used in this study, it was observed that beta phase transformed martensitically only during water quenching from solution temperatures >850°C. Microstructures of test specimens shown in Fig. 9, then, include martensite in the three samples having the lowest toughness. The presence of a martensitic structure was not included, per se, in the quantitative analysis of the microstructure. The parameters considered were volume fraction of primary alpha, and Al and V concentrations of the α and β phases. However, in the case of a martensitic matrix, the "beta phase" composition used in the analysis is actually the martensite composition.

Volume fraction measurements and phase composition determinations were made on specimens cut from broken Charpy bars of the slow cooled conditions, whereas microstructure parameters for water quenched specimens were taken from the phase diagrams (Figs. 2 and 3).

Linear regression analyses were performed on the data from twelve tests. The best fit of the data was

$$K_Q = 457 - 15.8(Al_\alpha) - 19.8(Al_\beta) - 3.3(V_\beta) + 23.7(V_\alpha) - 122(vf_{\alpha p}) \quad (1)$$

where Al_α and Al_β are aluminum concentrations (by at. pct.) in alpha and beta phases, V_α and V_β are vanadium concentrations (by at. pct.) in alpha and beta phases, and $vf_{\alpha p}$ is volume fraction of primary alpha. Units of toughness are MPa $\sqrt{m}$. A graphic demonstration of how well this expression predicts toughness in α-β processed Ti-6Al-4V is shown in Fig. 10, where observed values are plotted against calculated values using Eq. (1). The straight line is a 1-1 correlation and it can be seen that the expression reliably predicts toughness based solely on phase compositions and volume fraction of primary alpha.

3.1.1.3 Fatigue Crack Propagation

Compact tension specimens were solution treated at 700, 800, and 900°C and water quenched prior to fatigue crack propagation rate testing. In order to demonstrate the effect of solution temperature on da/dN (fatigue crack growth rate), growth rates at four stress intensity levels have been selected from growth rate curves and plotted as a function of solution temperature, Fig. 11. The plot clearly shows that fatigue crack growth resistance increases significantly with increasing solution temperature.

Regression analyses were performed on the data shown in Fig. 11 with volume fraction and phase compositions taken from the phase diagrams (Figs. 2 and 3). The best fit of the data was found to be

$$\ell n\ da/dN = 28 - 2.8(Al_\alpha) - 3.4(Al_\beta) + 8.9(V_\alpha) - 1.5(V_\beta) + 7(vf_{\alpha p}) + 0.2\ (\Delta K) \quad (2)$$

where Al_α, Al_β, and V_α are aluminum concentrations (by at pct) in alpha and beta phase and vanadium concentration in beta phase, $vf_{\alpha p}$ is volume fraction of primary alpha, and ΔK is stress intensity level. Units of da/dN are mm/cycle and those of stress intensity are MPa $\sqrt{m}$.

As an assessment of the ability of Eq. (2) to predict da/dN, measured values are plotted against calculated values in Fig. 12. The straight line is a one-to-one correlation and it can be seen that Eq. (2) predicts da/dN over a wide growth rate range based solely on volume fraction of primary alpha, phase compositions, and stress intensity level. The expression is remarkably accurate in predicting da/dN, especially considering that the fracture mode changes from cyclic cleavage at low growth rates to striation formation at higher growth rates.

3.1.2 Ti-4.5Al-5Mo-1.5Cr (CORONA 5)

3.1.2.1 Microstructure

The starting microstructure of CORONA 5 consisted of equiaxed primary alpha grains ~3 μm in diameter dispersed in a beta phase matrix. Solution treatments were carried out at 625 to 925°C in 50°C intervals (β transus was ~935°C), held for 1 to 4 hours depending on temperature, and water quenched to retain volume fractions and compositions of alpha and beta phases that existed at solution temperature. The beta phase transforms martensitically to α' when quenched from 875°C and above, but is retained when quenched from lower solution temperatures. In order to avoid precipitation of secondary alpha at the lower solution temperatures, specimens were slow cooled from high in the α+β phase field to room temperature prior to re-heating to the solution temperature. Slow cooling resulted in high volume fraction of primary alpha which was then reduced to equilibrium values during solution treatment.

The results of composition and volume fraction measurements are presented in the form of pseudo-binary phase diagrams, Figs. 13, 14, and 15. Construction of the diagrams was accomplished in the same manner as described for Ti-6Al-4V (see Section 3.1.1.1a).

3.1.2.2 Fracture Toughness

Notched Charpy bars were water quenched following solution treatment at several sub-transus temperatures. Toughness values are shown in Fig. 16. The behavior is similar to that observed for Ti-6Al-4V, with room temperature fracture toughness decreasing as prior solution temperature increased.

Volume fraction of primary alpha phase and compositions of alpha and beta phases were the parameters included in regression analyses for correlating microstructure with fracture toughness. The values for the microstructural parameters were measured on samples extracted from broken Charpy bars. The regression analysis selected as the best fit of the data was

$$K_Q = 44 - 40(Al_\alpha) + 82(Al_\beta) - 365(Mo_\alpha) + 242(Mo_\beta) + 364(Cr_\alpha) - 399(Cr_\beta) - 33(vf_{\alpha p}) \quad (3)$$

where Al_α, Al_β, Mo_β, and Cr_β are aluminum content of alpha phase, aluminum, molybdenum and chromium contents of beta phase, and $vf_{\alpha p}$ is volume fraction of primary alpha. The alpha and beta phase compositions are in atomic percent and toughness units are MPa $\sqrt{m}$. Figure 17 demonstrates the ability of Eq. (3) to predict fracture toughness in CORONA 5, where measured values are plotted against calculated values, with the straight line being a one-to-one correlation.

3.1.3 Combined Ti-6Al-4V and CORONA 5 Fracture Toughness

Regression analyses were made using both 6-4 and CORONA 5 data to explore the possibility of a more universal expression. The analysis resulted in the following:

$$K_Q = 110 - 0.7(Al_\alpha) - 7.7(Al_\beta) + 237(Cr_\alpha) - 315(Cr_\beta) - 57(Mo_\alpha) + 182(Mo_\beta) + 34\ (V_\alpha) + 0.88(V_\beta) - 85(vf_{\alpha p}) \quad (4)$$

where parameters are as described in Sections 3.1.1.2 and 3.1.2.2. A plot of measured values against calculated values, Fig. 18, reveals that Eq. (4) predicts fracture toughness reasonably well for the two alpha-beta alloys.

3.2 Part I. B. Effect of Sub-Transus Solution Temperature and Aging Temperature on Mechanical Properties of α/β Ti Alloys

3.2.1 Ti-6Al-4V

3.2.1.1 Microstructure

In order to assess the influence of microstructure on toughness, da/dN, and tensile properties in solution treated and aged (STA) 6-4, three solution temperatures and three aging temperatures were selected. The

standard STA for 6-4 is one hour at 954°C (1750°F), water quench followed by 6 hours at 538°C (1000°F) and air cool. The several microstructural parameters that can be varied in STA treatments are volume fractions and compositions of primary alpha, secondary alpha, and beta phases, and size and morphology of secondary alpha. These parameters were measured in the standard STA condition and used as target parameters to be achieved with varied aging temperatures. To this end, 6-4 was solution treated at 954°C and aged for various times at 438°C (820°F) and at 635°F (1175°F). It was found that 48 hours at 438°C and 1 hour at 635°C produced microstructures similar to that in the standard STA material. Typical microstructures are shown in Figs. 19-21. Also examined were two lower solution temperatures - 871°C (1600°F) and 788°C (1450°F) - followed by the standard age at 538°C. Lowering the solution temperature, of course, increased the volume fraction of primary alpha phase and the resulting secondary alpha was also significantly altered. The various parameters are summarized in Table IV.

Table IV. Microstructural Features in Ti-6Al-4V Quantified for This Study*

Solution Treatment	Age Treatment	Volume Pct α_p[1]	Volume Pct α_s[2]	Volume Pct β[3]	α_s Particle Size[2] Length, μm	Width, μm
954°C/1 hr	538°C/6 hrs	10	86	4	8.0	0.4
954°C/1 hr	438°C/48 hrs	10	81	9	5.6	0.3
954°C/1 hr	635°C/1 hr	9	83	8	8.0	0.5
871°C/1 hr	538°C/6 hrs	53	45	2	0.8	0.08
788°C/1 hr	538°C/6 hrs	60	37	3	0.8	0.07

* Values shown in Table are averages of individual test specimens.
1 α_p = primary alpha phase
2 α_s = secondary alpha phase
3 β = beta phase

3.2.1.2 Regression Analysis Technique

The microstructural variables that have been quantified for regression analysis are compositions and volume fractions of primary alpha, secondary alpha, and beta phases, and size of secondary alpha particles. The relative contribution of each of the parameters to toughness was evaluated by regression analyses wherein nine trials were run, each with only one parameter eliminated from the analysis. The resulting correlation coefficients[28] provided a quantified ranking of the contribution of each parameter.

It was anticipated that there would be synergistic effects among the several microstructural parameters, so that a single elimination test as just described, although a good first approximation, could be modified by considering parameters pairwise or in triplets. Therefore, numerous linear regression trials were made with systematic combinations of parameters. The objective was two-fold: 1) to establish a mathematical expression for each property based on only the significant parameters and 2) to determine a consistent direction (positive or negative) in which each parameter influences a particular mechanical property. The former is to demonstrate that alloys and heat treatments could be designed to improve properties based on particular microstructural features, whereas the latter provides a more general, though not quantitative, aspect of the influence of various microstructural parameters on properties.

Evaluation of the consistency of direction (positive or negative) in which the parameters influence each property was made by tabulating the sign of the coefficient of each parameter in numerous regression trials. When the sign of the coefficient of any parameter is unchanged in a large number of regression trials, i.e., the consistency of the sign is 100%, that parameter is considered to be significant in the correlation of microstructure with mechanical property. The reasons for a change in sign of the coefficient of a particular parameter could be synergistic effects or mathematical manipulation during regression analysis to obtain a "best fit." The latter is most likely the situation for those parameters having a consistently signed coefficient in

less than 90 pct of the trials, because no regular pattern could be discerned for synergism among the various parameters in those cases.

These two tests - single elimination and consistency of sign - were used to evaluate the significance of each microstructural parameter on particular mechanical properties. Regression analysis equations were then developed using only the significant parameters, resulting in a meaningful mathematical expression for each property. The results will be presented as a single list of microstructural parameters in decreasing order of contribution (significance) to each mechanical property and as a single mathematical expression equating mechanical property to quantified microstructural features. Although expressions were developed for numerous combinations of microstructural parameters, the one presented will include only the significant parameters. As a result the reader will be able to evaluate the qualitative and the quantitative effect of significant parameters on properties.

3.2.1.3 Fracture Toughness

Test specimens were heat treated according to the schedule in Table IV. Duplicates of the five solution treat and age (STA) conditions were tested.

The influence of solution temperature on toughness for 6-4 given an age treatment of 538°C/6 hrs/air cool is seen to be negligible, Fig. 22. This is in contrast to results observed for solution treated 6-4, Fig. 9, indicating that different combinations of microstructures can produce similar properties.

Evaluation of regression analyses resulted in a ranking of the relative contribution of each microstructural variable to toughness, as listed in Table V. The analyses indicated that only the first four parameters listed in the Table made a significant impact on toughness. The vanadium content of beta-phase and the average volume of secondary alpha particles add to toughness in a positive manner, i.e., toughness is increased as either of these parameters is increased. On the other hand, aluminum content of primary alpha

and volume fraction of beta phase lower toughness, i.e., decreasing either of these two parameters reduces toughness. The remaining parameters do not significantly affect toughness to an extent that can be reliably quantified.

Table V. Contribution of Each Microstructural Parameter to Fracture Toughness in STA Ti-6Al-4V, as Measured by Regression Analysis

Parameter	Significance(1)	Sign of Coefficient(2)
Vanadium content β	S	+
Aluminum content primary α	S	-
Size secondary α particles	S	+
Volume fraction β phase	S	-
Vanadium content primary α	NS	
Aluminum content secondary α	NS	
Vanadium content secondary α	NS	
Aluminum content β	NS	
Volume fraction secondary α	NS	

(1) S = significant contribution to toughness
NS = not significant contribution to toughness
(2) + = positive contribution to toughness
- = negative contribution to toughness

Regression analysis including the four significant variables resulted in the following expression:

$$K_Q = 127 - 12.9(Al_{\alpha p}) + 3.2(V_\beta) - 1.1(vf_\beta) + 24.9(\alpha_s) \qquad (5)$$

where $Al_{\alpha p}$ is aluminum concentration (at. pct.) in primary alpha, V_β is vanadium concentration (at. pct.) in beta, vf_β is volume percent of beta phase, and α_s is average volume of secondary alpha particles (cubic micrometers). Units of toughness are MPa $\sqrt{m}$. The accuracy of Eq. (5) in predicting toughness is shown in Fig. 23, where measured toughness values are

plotted against calculated values using Eq. (5). The straight line is a one-to-one correlation.

3.2.1.4 Fatigue Crack Propagation

Compact tension specimens were given heat treatments #3, 4, and 5 as listed in Table IV. In this way, a variation in microstructure was developed to provide a broad base for regression analyses.

The influence of prior solution temperature on fatigue crack propagation rate for 6-4 given an age treatment of 538°C/6 hours/air cool is seen to be negligible, Fig. 24. This is in contrast to results observed for solution treated 6-4, Fig. 11, indicating that different combinations of microstructures can produce similar properties. This effect was also observed for fracture toughness (see prior section).

The relative contributions of microstructural variables are presented in Table VI, as measured by regression analyses. Six of the nine parameters were evaluated as significantly influencing da/dN. In this case, a positive contribution actually increases crack growth rate, hence a negative sign of the regression coefficient indicates an improvement in crack growth resistance.

Regression analysis using the six significant variables resulted in the following:

$$\ell n\ da/dN = -82 - 0.8(vf_{\beta}) + 17.7(\alpha_s) - 1.5(Al_{\alpha p}) + 0.4(V_{\alpha p}) + 6.6(Al_{\alpha s})$$

$$+6.4(V_{\alpha s}) + 0.2(\Delta K) \qquad (6)$$

Table VI. Contribution of Each Microstructural Parameter to Fatigue Crack Propagation Rate in STA Ti-6Al-4V, as Measured by Regression Analysis

Parameter	Significance(1)	Sign of Coefficient(2)
Vanadium content secondary α	S	+
Aluminum content secondary α	S	+
Volume fraction β phase	S	-
Size secondary α particles	S	+
Vanadium content primary α	S	+
Aluminum content primary α	S	+
Aluminum content β	NS	
Volume fraction secondary α	NS	
Vanadium content β phase	NS	

(1) S = significant contribution to da/dN
NS = not significant contribution to da/dN
(2) + = positive contribution to da/dN
- = negative contribution to da/dN

where vf_β is volume fraction of beta phase, α_s is average volume of secondary alpha particles (in cubic micrometers), $Al_{\alpha p}$ and $Al_{\alpha s}$ are aluminum concentrations (at. pct.) in primary alpha and secondary alpha, respectively, $V_{\alpha p}$ and $V_{\alpha s}$ are vanadium concentration (at. pct.) in primary and secondary alpha, respectively, and ΔK is stress intensity in MPa $\sqrt{m}$. The accuracy with which Eq. (6) predicts da/dN in STA Ti-6Al-4V is illustrated in Fig. 25, where measured da/dn is plotted against calculated da/dn using Eq. (6). the straight line is a one-to-one correlation.

3.2.1.5 Tensile Tests

Test specimens were heat treated following the schedule in Table IV. Duplicate specimens of the five STA conditions were tested at room temperature to provide a broad base for correlation of properties and microstructure.

The influence of prior solution temperature on room temperature tensile properties of 6-4 aged at 538°C is illustrated in Fig. 26. It can be seen that ultimate and yield strengths increase and elongation decreases with increasing solution temperature. None of the quantified microstructural features individually correlates with the observed tensile behavior, indicating that an interaction of parameters contributes to the behavior of the alloy.

Regression analysis evaluations were made for the three tensile properties, the results of which are presented in Tables VII, VIII, and IX. The analyses indicate there are six significant microstructural parameters contributing to yield strength and to ultimate strength. In the case of tensile elongation, five microstructural variables have been assessed as significant. Regression analyses for each of the tensile properties yield the following:

$$Y.S. = -2344 - 49(vf_{\beta}) + 1296(vf_{\alpha s}) - 972(\alpha_s) + 165\ (Al_{\alpha s}) + 186(V_{\alpha s}) + 54(V_{\beta}) \quad (7)$$

$$U.T.S. = -662 + 765(vf_{\alpha s}) - 800(\alpha_s) + 87(Al_{\alpha p}) - 6.9(V_{\alpha p}) + 54(V_{\alpha s}) + 10(V_{\beta}) \quad (8)$$

$$\varepsilon = -57 - 1.0(vf_{\beta}) - 33(vf_{\alpha s}) + 5.6(Al_{\alpha p}) - 13.1(V_{\alpha p}) + 4.7(Al_{\alpha s}) \quad (9)$$

where vf_{β} is volume percent β phase, $vf_{\alpha s}$ is volume fraction secondary α, α_s is average volume of secondary α particles (in cubic micrometers), $Al_{\alpha p}$ and $Al_{\alpha s}$ are aluminum concentrations (at. pct.) in primary α and secondary α, respectively, and $V_{\alpha p}$, $V_{\alpha s}$, V_{β} are vanadium concentrations (at. pct.) in primary α, secondary α, and β phases, respectively. Units of stress are MPa; ε is in percent. The accuracy with which each equation predicts its respective property is illustrated in Figs. 27-29, where measured values are plotted against calculated values. The straight lines in the figures are one-to-one correlations.

Table VII. Contribution of Each Microstructural Parameter to Tensile Yield Strength in STA Ti-6Al-4V, as Measured by Regression Analysis.

Parameter	Significance(1)	Sign of Coefficient(2)
Volume fraction secondary α	S	+
Vanadium content secondary α	S	+
Vanadium content β phase	S	+
Volume fraction β phase	S	-
Size secondary α particles	S	-
Aluminum content secondary α	S	+
Aluminum content β phase	NS	
Vanadium content primary α	NS	
Aluminum content primary α	NS	

(1) S = significant contribution to yield strength
NS = not significant contribution to yield strength
(2) + = positive contribution to yield strength
- = negative contribution to yield strength

Table VIII. Contribution of Each Microstructural Parameter to Ultimate Tensile Strength in STA Ti-6Al-4V, as Measured by Regression Analysis

Parameter	Significance[1]	Sign of Coefficient[2]
Volume fraction secondary α	S	+
Vanadium content secondary α	S	+
Aluminum content primary α	S	+
Vanadium content primary α	S	-
Vanadium content β phase	S	+
Size secondary α particles	S	-
Aluminum content β phase	NS	
Volume fraction β phase	NS	
Aluminum content secondary α	NS	

(1) S = significant contribution to ultimate strength
NS = not significant contribution to ultimate strength
(2) + = positive contribution to ultimate strength
- = negative contribution to ultimate strength

Table IX. Contribution of Each Microstructural Parameter to Tensile Elongation in STA Ti-6Al-4V, as Measured by Regression Analysis.

Parameter	Significance(1)	Sign of Coefficient(2)
Vanadium content primary α	S	-
Aluminum content secondary α	S	+
Aluminum content primary α	S	+
Volume fraction secondary α	S	-
Volume fraction β phase	S	-
Vanadium content β phase	NS	
Vanadium content secondary α	NS	
Size secondary α particles	NS	
Aluminum content β phase	NS	

(1) S = significant contribution to elongation
NS = not significant contribution to elongation
(2) + = positive contribution to elongation
- = negative contribution to elongation

3.2.2 Ti-4.5Al-5Mo-1.5Cr (CORONA 5)

3.2.2.1 Microstructure

Three solution temperatures and three aging temperatures were selected to assess the influence of microstructure on toughness and tensile properties in STA CORONA 5. The standard treatment for CORONA 5 is four hours at 830°C (1525°F), air cool, followed by four hours at 593°C (1100°F) and air cooled. The same microstructural parameters that were evaluated for 6-4 were varied in STA CORONA 5, namely, volume fractions and compositions of primary alpha, secondary alpha and beta phases, and size of secondary alpha particles. The parameters were determined for the standard STA condition and used as goal values for other treatments. As a result, Ti-4.5Al-5Mo-1.5Cr was solution treated at 830°C and aged for various times at 510°C (950°F) and at 677°C (1250°F). Twenty-four hours at 510°C and twenty minutes at 677°C were treatments that produced microstructures similar to that in standard STA material. Typical microstructures are shown in Figs. 30-32. Two additional solution temperatures - 749°C (1380°F) and 885°C (1525°F) - were selected for material to be given standard age treatment of 4 hours at 593°C. The resulting (non-compositional) parameters are summarized in Table X.

3.2.2.2 Fracture Toughness

Test specimens were heat treated according to Table X. Duplicates of conditions 1, 2, 4, and 5 were tested, along with a single sample of condition 3.

The influence of solution temperature on toughness for Ti-4.5Al-5.0Mo-1.5Cr given an age treatment of 593°C/4 hrs/AC is shown in Fig. 33. The behavior is similar to that observed for the as-solution-treated condition, Fig. 16. There has been, however, a reduction in toughness after aging at 593°C, which is apparently the result of the change in volume fractions of alpha and beta phases. This effect is addressed in the Discussion (Section 4.2.1).

Table X. Microstructural Features in Ti-4.5Al-5Mo-1.5Cr Quantified for This Study*

Solution Treatment	Age Treatment	Volume Pct α_p[1]	Volume Pct α_s[2]	Volume Pct β[3]	α_s Particle Size[2] Length, μm	Width, μm
830°C/4 hrs	593°C/4 hrs	51	27	22	1.0	0.07
830°C/4 hrs	510°C/24 hrs	51	30	19	1.0	0.04
830°C/4 hrs	677°C/20 min	46	30	24	1.4	0.10
749°C/6 hrs	593°C/4 hrs	58	17	25	0.6	0.08
885°C/4 hrs	593°C/4 hrs	18	60	22	1.9	0.08

* Values shown in Table are averages of individual test specimens.
1 α_p = primary alpha phase
2 α_s = secondary alpha phase
3 β = beta phase

The microstructural variables that have been quantified for regression analysis are the same as those for 6-4, and the regression analysis for STA CORONA 5 is similar to that described in Section 3.2.1.2. The number of variables for CORONA 5 is twelve (compared to only nine for 6-4), while the number of test specimens was nine. Consequently, single elimination regression analyses (see Section 3.2.1.2) could not be run, rather quintuple elimination trials were used to develop a ranking of the parameters.

The relative contribution to toughness of each variable is listed in Table XI. The analyses indicated that only seven parameters significantly impacted toughness, with a positive coefficient corresponding to an increase in toughness.

The following expression resulted from regression that included only the seven significant variables:

Table XI. Contribution of Each Microstructural Parameter to Fracture Toughness in STA Ti-4.5Al-5Mo-1.5Cr, as Measured by Regression Analysis

Parameter	Significance(1)	Sign of Coefficient(2)
Volume fraction β phase	S	+
Aluminum content β phase	S	-
Chromium content primary α	S	+
Chromium content β phase	S	+
Size secondary α particles	S	-
Aluminum content primary α	S	-
Volume fraction secondary α	NS	
Molybdenum content β phase	NS	
Chromium content secondary α	NS	
Molybdenum content primary α	NS	
Molybdenum content secondary α	NS	

(1) S = significant contribution to toughness
NS = not significant contribution to toughness
(2) + = positive contribution to toughness
- = negative contribution to toughness

$$K_Q = -154 - 0.5(Al_{\alpha p}) + 13(Al_{\alpha s}) - 20(Al_\beta) + 308(Cr_{\alpha p}) + 0.4(Cr_\beta) + 615(vf_\beta)$$
$$-2553(\alpha_s) \qquad (10)$$

where $Al_{\alpha p}$, $Al_{\alpha s}$, Al_β are aluminum concentrations (at.pct.) in primary alpha, secondary alpha, and beta phases, respectively, $Cr_{\alpha p}$ and Cr_β are chromium concentrations (at.pct) in primary alpha and beta phases, vf_β is volume fraction of beta phase, α_s is average volume of secondary alpha particles (cubic micrometers), and K_Q is in units of MPa $\sqrt{m}$. The accuracy of Eq. (10) in predicting toughness is shown in Fig. 34 where measured toughness is plotted against calculated values.

3.2.2.3 Tensile Tests

Tensile specimens were heat treated according to Table X. Duplicates of conditions 1, 3, 4, and 5 and a single sample of condition 2 were tested.

The influence of prior solution temperature on room temperature tensile properties of Ti-4.5Al-5Mo-1.5Cr given an age treatment of 583°C/4 hrs/AC is shown in Fig. 35. The behavior is similar to that observed for 6-4, Fig. 26, where strength levels increase and ductility decreases with increasing solution temperature.

Regression analysis trials were performed in a manner similar to that described for fracture toughness, Section 3.2.2.2, for the three tensile properties. The relative contribution of each parameter to tensile properties are listed in Tables XII, XIII and XIV. The analysis indicated that seven variables significantly affected each of the three tensile properties; the seven parameters were identical for yield and ultimate strengths, but a different set of seven was found to influence elongation. Regression analysis on each of the properties yields the following:

$$Y.S. = 1055 - 61(vf_{\beta}) + 807(vf_{\alpha s}) + 121(Mo_{\alpha p}) - 61(Cr_{\alpha p}) + 229(Mo_{\alpha s}) - 379(Cr_{\alpha s}) - 23(Mo_{\beta}) \quad (11)$$

$$U.T.S. = 1611 - 385(vf_{\beta}) + 39(vf_{\alpha s}) + 137(Mo_{\alpha p}) - 1089(Cr_{\alpha p}) + 283(Mo_{\alpha s}) - 399(Cr_{\alpha s}) - 41(Mo_{\beta}) \quad (12)$$

$$\varepsilon = 7.4 - 17.8(vf_{\alpha s}) + 53(\alpha_s) + 1.7\ (Mo_{\alpha p}) + 1.1(Al_{\alpha s}) - 1.8(Mo_{\alpha s}) + 1.2(Mo_{\beta}) - 1.6(Cr_{\beta}) \quad (13)$$

Table XII. Contribution of Each Microstructural Parameter to Tensile Yield Strength in STA Ti-4.5Al-5Mo-1.5Cr, as Measured by Regression Analysis

Parameter	Significance(1)	Sign of Coefficient(2)
Volume fraction secondary α	S	+
Vanadium content secondary α	S	+
Chromium content secondary α	S	-
Volume fraction β phase	S	-
Molybdenum content β phase	S	-
Molybdenum content primary α	S	+
Chromium content primary α	S	-
Size secondary α particles	NS	
Chromium content β phase	NS	
Aluminum content β phase	NS	
Aluminum content primary α	NS	
Aluminum content secondary α	NS	

(1) S = significant contribution to yield strength
NS = not significant contribution to yield strength
(2) + = positive contribution to yield strength
- = negative contribution to yield strength

Table XIII. Contribution of Each Microstructural Parameter to Ultimate Tensile Strength in STA Ti-4.5Al-5Mo-1.5Cr, as Measured by Regression Analysis

Parameter	Significance[1]	Sign of Coefficient[2]
Molybdenum content primary α	S	+
Chromium content secondary α	S	-
Molybdenum content secondary α	S	+
Chromium content primary α	S	-
Molybdenum content β phase	S	-
Volume fraction secondary α	S	+
Volume fraction β phase	S	-
Size secondary α particles	NS	
Chromium content β phase	NS	
Aluminum content primary α	NS	
Aluminum content secondary α	NS	
Aluminum content β phase	NS	

(1) S = significant contribution to ultimate tensile strength
NS = not significant contribution to ultimate tensile strength
(2) + = positive contribution to ultimate tensile strength
- = negative contribution to ultimate tensile strength

Table XIV. Contribution of Each Microstructural Parameter to Tensile Elongation in STA Ti-4.5Al-5Mo-1.5Cr, as Measured by Regression Analysis

Parameter	Significance(1)	Sign of Coefficient(2)
Volume fraction secondary α	S	-
Molybdenum content β phase	S	+
Molybdenum content secondary α	S	-
Size secondary α particles	S	+
Molybdenum content primary α	S	+
Aluminum content secondary α	S	+
Chromium content β phase	S	-
Aluminum content primary α	NS	
Aluminum content β phase	NS	
Chromium content secondary α	NS	
Volume fraction β phase	NS	
Chromium content primary α	NS	

(1) S = significant contribution to tensile elongation
NS = not significant contribution to tensile elongation
(2) + = positive contribution to tensile elongation
- = negative contribution to tensile elongation

where vf_β is volume fraction β phase, $vf_{\alpha s}$ is volume fraction secondary α, α_s is average volume of secondary alpha particles (in cubic micrometers), $Mo_{\alpha p}$, $Mo_{\alpha s}$, and Mo_β are molybdenum concentrations (at.pct.) in primary alpha, secondary alpha, and beta phases, respectively, $Cr_{\alpha p}$, $Cr_{\alpha s}$, and Cr_β are chromium concentrations (at.pct.) in primary alpha, secondary alpha, and beta phases, respectively, and $Al_{\alpha s}$ is aluminum concentration (at.pct.) in secondary alpha. Units of stress are MPa; ε is in percent. Measured values are plotted against calculated values in Figs. 36-38 to illustrate the accuracy of each equation in predicting tensile properties.

3.3 Part II. Characterization of Powder Processed Ti-6Al-4V

3.3.1 Material

The powder processed Ti-6Al-4V examined in this study was obtained from the Boeing Company where mechanical properties tests had been performed.[6] The pre-alloyed powder was hot isostatically pressed (HIP) at 900°C for 2 hours and 103 MPa following consolidation and sintering.[6] This HIP'ed material exhibited reduced tensile, fracture toughness, and fatigue properties.[6]

3.3.2 Microstructure

Microstructure of the as-HIP'ed 6-4 is shown in Fig. 39, where numerous voids and large inclusions can be seen. Transmission electron microscopy revealed the presence of voids, bubbles, and particles in the size range of less than 1 μm. A typical view of the microstructure is illustrated in Fig. 40.

The bubbles and voids, which are on the order of 10-100 nm, tend to occur in clusters about 2 or 3 μm across. Voids and bubbles are distinguishable in two ways. First, x-ray energy dispersive spectroscopy (EDS) reveals foreign elements (gas) in bubbles, whereas none is detected in voids. Second, voids tend to exhibit planar (crystallographic) sides while bubbles are spher-

ical, Fig. 40. All the bubbles analyzed contained chlorine; other elements detected in bubbles were calcium and sodium, generally only as trace amounts.

Small particles on the order of 20-50 nm in diameter exhibit a line of no-contrast when imaged in two-beam dynamical contrast, Fig. 41. This behavior indicates the particles are coherent with the alpha phase matrix.[29] The particles were not sufficiently large to generate discrete electron diffraction patterns nor was a significant EDS analysis obtained from the particles. Further identification of the particles was not attempted. Occasional large particles (~100 nm) were detected in the powder processed material that were analyzed by EDS as containing yttrium.

In addition to analyses of submicron defects, compositions of alpha and beta phases were measured to compare powder with wrought 6-4. The as-HIP'ed powder alloy was heat treated at 700, 800, and 900°C to observe partitioning of Al and V between alpha and beta phases. Results are presented in Table XV and Figs. 42 and 43. The data reveal that HIP'ing at 900°C for 2 hours does not develop equilibrium partitioning observed in wrought 6-4 solution treated at 900°C. However, solution treating the powder material for 1 hour brings alpha and beta phases close to equilibrium compositions.

3.4 Part III: Fatigue Crack Initiation in Ti-6Al-4V

3.4.1 Test Results

Results of fatigue tests at R = +0.1 are given in Tables XVI, XVII, XVIII, XIX, XX, and XXI for Ti-6Al-4V in the STOA, RA and βF conditions, respectively. These results are also plotted on the maximum stress-cycles to failure (σ_{max}-N_f) diagrams in Figs. 44, 45, and 46, respectively. It should be noted in the tabulated results that there is a substantial variation in the surface residual stresses resulting from the various surface treatment techniques. Shot peening produced the largest magnitude of surface residual compressive stress while electropolishing resulted in surface residual stresses essentially near zero. Surprisingly, the as-machined (AM) condition, which was produced by a procedure very near the ASTM E-606 standard, exhibited moderate compressive residual surface stresses.

Table XV. Comparison of Al and V Partitioning Between Powder Processed and Wrought Ti-6Al-4V*

Treatment	Wt Pct Al in Alpha		Wt Pct Al in Beta		Wt Pct V in Alpha		Wt Pct V in Beta	
	Powder	Wrought	Powder	Wrought	Powder		Wrought	
As HIP'ed	6.3	7.2	0.9	5.1	2.0	1.9	28.3	6.5
700°C/1 hr/WQ	6.6	6.6	2.6	1.9	2.3	1.4	15.9	17.7
800°C/1 hr/WQ	6.5	7.0	3.6	3.9	2.2	2.0	10.2	9.7
900°C/1 hr/WQ	6.8	7.2	5.3	5.1	1.8	1.9	5.9	6.5

*Powder material hot isostatically pressed at 900°C.

Table XVI Fatigue Results for Ti-6Al-4V, STOA With Various Internal Hydrogen Contents and Surface Treatments

Solution Treated and Over-Aged (STOA)
R = +0.1, $S_{0.2\%}$ = 980 MPa (142 ksi)

H_2, ppm	As-Machined (AM)				Electropolished (EP)				Shot Peened (SP)			
	No.	σ_{max}	σ_r	N_f	No.	σ_{max}	σ_r	N_f	No.	σ_{max}	σ_r	N_f
3	C7-7	552 (80)	-207 (-30)	1.2×10^7	C7-11	620 (90)	+12.4 (+1.8)	7.7×10^5	C7-9	614 (89)	-634 (-92)	1.8×10^6
	C7-8	614 (89)	-276 (-40)	6.8×10^6	C7-12	603 (87.5)	+15.2 (+2.2)	1.7×10^6	C7-10	614 (89)	-600 (-87)	1.6×10^6
100	C7-F1	614 (89)	-130.0 (-18.8)	1.5×10^5	CF-F2	676 (98)	-5.5 (-0.8)	5.5×10^4	C7-F3	614 (89)	-724 (-105)	1.9×10^6
300	C7-G1	676 (98)	-165 (-24)	4.3×10^4	C7-G2	676 (98)	-6.2 (-0.9)	$1.5 \times 10^{7+}$	C7-G3	-552 (89)	$1 \times 10^{7+}$ (-80)	
									Retest	676 (98)	-552 (-80)	1.3×10^5

No. = specimen number
σ_{max} = maximum stress @ R = +0.1
σ_r = surface residual stress; - is compressive, + is tensile
N_f = cycles to failure
+ indicates a runout
Stress values in MPa, those in parenthesis in ksi

Table XVII. Fatigue Results for Ti-6Al-4V, STOA with 3 ppm Internal Hydrogen and Electropolished Surface; R = +0.1 (Ref. 16)

Spec. No.	σ_{max}, MPa (ksi)	Cycles to Failure, N_f
1	700 (101.5)	99,000
8	650 (94.25)	141,000

Table XVIII. Fatigue Results for Ti-6Al-4V, RA with Various Internal Hydrogen Contents and Surface Treatments

Recrystallization Annealed (RA)
R = +0.1, $S_{0.2\%}$ = 876 MPa (127 ksi)

H_2, ppm	As-Machined (AM)				Electropolished (EP)				Shot Peened (SP)			
	No.	σ_{max}	σ_r	N_f	No.	σ_{max}	σ_r	N_f	No.	σ_{max}	σ_r	N_f
3	C1-14	400 (58)	-414 (-60)	4.0×10^6	C1-15	400 (58)	-110 (-16)	3.8×10^6	C1-16	400 (58)	-634 (-92)	3.4×10^6
100			-		C1-F2	400 (58)	-41 (-6)	2.1×10^6	C1-F3	400 (58)	-614 (-89)	2.6×10^6
300			-		C1-G2	496 (72)	+28 (+4)	9.1×10^4	C1-G3	400 (58)	-607 (-88)	4.9×10^6
					C1-G4	400 (58)	~0 (0)	3.8×10^6				

No. = specimen number
σ_{max} = maximum stress @ R = +0.1
σ_r = surface residual stress; - is compressive, + is tensile
N_f = cycles to failure
Stress values in MPa, those in parenthesis in ksi

Table XIX. Fatigue Results for Ti-6Al-4V, RA with 3 ppm Internal Hydrogen and Electropolished Surface; R = +0.1 (Ref. 16)

Spec. No.	σ_{max}, MPa (ksi)	Cycles to Failure, N_f
1	700 (101.5)	27,000
2	650 (94.25)	28,000
3	550 (79.75	59,000
4	500 (65.25)	212,000
6	430 (62.35)	285,000
7	385 (55.83)	5,212,000
8	370 (53.65)	10,094,000*

* Did not fail.

Table XX Fatigue Results for Ti-6Al-4V, βF With Various Internal Hydrogen Contents and Surface Treatments

Beta Forged (βF)
R = +0.1, $S_{0.2\%}$ = 855 MPa (124 ksi)

H_2, ppm	As-Machined (AM)				Electropolished (EP)				Shot Peened (SP)			
	No.	σ_{max}	σ_r	N_f	No.	σ_{max}	σ_r	N_f	No.	σ_{max}	σ_r	N_f
3	C1-14	496 (72)	-490 (-71)	1.4×10^7	C4-15	496 (72)	~0	1.4×10^6	C4-16	496 (72)	-634 (-92)	4.5×10^6
					C4-17	400 (58)	-29 (-4.2)	1.1×10^7+				
100			-		C4-F2	496 (72)	-28 (-4)	1.6×10^7	C4-F3	496 (72)	-703 (-102)	2.6×10^6
300	C4-G1	517 (75)	-	2.2×10^6	C4-G2	496 (72)	-110 (-16)	1×10^7+	CA-G3	496 (72)	-	2.0×10^7

No. = specimen number
σ_{max} = maximum stress @ R = +0.1
σ_r = surface residual stress; - is compressive, + is tensile
N_f = cycles to failure
Stress values in MPa, those in parenthesis in ksi
+ indicates a runout

Table XXI. Fatigue Results for Ti-6Al-4V, βF with 3 ppm Internal Hydrogen and Electropolished Surface; R = +0.1 (Ref. 16)

Spec. No.	σ_{max}, MPa (ksi)	Cycles to Failure, N_f
42	600 (87)	74,000
43	550 (79.75)	140,000
45	525 (76.13)	204,000
47	500 (72.50)	169,000
46	475 (68.88)	10,000,000*

* Did not fail

The curves in Figs. 44-46 are "hand-fit" to the data from this program plus the data from Ref. 16. The general conclusion for all data shown in the figures is that there is no systematic trend with residual stress.

If, however, particular attention is focused on the tabulated results for the shot peened specimens in Tables XVI, XVIII, and XX, there is a trend of increased fatigue life with increased internal hydrogen content for STOA and βF microstructures. For the electropolished condition, the trend for increased fatigue life with increased internal hydrogen content is exhibited in the higher strength STOA microstructure, but not in the RA or βF microstructures.

To compare all results on a more equitable basis, attempts were made to account for the effects of mean stress, residual stress, and ultimate strength on fatigue life. The effect of mean stresses, σ_o, on fatigue resistance is often taken in account by one of several relationships;[26] for example, the Goodman relationship

$$\sigma_a = \sigma_{cr} \left[1 - \frac{\sigma_o}{\sigma_u}\right] \tag{14}$$

where σ = stress amplitude
σ_{cr} = completely reversed stress (R = -1) for a given life
σ_u = ultimate strength of material

or the Gerber relationship

$$\sigma_a = \sigma_{cr} \left[1 - \left(\frac{\sigma_o}{\sigma_u}\right)^2\right] \tag{15}$$

or the Morrow relationship

$$\sigma_a = \sigma_{cr} \left[1 - \frac{\sigma_o}{\sigma_f}\right] \tag{16}$$

where σ_f = true fracture strength of material.

Residual stress, σ_r is often taken in account by algebraic addition (compressive) or subtraction (tensile) from the mean stress.

Through the equation

$$\sigma_a = (\sigma_f + \sigma_o + \sigma_r)(2N_f)^b \qquad (17)$$

where $2N_f$ = reversals to failure (double the number of cycles to failure)
b = fatigue strength exponent

stress amplitude may be related to life for the Morrow mean stress relationship. Similar equations may be developed for stress and life for the Gerber and Goodman relationships. Since all present stress-life tests were performed at $R = 0.1 \equiv \frac{\sigma_{min}}{\sigma_{max}}$ and the mean stress, $\sigma_o = \frac{\sigma_{max} + \sigma_{min}}{2}$, the following expression can be derived from Eq. (17):

$$N_f = \left[\frac{0.45\ \sigma_{max}}{\sigma_f - 0.55\ \sigma_{max} + \sigma_r}\right]^{1/b} \qquad (18)$$

where $b \cong -\frac{1}{6} \log \left[\frac{2\sigma_f}{\sigma_u}\right]$,

similar expressions are also obtained from Eqs. (14) and (15).

Equation (18) and similar expressions for fatigue life from Eqs. (14) and (15) were used to predict the failure lives of several of the specimens tested. However, the predicted lives were not consistently accurate enough to produce meaningful correlations.

3.4.2 Fractography

Fractographic analysis revealed that all fractures, except two, were initiated at specimen surfaces. The two specimens with sub-surface crack ini-

tiation were in the intermediate strength level RA condition, in one case shot peened and containing 3 ppm hydrogen (C1-16) and in the other case electropolished and containing 100 ppm hydrogen (C1-F2), Fig. 47. There was no evidence of microstructural anomalies at the sub-surface initiation sites.

Figure 48 illustrates the change in fracture topography at the surface initiation sites that occurred with increasing hydrogen in STOA condition. There is significantly more cyclic cleavage in the low hydrogen sample, Fig. 48a, than in the higher hydrogen containing sample, Fig. 48b. A similar effect is observed for the RA condition, as shown in Fig. 49, where the 3 ppm hydrogen sample exhibits extensive cyclic cleavage fracture while the 300 ppm hydrogen sample displays a more ductile fracture mode, again at the surface initiation sites. The presence of internal hydrogen appears to promote a more ductile, or higher energy absorbing fracture mode as compared to a nominal (3 ppm) hydrogen content.

4.0 DISCUSSION

4.1 Effect of Sub-Transus Solution Temperature on Properties

4.1.1 Fracture Toughness

4.1.1.1 Ti-6Al-4V

Attempts to correlate microstructural parameters individually revealed no correlation of volume fractions or phase compositions separately with K_Q. Regression analysis, on the other hand, indicated an excellent correlation of the combination of parameters, see Eq. (1) and Fig. 10. The results show that volume fraction primary alpha, aluminum content primary alpha, aluminum content beta, and vanadium content beta all reduce K_Q, whereas vanadium content of alpha increases K_Q.

A fracture toughness crack propagating in α/β processed 6-4 having 80-90% primary α progresses by microvoid coalescence as the microvoids nucleate and grow within individual primary alpha grains. Failure occurs as the microvoids link up, hence an increase in volume fraction of primary alpha will provide a more continuous path for the linking of voids, resulting in lower toughness. Increasing the aluminum content of primary alpha promotes an increase in the intensity of planar slip and concomittant increase in yield strength and decrease in ductility.[30] The expected attendant reduction in plastic zone size would account for the decrease in K_Q due to aluminum concentrated in primary α. Similarly, increases in aluminum and vanadium concentration in β phase provide solid solution strengthening which assists in constraining the plastic zone size to primary alpha grains. It is not clear how small increments in vanadium concentration in primary alpha can increase fracture toughness; the effect may be a result of offsetting the influence of aluminum although there is no evidence for that at this point.

4.1.1.2 Ti-4.5Al-5Mo-1.5Cr

The quantitative analyses have shown an effect similar to that observed for Ti-6Al-4V, in which volume fraction primary alpha, aluminum and molybdenum contents of primary alpha, and chromium content of beta phase reduce toughness while aluminum and molybdenum contents of beta phase and chromium content of primary alpha increase toughness. The same rationale as that used for 6-4 applies here for assessing the manner in which the microstructural parameters influence toughness. The interesting situation for CORONA 5 is that Mo and Cr tend to act in opposite directions; i.e., Cr in β reduces toughness but Mo in β increases toughness, see Eq. (3).

4.1.1.3 Combination of Ti-6Al-4V and Ti-4.5Al-5Mo-1.5CR

The analyses of each of the two alloys resulted in expressions that very accurately predicted toughness, see Fig. 10 and 17. Regression analysis on the combination of the two alloys produced an expression that had similarities to the individual analyses, see Eq. (4). However, there were some discrepancies, e.g., vanadium and aluminum contents of beta phase, and it is possible that the combined analysis is more a statistical result than a physical one. This is a point that only testing of new alloy compositions would resolve.

4.1.2 Fatigue Crack Propagation, Ti-6Al-4V

The microstructural parameters did not correlate individually with da/dN, however regression of the combined parameters revealed an excellent correlation, see Eq. (2) and Fig. 12. Equation (2) shows that aluminum concentration in alpha and beta phases and vanadium content of beta phase increase the alloy's resistance to fatigue crack propagation, whereas volume fraction and vanadium content of primary alpha tend to decrease crack resistance. The fatigue crack propagates through the microstructure by cyclic cleavage of primary α at low stress intensities and by striation formation through primary alpha at higher stress intensities. Because the crack propa-

gates more readily through the primary alpha, an increase in volume fraction will lead to reduced crack propagation resistance, analogous to the situation observed for fracture toughness. It is not obvious how increasing Al in alpha and V in beta leads to increased crack resistance.

4.1.3 Summary of Observations

The quantitative analysis results described in Eqs. (1), (2), and (3) are extremely accurate in predicting toughness and fatigue crack propagation rate as evidenced by Figs. 10, 12 and 17. The equations, of course, are limited to the composition bounds as measured within the two alloys, but nevertheless the behavior described for 6-4 and CORONA 5 in Figs. 9, 11, and 16 has adequately been accounted for in terms of α and β phase compositions and distribution. The important parameters for toughness and da/dn are volume fraction primary alpha, aluminum concentration in primary alpha and vanadium content of beta phase. These parameters, however, act in concert to produce observed property effects and cannot be correlated to properties individually.

4.1.4 Cooling Rate Effects, Ti-6Al-4V

The vanadium and aluminum composition gradients detected in the beta phase of slowly cooled 6-4 are the result of nonequilibrium conditions. In contrast, the rapidly cooled samples did not exhibit beta phase composition gradients. The gradient phenomenon can account for the frequently observed effect in air-cooled and aged 6-4 in which central regions of broad beta phase patches transform to $\alpha + \beta$ while narrow strips and the periphery of the larger patches remain untransformed. In those cases, a high vanadium concentration in the beta phase inhibits transformation, whereas a lower concentration cannot prevent the transformation during the aging treatment. The resulting microstructure is an inhomogeneous mixture of primary alpha, retained beta, and partially transformed beta. Mechanical properties will be influenced, therefore, by the size distribution of beta phase after solution treatment.

4.2 Effect of Sub-Transus Solution Temperature and Aging Temperature on Mechanical Properties of α/β Alloys

4.2.1 Fracture Toughness

4.2.1.1 Ti-6Al-4V

Figure 22 reveals that different combinations of microstructures can result in similar toughness values for 6-4. Examination of the raw data from these samples and Eq. (5) indicates that it is primarily the contribution of volume fraction beta phase and size of secondary alpha particles that account for leveling of toughness in the three conditions. That is, the low toughness of the high solution temperature condition is improved relative to the other two conditions by the larger secondary alpha particles present. On the other hand, the intermediate solution temperature condition has improved toughness after aging due to smaller amounts of beta phase than is present in low solution temperature condition.

Comparison of Eqs. (1) and (5) shows that, after aging, some of the microstructural parameters appear to contribute to toughness in an opposite manner than was observed prior to aging. This is likely because the added microstructural parameters after aging result in more complex interactive effects. At any rate, Eq. (5) demonstrates that toughness is increased by increasing vanadium content of β phase and by reducing volume fraction of beta phase. These two effects are, of course, interdependent and, in conjunction with size of secondary alpha particles, point out the importance of the "transformed beta" regions in toughness of STA 6-4. Larger secondary alpha particles result in a more tortuous path for the crack as it passes through transformed beta regions. Higher toughness values are observed when the crack follows a more tortuous path absorbing more energy per linear crack extension.[31] Increasing aluminum content of primary alpha can reduce toughness in the manner described for the ST condition, Section 4.1.1.1.

4.2.1.2 Ti-4.5Al-5Mo-1.5Cr

Unlike Ti-6Al-4V, CORONA 5 did not undergo a leveling of toughness after aging, see Figs. 16 and 33, but rather exhibited a blanket reduction. The difference in behavior of the two alloys can be attributed to microstructural variations. In the case of CORONA 5 there is 50% or less of primary alpha, so that the crack progresses primarily through beta or transformed beta region whereas the crack propagates essentially through primary alpha in 6-4. After aging, the transformed beta regions of CORONA 5 contain a high volume fraction of relatively small secondary alpha particles. This combination results in a strengthening effect within the transformed beta and a concomittant reduction of plastic zone size, leading to reduced toughness.

Examination of Eq. (10) and the raw data reveals no one or two significant parameters that produces the large differences in toughness presented in Fig. 33. It appears that the small differences in all of the parameters contribute to the total large variation in toughness after aging.

The manner in which some of the microstructural parameters influence toughness in STA CORONA 5 is opposite to that observed for STA 6-4, cf Eqs (5) and (10). For instance, volume fraction beta and size of secondary alpha particles contribute in opposing ways in the two alloys. This can be understood when considering the relative amounts of each phase in the alloys; that is, there is up to an order of magnitude more beta phase in CORONA 5; while the size of the secondary alpha particles varies from 1 to 2 orders of magnitude smaller in CORONA 5. Volume fraction beta influences toughness in a positive manner in CORONA 5 because the crack propagates through transformed beta regions and, consequently, increasing the amount of beta phase (relative to amount of secondary alpha) reduces the strengthening effect of secondary alpha, allowing a larger plastic zone to develop which results in higher toughness. The secondary alpha particles in CORONA 5 remain relatively small and contribute only to an increase in strength and reduced plastic zone size. In the case of 6-4, the secondary alpha particles have grown sufficiently large to reduce strengthening effects and to provide crack branching during propagation.

Comparison of Eqs. (5) and (10) also shows that beta stabilizer content of beta phase increases toughness and aluminum concentration in primary alpha reduces toughness in both alloys. These effects have been described previously, Sections 4.1.1.1 and 4.2.1.1

4.2.2 Fatigue Crack Propagation, Ti-6Al-4V

Two observations are apparent when Eq. (6) and raw da/dN data for STA 6-4 are examined: (1) aging has increased the fatigue crack growth rate, cf. Figs. 11 and 24, and (2) the influence of prior solution treatment has been minimized by aging, Fig. 24. The crack growth rate has increased after aging due to changes in the transformed beta regions of the microstructure. Small secondary alpha particles (specimens with larger secondary alpha particles were not tested) serve to strengthen these regions, thereby reducing plastic zone size and increasing crack growth rates.

As was observed for ST 6-4, crack growth rate is controlled by volume fraction primary alpha (implied in Eq. (6) by the volume fraction beta factor) and by aluminum and vanadium concentrations of primary alpha. Average size of secondary alpha particles increases da/dN because their limited small size in the test specimens acts only to strengthen the transformed beta regions. Aluminum and vanadium concentrations of secondary alpha provide strengthening effects to increase growth rate. Crack growth rate has levelled after aging due to the effects of volume fraction beta and size of secondary alpha particles. The lower solution temperature specimen has a higher volume fraction beta while the higher solution temperature sample has a smaller secondary alpha particle size; each of these leads to reduced da/dN.

4.2.3 Tensile Tests

4.2.3.1 Ti-6Al-4V

Regression analyses, Eqs (7)-(9), show that yield and ultimate strengths are increased by increasing volume fraction secondary alpha and vanadium contents of beta and secondary alpha, whereas strengths are reduced

by increasing size of secondary alpha particles. In addition, aluminum content of secondary alpha or primary alpha increases yield or tensile strength, respectively, while volume fraction beta or vanadium content of primary alpha reduces yield or tensile strengths, respectively.

Vanadium in beta phase provides solid solution strengthening and secondary alpha particles create a precipitation hardening effect. Increasing the size of secondary alpha particles can result in overaging and reduced strength. Aluminum in alpha phase also produces solid solution strengthening.

The influence of parameters on tensile elongation, Eq. (9), is more difficult to interpret. Although it follows from precipitation hardening theories that a reduction in volume fraction secondary alpha contributes to increased elongation, the positive effect of aluminum in alpha is less obvious.

4.2.3.2 Ti-4.5Al-5Mo-1.5Cr

Regression analyses Eqs. (11)-(13) show a microstructural effect on tensile properties similar to that observed for 6-4. Yield and ultimate strengths are increased by increasing volume fraction of secondary alpha and molybdenum contents of primary and secondary alpha, whereas strengths are reduced by volume fraction beta, chromium content of primary and secondary alpha and molybdenum content of beta phase.

Solid solution hardening and precipitation hardening are the primary reasons for increased strengths, as was described for 6-4. Chromium and molybdenum appear to act in opposition in alpha and beta phases. Chromium seems to strengthen beta phase and reduce effects of aluminum in alpha phase whereas molybdenum has the opposite effects in alpha and beta phases. Similar behavior was observed in fracture toughness analyses.

A different set of microstructural parameters influences tensile elongation than influenced tensile strengths. Eq. (13) shows that increased volume fraction of secondary alpha reduces elongation as do chromium content

of beta phase and molybdenum content of secondary alpha. On the other hand, molybdenum contents of beta phase and primary alpha, size of secondary alpha particles, and aluminum content of secondary alpha all act to increase elongation. The general trend seems to be that chromium in solution tends to reduce elongation while aluminum and molybdenum in solution tend to increase elongation.

4.3 Characterization of Powder Processed Ti-6Al-4V

The presence of clustered bubbles and voids is apparently the result of (1) trapping of impurities that are present on powder particles surfaces and (2) incomplete sintering. Because fractography was beyond the scope of this program, no assessment was made of the influence of these defects on the fracture process. However, voids and bubbles dispersed throughout the microstructure can lead to degradation of properties, such as has been observed in nickel-base and iron-base alloys.[32-33] The unidentified coherent precipitates were widely dispersed in a low volume fraction through the alloy and likely do not present a serious problem as far as properties are concerned.

The "as-HIP'ed" powder material exhibited properties inferior to those for the alloy in the wrought condition[6] and Table XV reveals deviations in equilibrium compositions of both alpha and beta phases, especially the latter. Equations (1) and (2) were developed for α/β processed 6-4 and it has not been demonstrated that they hold for β processing such as the powder material examined here. The equations, however, can give some insight into the influence of microstructure in the powder processed 6-4. Inspection of Eq. (1) shows that volume fraction of alpha phase is a major contributor to reduction in toughness, and the "as HIP'ed" powder material contains 92 volume percent primary alpha compared to 46 percent for wrought 6-4 solution treated at 900°C. Such a significant variation could account for a portion of the reduced toughness of the powder processed 6-4. Equation (2) reveals no one parameter that most significantly affects da/dN, but inspection of Table XV indicates that volume fraction, aluminum content, and vanadium content of

alpha phase together with aluminum content of beta phase all vary from the corresponding values in the wrought material so as to contribute to reduced crack propagation resistance. So that, although the coefficients in Eqs. (1) and (2) may not be valid for β-processed 6-4, the toughness and da/dN equations can account qualitatively for the observed effects.

4.4 Fatigue Crack Initiation in Ti-6Al-4V

The lack of significant surface residual stress effects and internal hydrogen effects on fatigue life and subsurface initiation in this study is an apparent paradox when compared to other alloy systems. To understand this apparent paradox, one must consider the cyclic stability of the three microstructures studied. In a study on the influence of shot peening on fatigue behavior of titanium alloys, Wagner and Luetjering[34] demonstrated that, due to the "fatigue process" occurring during shot peening, the yield strength will increase with peening pressure and exposure time if the alloy cyclically hardens. However, there will be a decrease in yield strength if the alloy cyclically softens. This partial exhaustion of the cyclic softening response during shot peening will cause the onset of plastic deformation to occur at lower stress levels in the S-N test, thereby relaxing the surface residual stress. Further, the greater the degree of cyclic softening, the greater the relaxation rate of surface residual stresses.

Previous work[16] has shown that all three microstructural conditions cyclic soften. Pre- and post-test surface residual stress measurements for specimens tested in this program are given in Table XXII. There does not appear to be a significant amount of residual stress relaxation in these specimens on a macroscopic basis. There is, however, a strong potential for cyclic softening and residual stress relaxation at the microscopic level of a crack initiation site where stress intensification is present as a result of the local deformation. This situation is analogous to the response of a geometrically notched member subjected to nominally elastic strains wherein cyclic local stress relaxation will occur. Local residual stress relaxation

could then account for the lack of correlation of surface condition with fatigue life or crack initiation sites.

Table XXII. Surface Residual Stress Before and After Fatigue

Spec. No.	Surface Residual Stress in MPa (ksi) Before	After
C1F2	-41(-6)	-40.3(-5.86)
C4F2	-28(-4)	-45.5(-6.60)
C7F2	-5.5(-0.8)	-56.2(-8.2)
C1-16	-634(-92)	-598(-86.7)
C4-16	-634(-92)	-670(-97.2)
C7-7	-207(-30)	-270(-39.1)
C7-G3	-522(-80)	-385(-55.8)

In contrast to the effect of internal hydrogen on crack propagation,[17] hydrogen appears to have no deleterious effect on fatigue life nor does it promote internal initiation. Lankford, et al. have noticed a similar lack of hydrogen effect in smooth bar, LCF testing of beta-annealed Ti-6Al-4V.[35] In their study, they found a dwell-debit in microstructures which contained little beta phase or discontinuous beta phase, but none in the beta annealed, Ti-6Al-4V which contained continuous beta phase. The lack of a dwell-debit was attributed to a combination of hydrogen solubility in the beta phase and an absence of large uninterrupted slip length in the Ti-64. The microstructural conditions of this study, which contain approximately 10 vol. % retained beta phase, also satisfy the latter condition.

Fractographic examination revealed a decrease of cyclic cleavage with increasing hydrogen in the STOA and RA conditions, Figs. 48 and 49. There appears to be some local enhancement of ductility at the initiation site due to increased hydrogen levels. Such behavior is in agreement with observations by Rhodes and Paton[27] in previous ONR work and by Chesnutt et al.[16] for room

temperature tensile behavior of RA, Ti-6Al-4V which showed an increase in elongation from 12.4 to 20.7 pct with hydrogen level increasing from 3 to 300 ppm. Similar "softening" behavior as a result of increased hydrogen concentrations has been observed in pure iron by Kimura et al.[36]

The occurrence of only two instances of subsurface initiation in spite of considerable efforts to promote such behavior, confirms the generally accepted conclusion that it is difficult to obtain subsurface initiation in Ti-6Al-4V in the absence of inclusions or significant microstructural inhomogenieties. The causes of sub-surface crack initiation in the two RA specimens are not apparent. There were no microstructure anomalies at initiation sites and calculations show that in the case of the shot-peened specimen, the initiation site does not correspond to a depth where subsurface tensile stresses would be maximum.

Finally, it should be noted that the present experiments were conducted on a material with a low oxygen content (0.122 wt. pct.) in order to determine if other parameters significantly contribute to internal fatigue crack initiation. The results indicate that subsurface crack initiation can be avoided by lowering the oxygen level in Ti-6Al-4V, even in the presence of internal hydrogen and compressive surface residual stresses.

5.0 CONCLUSIONS

5.1 Part I.A. Effect of Sub-Transus Solution Temperature on Mechanical Properties of α/β Ti Alloys

1. Room temperature fracture toughness in Ti-6Al-4V and CORONA 5 decreases with increasing prior solution temperature.

2. Results of quantitative analysis of volume fraction of primary alpha and alloy partitioning in alpha and beta phases correlate with toughness behavior in Ti-6Al-4V and CORONA 5.

3. Increasing volume fraction of primary alpha, aluminum content of primary alpha, aluminum content of beta phase, and vanadium content of beta phase reduces toughness of Ti-6Al-4V.

4. Increasing volume fraction of primary alpha, aluminum and molybdenum contents of primary alpha, and chromium content of beta phase reduces toughness of CORONA 5.

5. Room temperature fatigue crack growth rate in Ti-6Al-4V decreases with increasing prior solution temperature.

6. Increasing aluminum concentration in alpha and beta phases and vanadium content of beta phase increase fatigue crack propagation resistance in Ti-6Al-4V, whereas volume fraction and vanadium content of primary alpha tend to decrease crack propagation resistance.

7. Slow cooling of Ti-6Al-4V results in vanadium and aluminum concentration gradients in the beta phase. The gradients account for the frequently observed effect in air-cooled and aged Ti-6Al-4V in which central regions of beta phase patches

transform to $\alpha + \beta$ while narrow strips and periphery of larger patches remain untransformed.

5.2 Part I.B. Effect of Sub-Transus Solution Temperature and Aging Temperature on Mechanical Properties of α/β Ti Alloys

1. Aging can eliminate the influence of solution temperature on toughness of Ti-6Al-4V.

2. Increasing the size of secondary alpha particles and vanadium content of beta phase increases toughness while increasing volume fraction of primary alpha and volume fraction of beta phase decrease toughness in Ti-6Al-4V.

3. The influence of prior solution temperature on fatigue crack propagation rate is minimized by subsequent aging of 6-4.

4. Unlike Ti-6Al-4V, conventional aging does not eliminate the influence of solution temperature on toughness of CORONA 5.

5. Quantitative analyses show that toughness and tensile behavior can be explained in terms of volume fractions and chemical compositions of alpha and beta phases in Ti-6Al-4V and CORONA 5.

5.3 Part II. Characterization of Powder Processed Ti-6Al-4V

1. Powder processed Ti-6Al-4V contains voids, bubbles, and particles on the order of 20-50 nm in diameter.

2. The alpha and beta phases do not reach chemical equilibrium during hot isostatic pressing at 900°C.

3. Solution treatment of as-hot-isostatically pressed Ti-6Al-4V results in equilibrium partitioning of aluminum and vanadium between alpha and beta phases.

5.4 Part III. Fatigue Crack Initiation in Ti-6Al-4V

1. Surface residual stresses do not significantly affect fatigue life of Ti-6Al-4V because such residual stresses are relaxed due to cyclic softening.

2. Increasing the hydrogen content of Ti-6Al-4V up to 300 ppm does not reduce fatigue life or promote internal fatigue crack initiation.

3. Ductility at the initiating crack tip is increased with increasing internal hydrogen in fatigue tested Ti-6Al-4V.

6.0 APPENDIX

QUANTITATIVE ANALYSIS BY MEANS OF X-RAY ENERGY DISPERSIVE SPECTROSCOPY IN TRANSMISSION ELECTRON MICROSCOPY

Each manufacturer of multichannel analyzers for x-ray spectra supplies a computer program to calculate weight fractions of the elements in an alloy. In order for the calcualtion to be accurate, however, the program requires the input of numerous parameters, some of which are properties of the microscope system and some of which are properties of the sample being studied. Determination of the values of many of these parameters is a trivial matter for the microscopist, but there are others that require time and effort to measure, or perhaps are even unmeasurable.

For instance, fluorescence and absorption of x-rays can influence intensities of elemental peaks in an x-ray energy spectrum.[37] In the case of transmission electron microscope thin foil specimens, the measurable parameters that influence fluorescence and absorption are take-off (tilt) angle, accelerating voltage, foil thickness, and density of the phase being examined. Values of the first two parameters are easily determined, but accurate measurements of the latter two can be elusive. As far as foil thickness is concerned, the microscopist must either estimate it or measure it for each spectrum acquired. Unfortunately, the former can introduce significant error, while the latter requires a great deal of time and effort. As for density of the phase being analyzed, it can only be estimated since density is a function of composition, which in this case is unknown.

If the research requires analyses of a large number of similar spectra, as was the case for the work described in this report, then, in the interest of time and accuracy, a quantitative analytical technique that requires less input for each spectrum is desirable. Such a technique was developed for Ti-6Al-4V and Ti-4.5Al-5Mo-1.5Cr and is described in the remainder of this Appendix.

When a foil is sufficiently thin, the contributions of fluorescence and absorption to the spectrum are insignificant and can be ignored for quantitative analysis.[37] Unfortunately, for these phenomena to be disregarded in the analysis, the microscopist must be certain that the spectrum is acquired from a region of the foil that is less than some critical thickness. Again, this requires an estimate or measurement of foil thickness. Of course, spectra could be taken from the thinnest edge of the specimen where the probability of meeting the thin foil criterion is almost certainly 1.0, but the x-ray production rate will be sufficiently low in these extremely thin areas that acquisition times become inordinately long and other factors affecting peak intensities, such as surface contamination, creep into the picture.

The foregoing restrictions and requirements for quantitative analysis of thin foils led to the formulation of a technique that takes the system and sample variables into account and normalizes them. This results in a simple, but accurate, approach to quantifying the data in energy spectra from two-phase Ti alloys. The technique uses the concept of ignoring fluorescence and absorption, but does so not by examining foils only in very thin regions but rather by establishing correction factors for the alloying elements under controlled conditions that can be reproduced in all specimens examined. In this way, all variables that can affect peak intensities are identical in both unknown and standard samples, hence elemental correction factors will be valid for all spectra. The technique, then, could be considered a modification of the Cliff-Lorimer[38] approach.

The expression used to calculate elemental concentrations was

$$\text{wt pct } A_i = \frac{(C_{A_i})(A_{i_{K\alpha}})}{(C_{A_i})(A_{i_{K\alpha}}) + (C_{A_j})(A_{j_{K\alpha}}) + (\text{Ti})} \qquad \text{(A1)}$$

where $A_{i,j,k...}$ = alloying additions Al, V, Mo, Cr, or Fe
C_{A_i} = correction factor of alloying addition A_i
$A_{i_{K\alpha}}$ = integrated Kα peak intensity above background for element A_i (for Mo, Lα peak intensity)
Ti = integrated Kα peak intensity above background for Ti

Implicit in the correction factors, C_{A_i}, are those parameters that influence peak intensity, such as foil thickness, tilt (take-off) angle, etc. In order for the correction factors to be valid, the spectra to which they are applied must be acquired under precisely the same conditions as those prevailing when the correction factors were established.

Binary Ti alloy standards that could be heat treated to produce either α or β single phase microstructures (and, therefore, uniform distribution of the alloying additive) were used to establish the various correction factors. Ti-6Al, Ti-20V, Ti-6Cr, Ti-28Mo, and Ti-13Fe were examined to calculate correction factors. All spectra were acquired under the following conditions:

120 Kv accelerating voltage
15-20 μA beam current
21° tilt angle
30-40% dead time
20 nm probe size

A constant foil thickness was maintained indirectly by acquiring spectra only from those regions of the foil where the time to acquire a fixed size $Ti_{K\alpha}$ peak was approximately 100 seconds. This criterion was deduced to result in a constant foil thickness because x-ray production rate is a function of foil thickness and because the concentration of Ti varied by only a few percent within the α or β phase.

The problem of overlapping peaks is common in quantitative microanalysis and it arose here in the case of Ti-6Al-4V in which the Ti K_β peak overlaps the V K_α peak. Two approaches were considered for the application of Eq. (A1) to calculate vanadium concentrations: (1) use the non-overlapped V K_β peak intensity or (2) mathematically separate the Ti K_β and V K_α peak intensities. The former was found to be impractical because the alpha phase contained such small concentrations of vanadium that the V K_β peak was frequently undetectable above background. The second approach was therefore pursued and was developed in the following manner.

The Ti peak intensity (above background) ratio of K_α to K_β was measured in those binary standards not containing vanadium. A statistically significant number of spectra was measured and the mean value of K_α:K_β was established. This value was then used to calculate Ti K_β peak intensity in Ti-V standard spectra based on the corresponding Ti K_α peak intensity. The calcualted Ti K_β intensity was then subtracted from the total overlapped Ti K_β and V K_α peak intensity, resulting in a calculated V K_α peak intensity. The correction factor for vanadium was based on the calculated K_α peak intensity. This technique was used to determine vanadium concentrations in both α and β phases of Ti-6Al-4V.

The application of Eq. (A1) using correction factors developed from binary standards has proven to be a simple, straightforward, and reliable technique for quantitative analysis. The microscopist need only set up the sample and microscope to conform to the predetermined conditions and simply measure peak intensities above background for each element in the spectrum. The peak intensities are the only input to the computer program that calculates concentrations via Eq. (A1). Reproducibility of the results attests to the accuracy of the technique, especially as manifested by the pseudo-binary phase diagrams displayed in Figs. 2, 3, 13-15.

7.0 REFERENCES

1. A. M. Adair, F. J. Gurney and A. T. Male, ibid, pp. 1755-67.

2. N. L. Richards and J. T. Barnby, Mat. Sci. and Engr. Vol. 26, 1976, pp. 221-29.

3. M. G. Ulitchny, H. J. Rack and D. B. Dawson, Toughness and Fracture Behavior of Titanium, ASTM-STP 651, ASTM, Philadelphia, 1978, pp. 17-42.

4. C. A. Stubbington and A. W. Bowen, J. Mat. Sci., vol. 9, 1974, pp. 941-47.

5. J. C. Williams, et al., Toughness and Fracture Behavior of Titanium, ASTM-STP 651, ASTM, Philadelphia, 1975, pp. 64-114.

6. J. E. Magnuson, J. W. Tripp, and R. Boyer, "Characterization of Pressed Sintered and HIPped Ti-6Al-4V," paper presented at 109th AIME Annual Meeting, Las Vegas, Nev., Feb. 1980.

7. R. H. Witt and W. T. Highberger, "Hot Isostatic Pressing of Near Net Titanium Structural Parts," ibid.

8. C. S. Barker and W. P. Schimmel, "Application of HIP Ti-6Al-4V Powder to the Radial Compressor Rotor of the F-107 Cruise Missile Engine," ibid.

9. R. F. Geisendorfer, "Powder Metallurgy of Ti-6Al-4V Powder," ibid.

10. R. W. Landgraf, "Materials Selection for Fatigue Performance," Proc. Fatigue Fundamentals and Applied Aspects Seminar, Saabgarden, Rimforsa, Sweden, Aug. 1977.

11. H. O. Fuchs, Metal Fatigue, Chapter 9, "Techniques of Surface Stressing to Avoid Fatigue," edited by G. Sines and J. L. Weisman, McGraw Hill, 1959, pp. 197-231 (reprinted 1979).

12. Jo Dean Morrow, A. S. Ross, and G. M. Sinclair, SAE Trans. V68, 196C, pp. 40-48.

13. R. W. Landgraf, and R. C. Francis, "Material Processing Effects on Fatigue Performance of Leaf Springs," paper presented at SAE Exposition and Congress, Detroit, Mich., Feb. 1979.

14. B. A. Kolacheu, and S. A. Vigdorchick, Titanium "80" Science and Technology, Kyoto, Japan, Proc. 4th Int. Conf. on Ti, H. Kimura and O. Izumi, eds., Met. Soc. AIME, 1980, pp. 1671-1683.

15. W. W. Gerberich, N. R. Moody, C. L. Jansen, C. Hagman, and K. Jatavallabhula, Hydrogen Effects in Metals, I. M. Bernstein and A. W. Thompson, eds., TMS/AIME, New York, 1981, pp. 731-44.

16. J. C. Chesnutt, A. W. Thompson, and J. C. Williams, "Influence of Metallurgical Factors on the Fatigue Crack Growth Rate in Alpha-Beta Titanium Alloys," AFML-TR-78-68, May 1978.

17. W. J. Pardee, and N. E. Paton, Met. Trans. A., vol. 11A, 1980, pp. 1391-1400.

18. R. A. Spurling, Met. Trans., Vol. 6A, 1975, pp. 871-93.

19. R. A. Spurling, C. G. Rhodes, and J. C. Williams, Met. Trans. Vol. 5A, 1975, pp. 2597-600.

20. C. G. Rhodes, "Quantitative X-ray Microanalysis of Ti Alloys," Proc. 38th Annual EMSA Conf. Reno, Nev. 1980.

21. J. E. Hilliard and J. W. Cahn, Trans. Met. Soc. AIME, Vol. 221, 1961, pp. 344-52.

22. G. H. Gessinger, and C. W. Corte, Titanium '80 Science and Technology, Proc. 4th Int'l Conf. on Ti, Kyoto, Japan, H. Kimwra and O. Izumi, eds., TMS/AIME, New York, 1980, pp. 1787-1985.

23. Y. Mahajau, S. Fujishiro, L. R. Bidwell, and F. H. Froes, ibid, pp. 1807-1814.

24. Section 18.3 "Surface Integrity," Machining Data Handbook, 3rd Edition, V2, Machinability Data Center, Cincinnati, OH, 1980, pp. 18-116, 127.

25. C. J. Beevers, Science, Technology and Application of Titanium, Int. Conf. on Ti, R. I. Jaffee and N. E. Promisel, eds., Pergamon Press, 1970, pp. 535-543.

26. M. R. Mitchell, Fatigue and Microstructure, ASM, 1979, pp. 385-437.

27. C. G. Rhodes and N. E. Paton, "Mechanical Behavior of Titanium Alloys," Final Report, SC5056.4FR, April 1979.

28. M. Ezekiel and K. A. Fox, Methods of Correlation and Regression Analysis, J. Wiley & Sons, Inc., New York, 1959, p. 190.

29. P. B. Hirsh, et al., Electron Microscopy of Thin Crystals, Butterworths, London, 1965, p. 190.

30. N. E. Paton, J. C. Williams, and G. P. Rauscher, Ti Sci. and Tech., R. I. Jaffee and H. M. Burte, eds., Plenum Press, New York, 1973, pp. 1049-69.

31. J. C. Chesnutt and J. C. Williams, Scanning Electron Microscopy 1974 (Part IV), O. Johari, ed., SEM Inc., O'Hare, IL: p. 895-902.

32. R. V. Miner and R. L. Dieshfield, Met. Trans. A, Vol. 12A, 1981, pp. 261-67.

33. D. Kramer, K. R. Garr, C. G. Rhodes, and A. G. Pard, "He Embrittlement of Fuel Cladding Alloys for Potential Service in Fast Breeder Reactors" Symposium on Radiation Damage in Reactor Materials, Vienna, Austria, 1969.

34. L. Wagner and G. Luetjering, "Influence of Shot Peening on the Fatigue Behavior of Titanium Alloys," First Int'l Conf. on Shot Peening," Paris, Sept. 1981, A. Niku-Lari, ed., Pergamon Press, Oxford, pp. 453-460.

35. J. Lankford, D. L. Davidson, G. R. Leverant, and J. E. Hack, "Study of Fatigue Mechanisms in Aerospace Structural Materials," AFOSR Final Report, Contract F49620-78-2-0022, Southwest Research Institute, Feb. 1981.

36. H. Kimura, H. Matzui, A. Kimura, T. Kimura, and K. Oguri, Hydrogen Effects in Metals, I. M. Bernstein and A. W. Thompson, eds., TMS/AIME, New York, 1981, pp. 191-208.

37. Introduction to Analytical Electron Microscopy, J. J. Hren, J. I. Goldstein, and D. C. Joy, eds., Plenum Press, New York, 1979.

38. G. Cliff and G. W. Lorimer, J. Microsc., Vol. 103, 1975, p. 203.

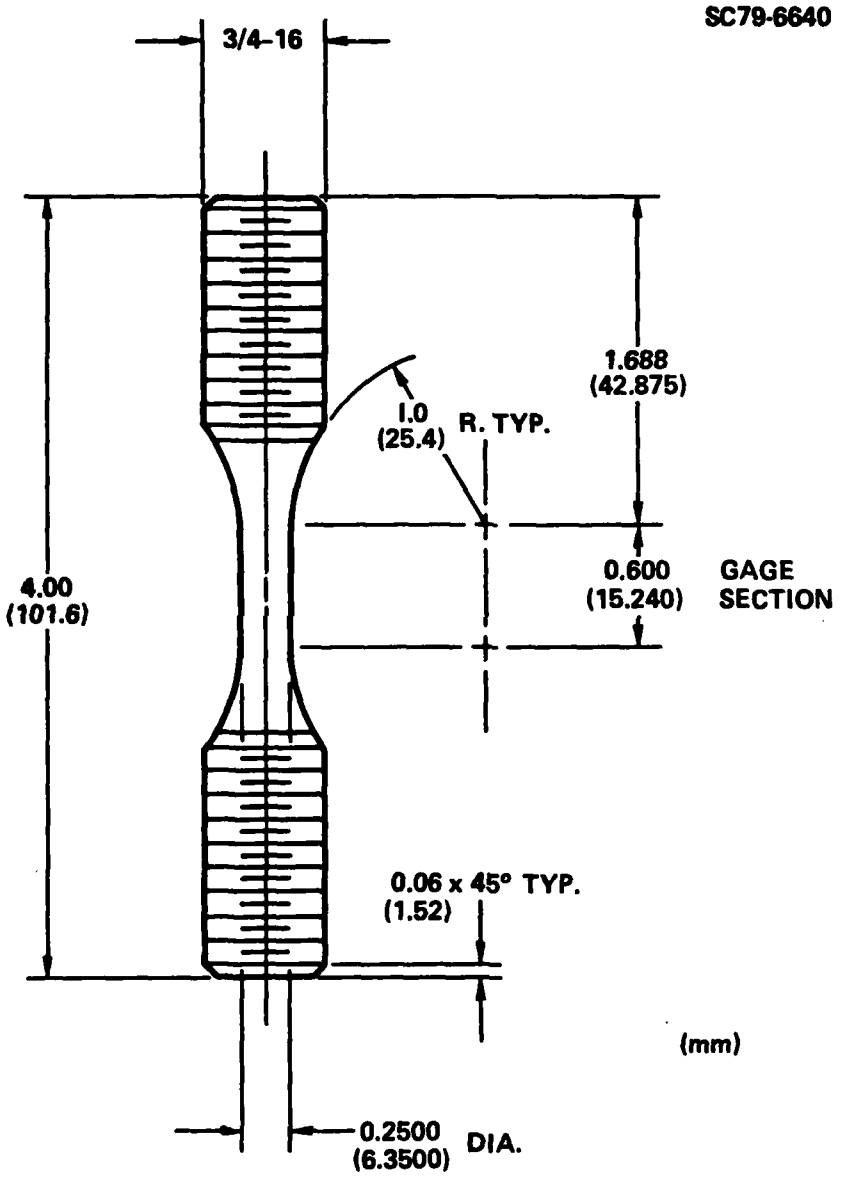

Fig. 1 Fatigue specimen configuration used in Part III.

SC81-11903

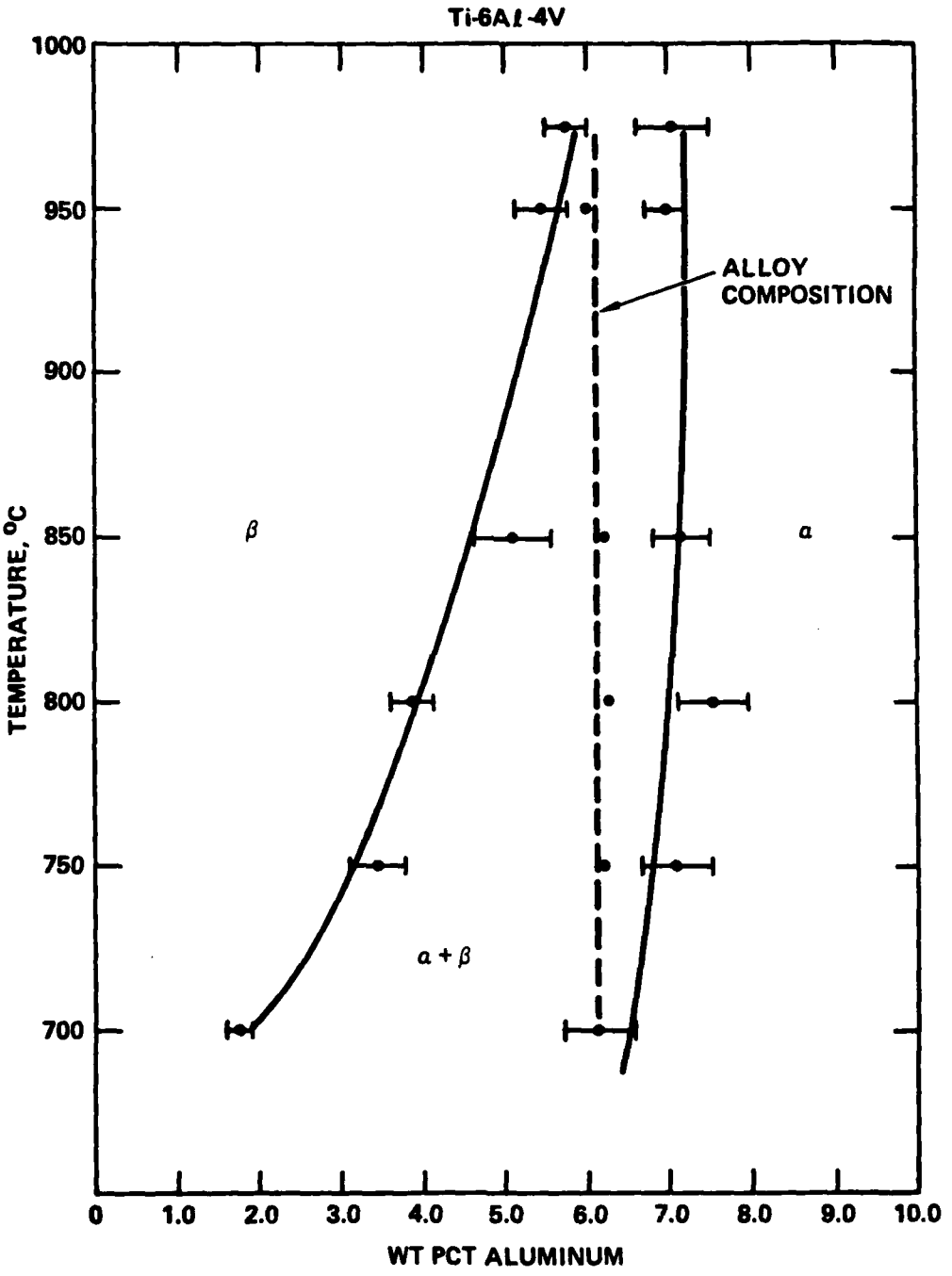

Fig. 2 Al-Ti4V phase diagram constructed from microanalysis data from Ti-6Al-4V.

SC81-11883

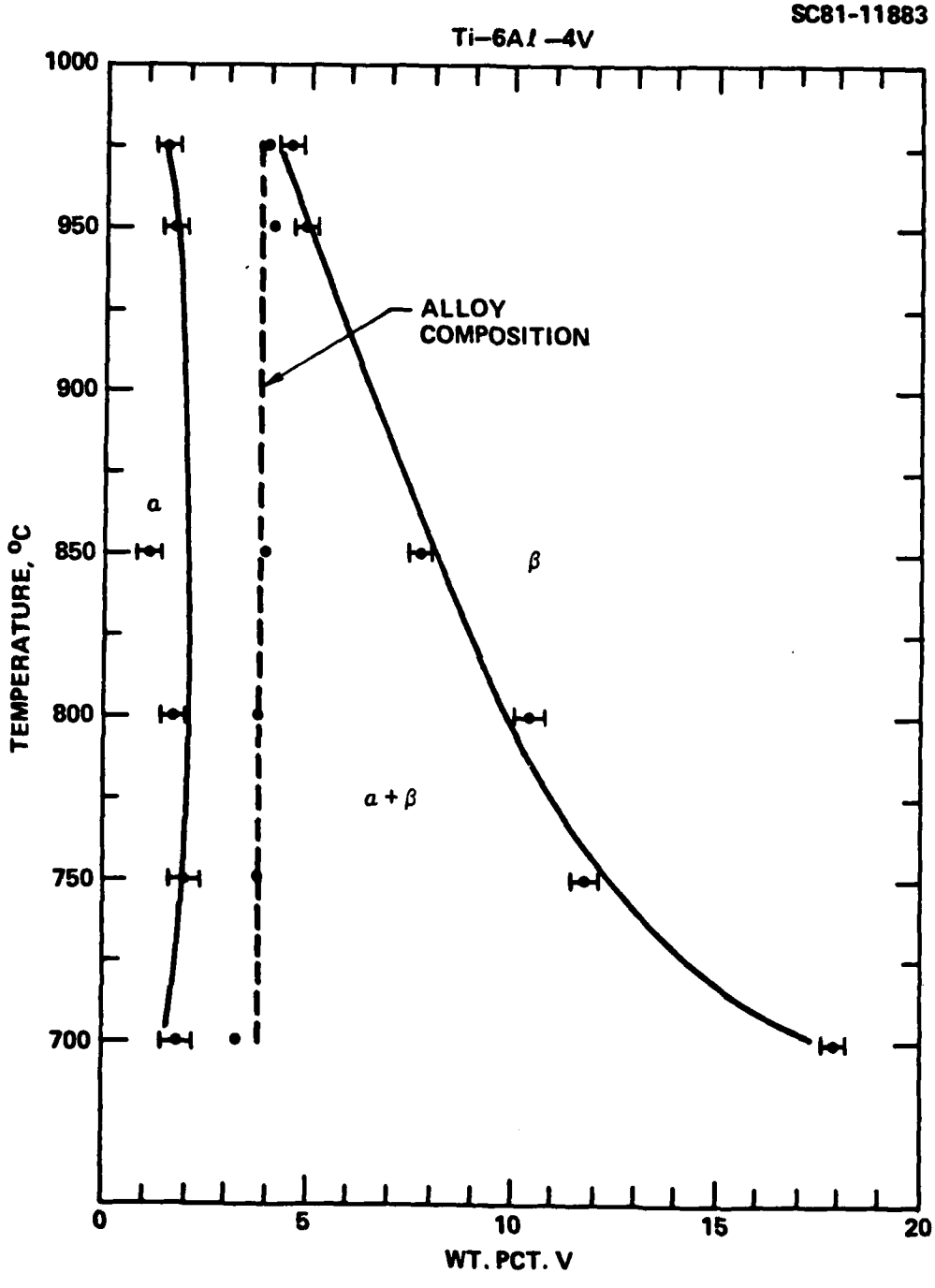

Fig. 3 V-Ti6Al phase diagram constructed from microanalysis data from Ti-6Al-4V.

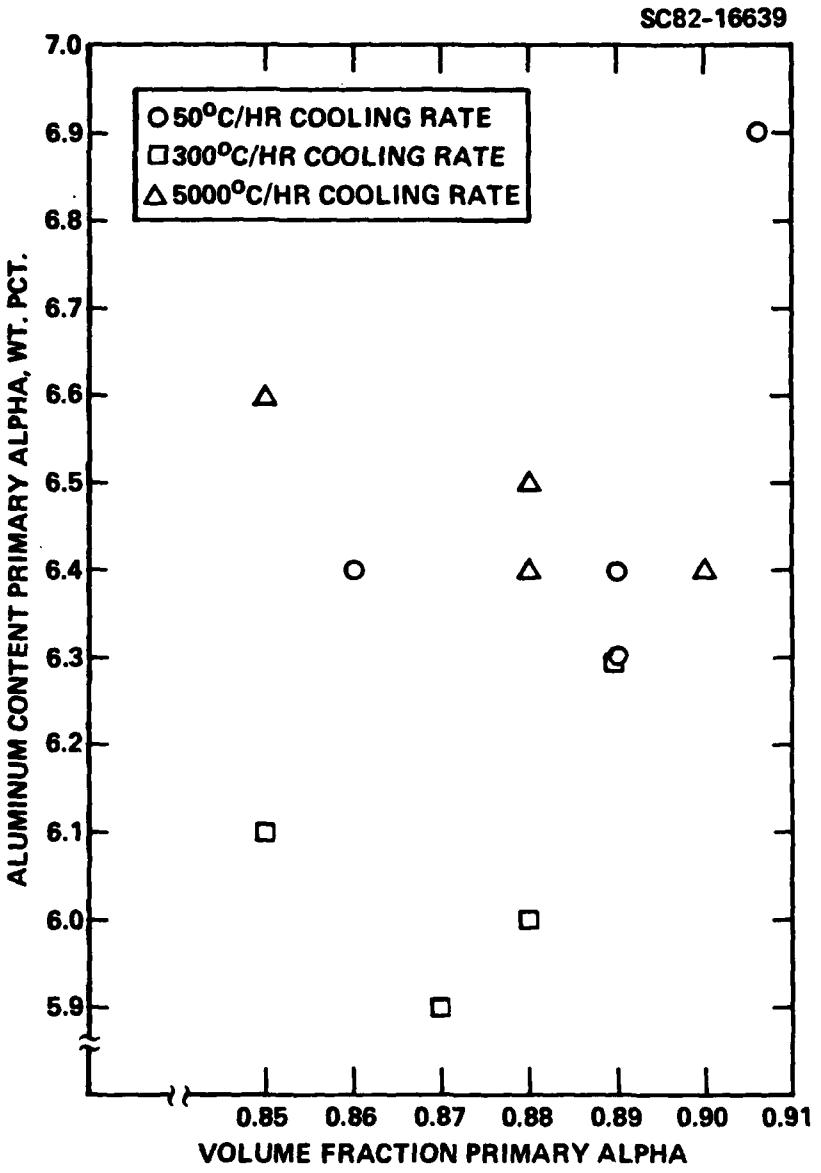

Fig. 4 Al content vs volume fraction of primary alpha in solution treated Ti-6Al-4V cooled at three cooling rates.

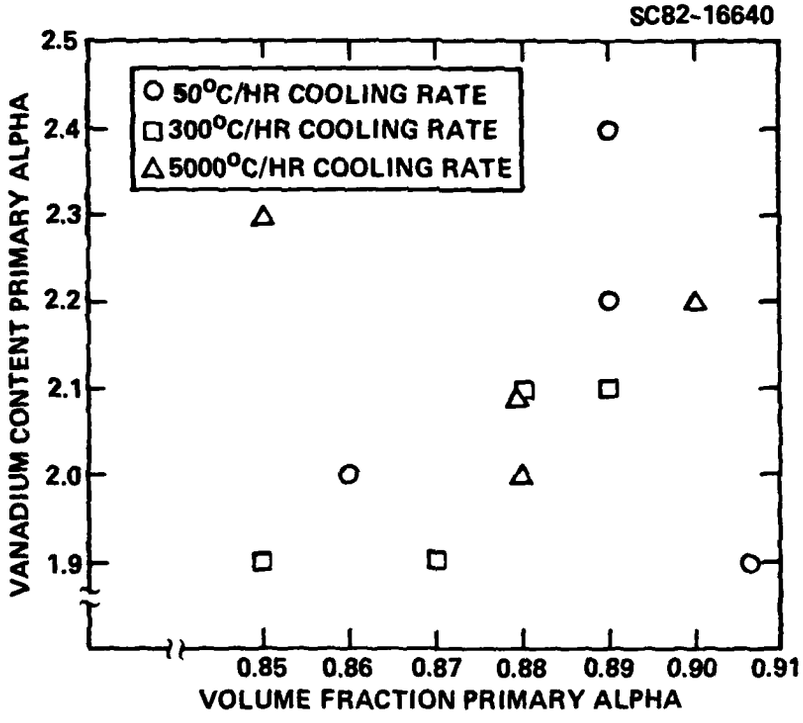

Fig. 5 V content vs volume fraction of primary alpha in solution treated Ti-6Al-4V cooled at three cooling rates.

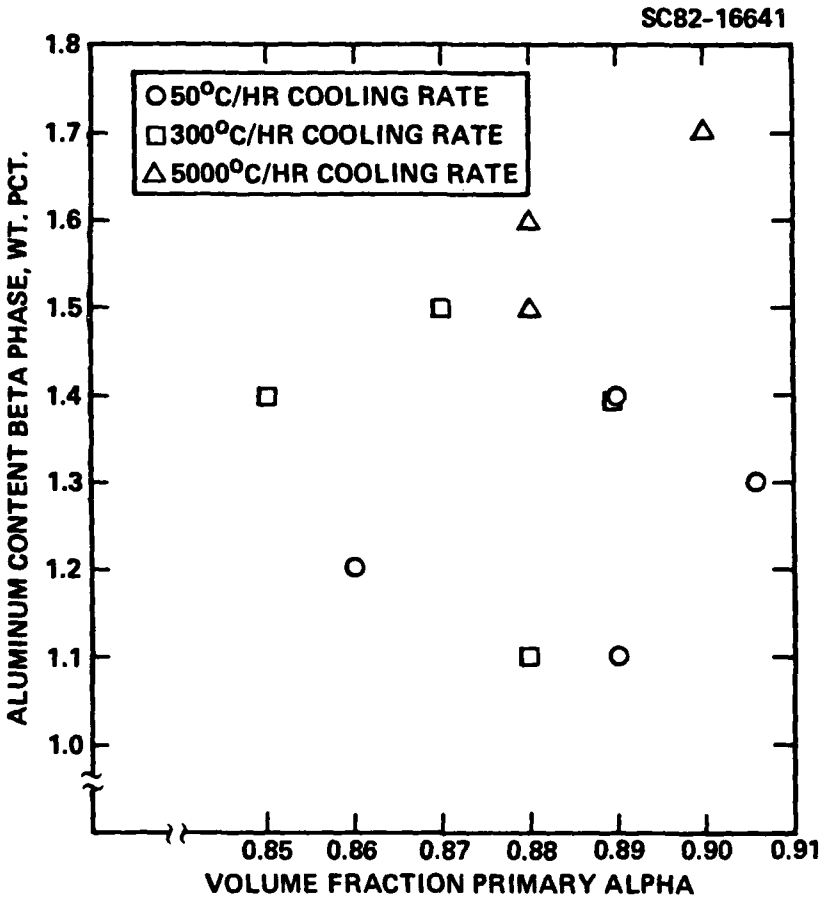

Fig. 6 Al content of beta phase vs volume fraction of primary alpha in solution treated Ti-6Al-4V cooled at three cooling rates.

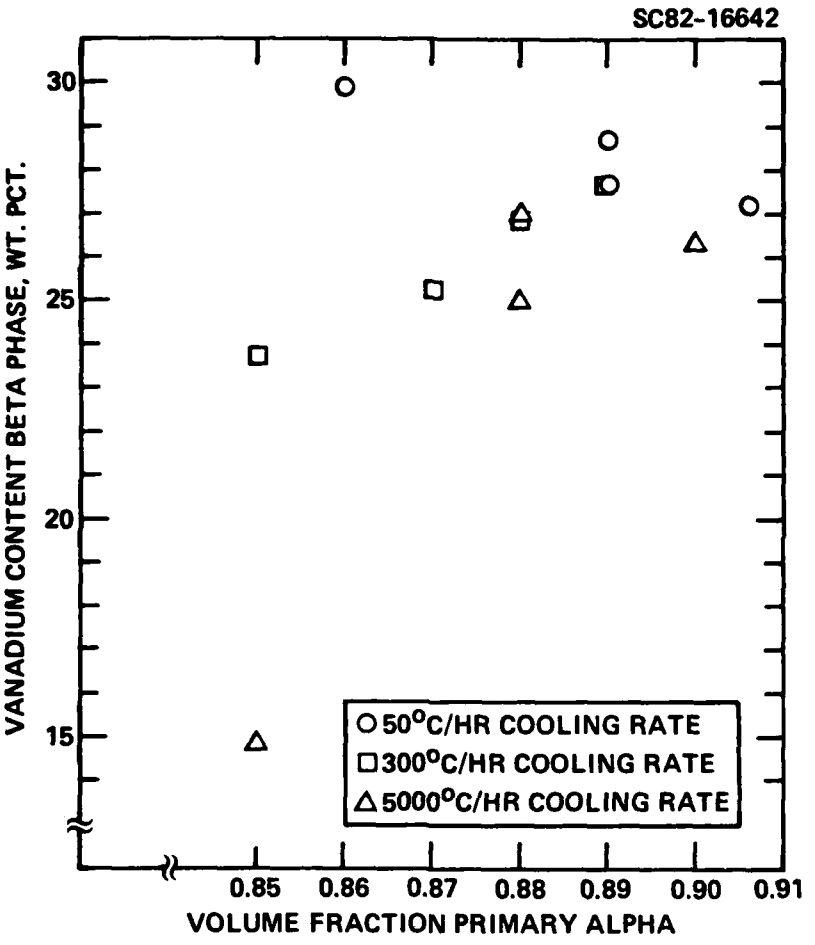

Fig. 7 V content of beta phase vs volume fraction of primary alpha in solution treated Ti-6Al-4V cooled at three cooling rates.

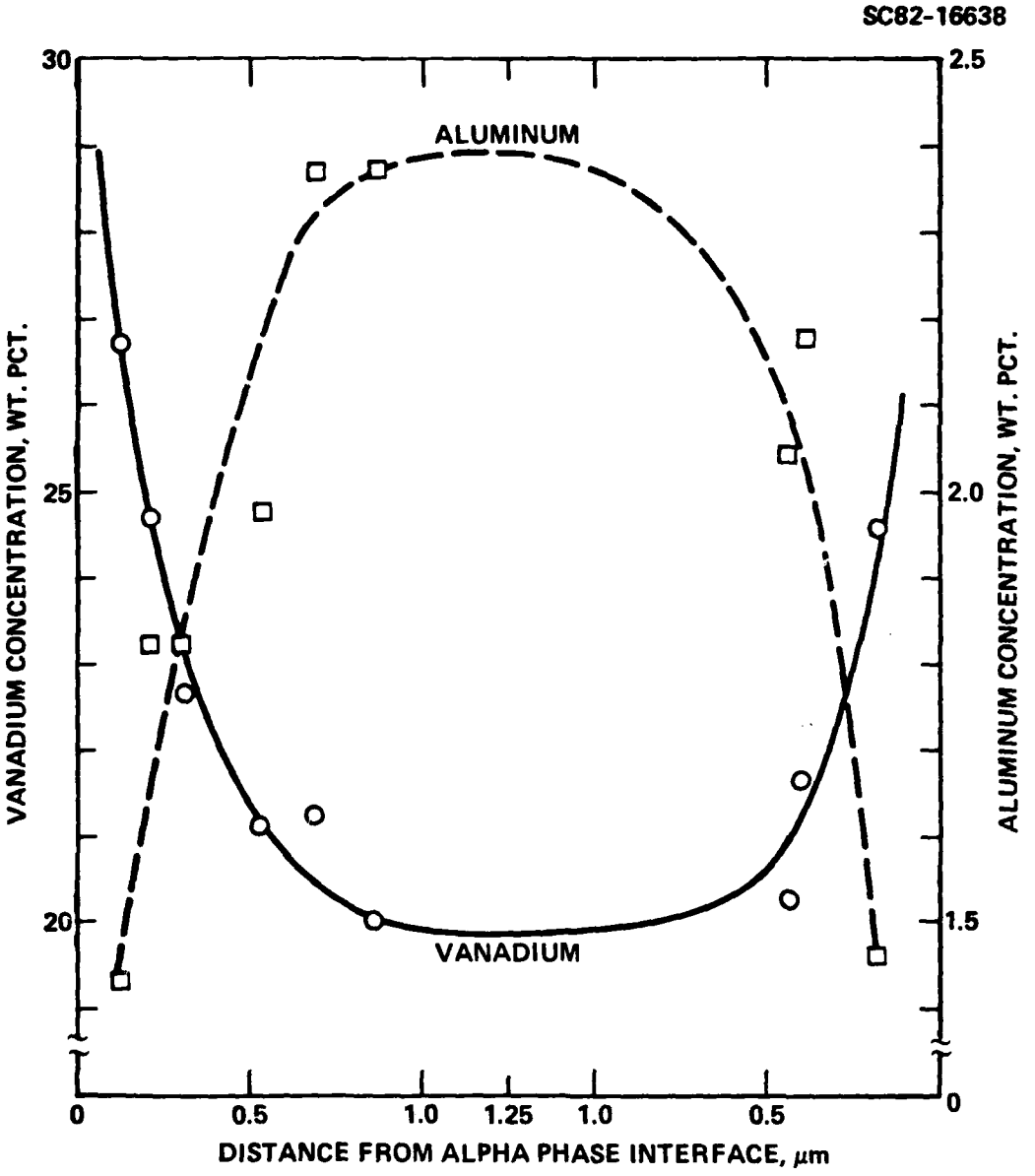

Fig. 8 Profile of Al and V concentrations in beta phase of Ti-6Al-4V cooled 50°C/hr from 900°C.

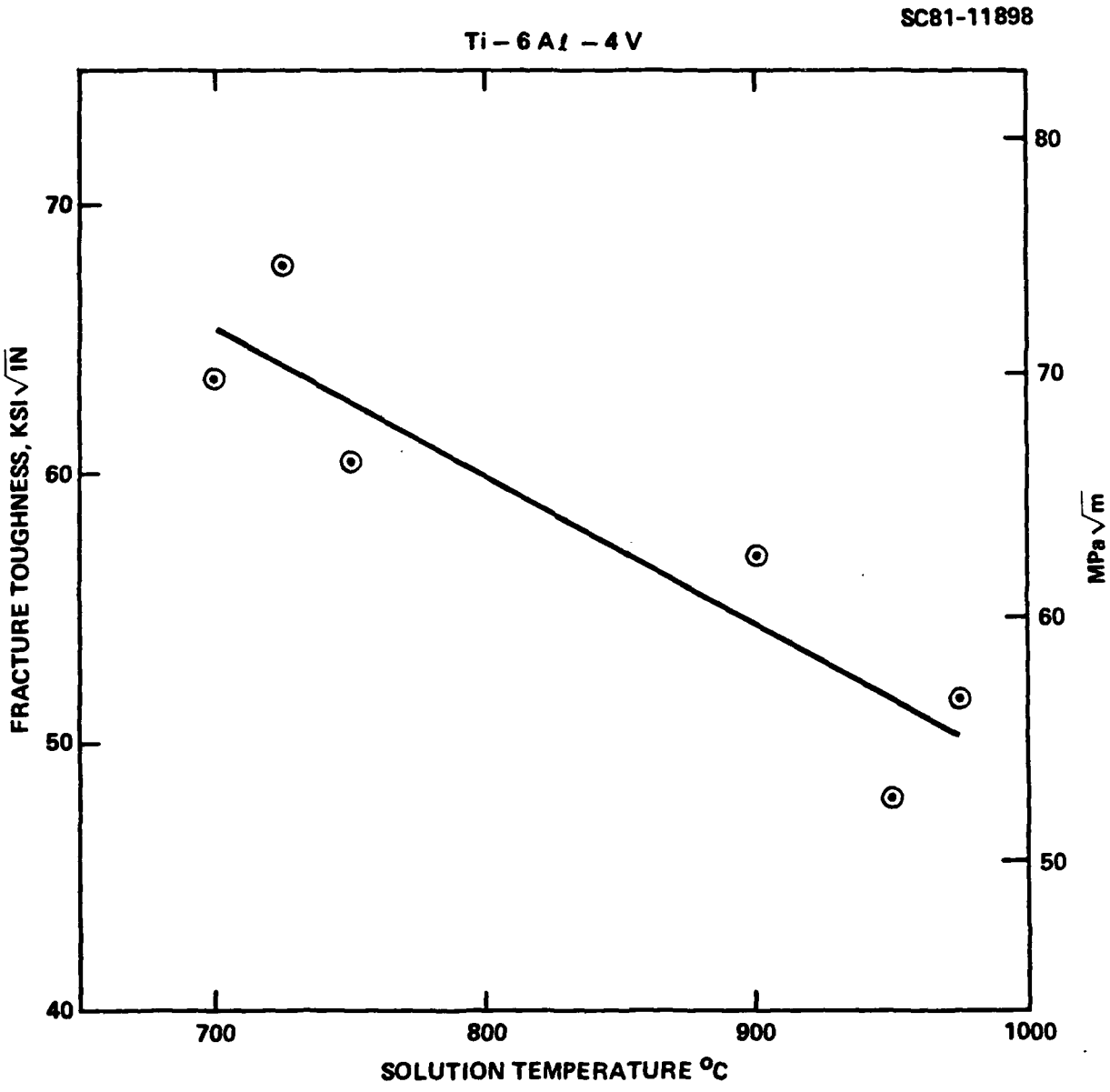

Fig. 9 Room temperature fracture toughness as a function of prior solution temperature for quenched Ti-6Al-4V.

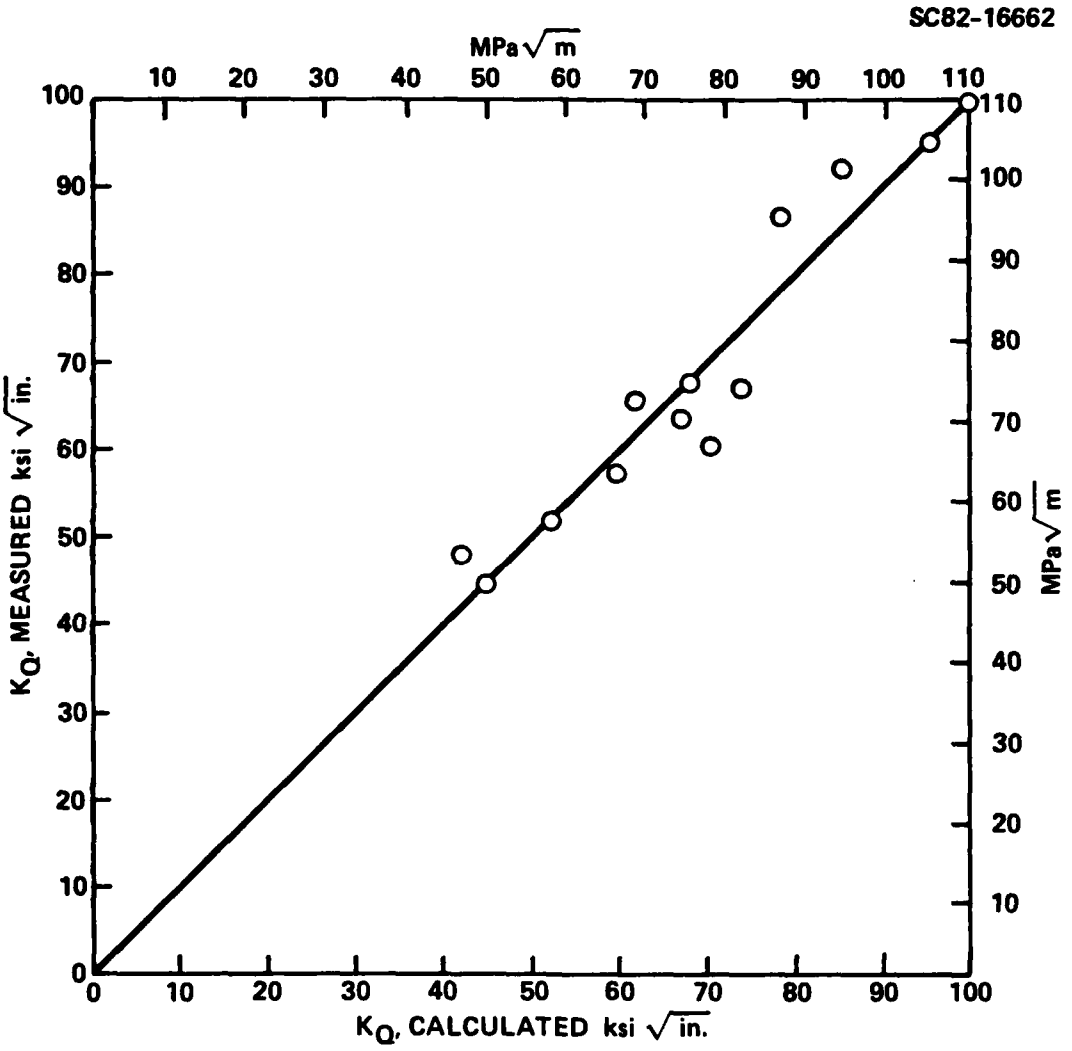

Fig. 10 Measured fracture toughness of solution treated Ti-6Al-4V vs fracture toughness calculated using Eq. (1).

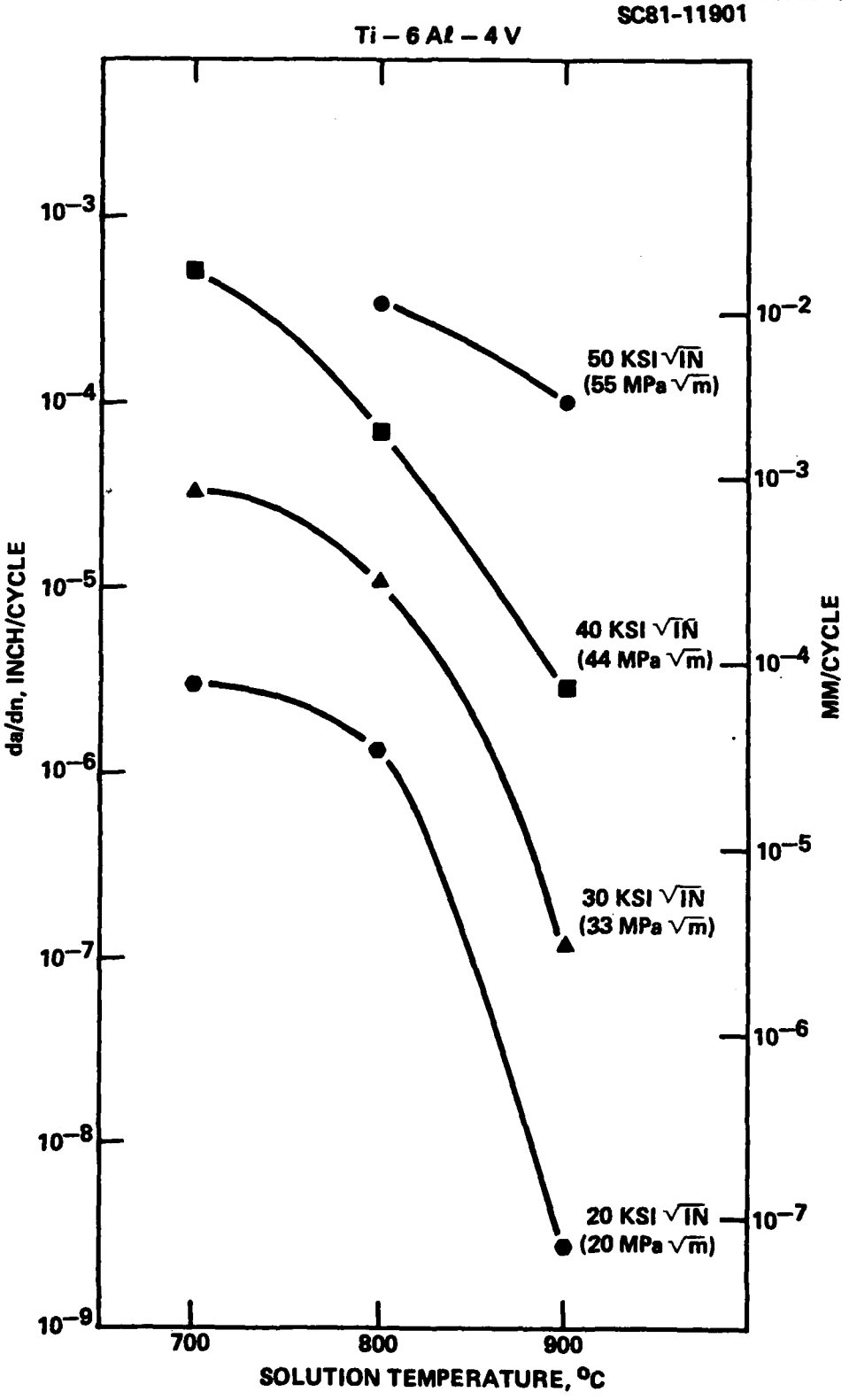

Fig. 11 Fatigue crack growth rate as a function of prior solution temperature for Ti-6Al-4V at four stress intensity levels.

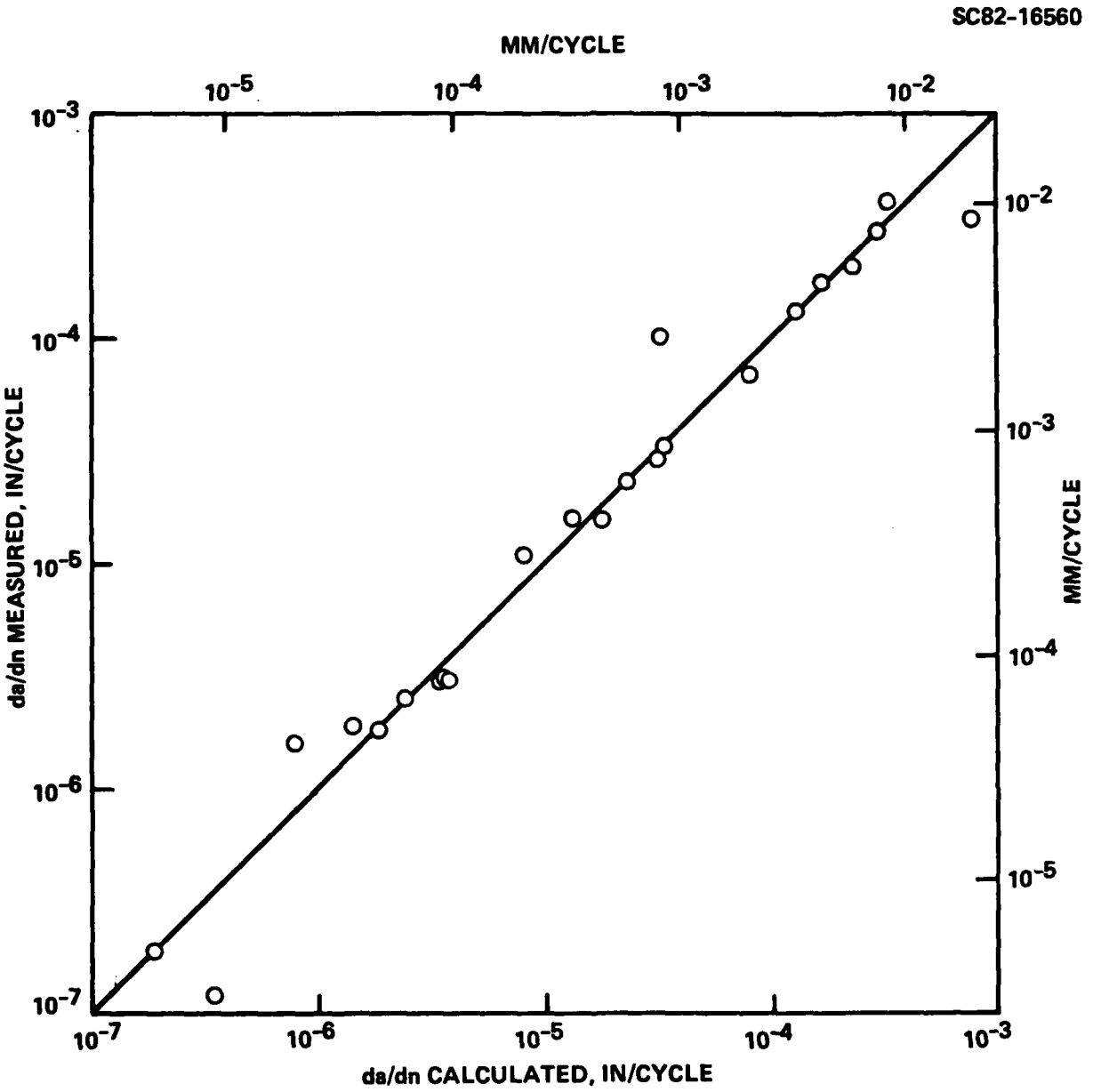

Fig. 12 Measured fatigue crack growth rate of solution treated Ti-6Al-4V vs fatigue crack growth rate calculated using Eq. (2).

SC81-11882

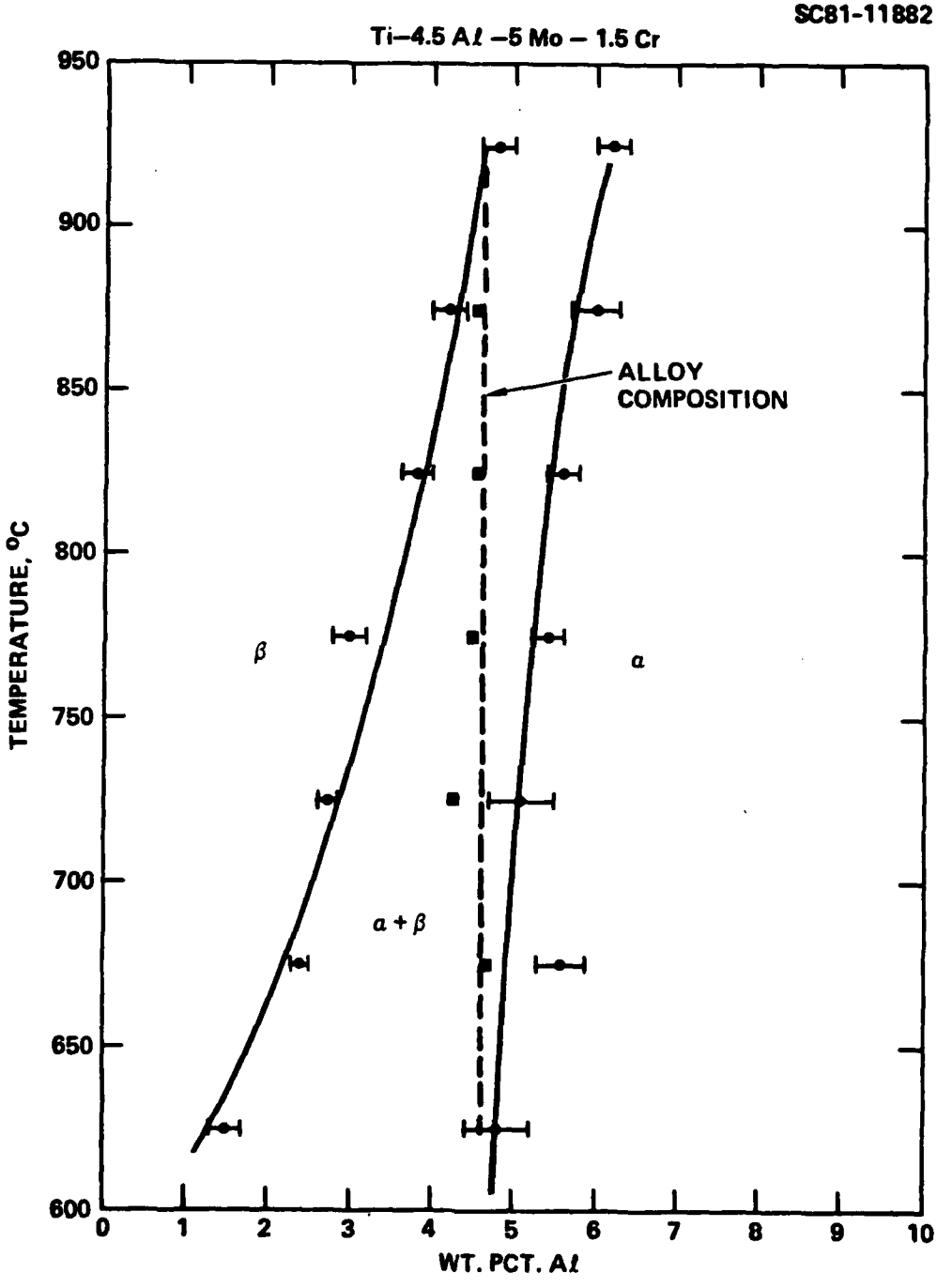

Fig. 13 Al-(Ti-5Mo-1.5Cr) phase diagram constructed from microanalysis data from Ti-4.5Al-5Mo-1.5Cr.

SC81-11897

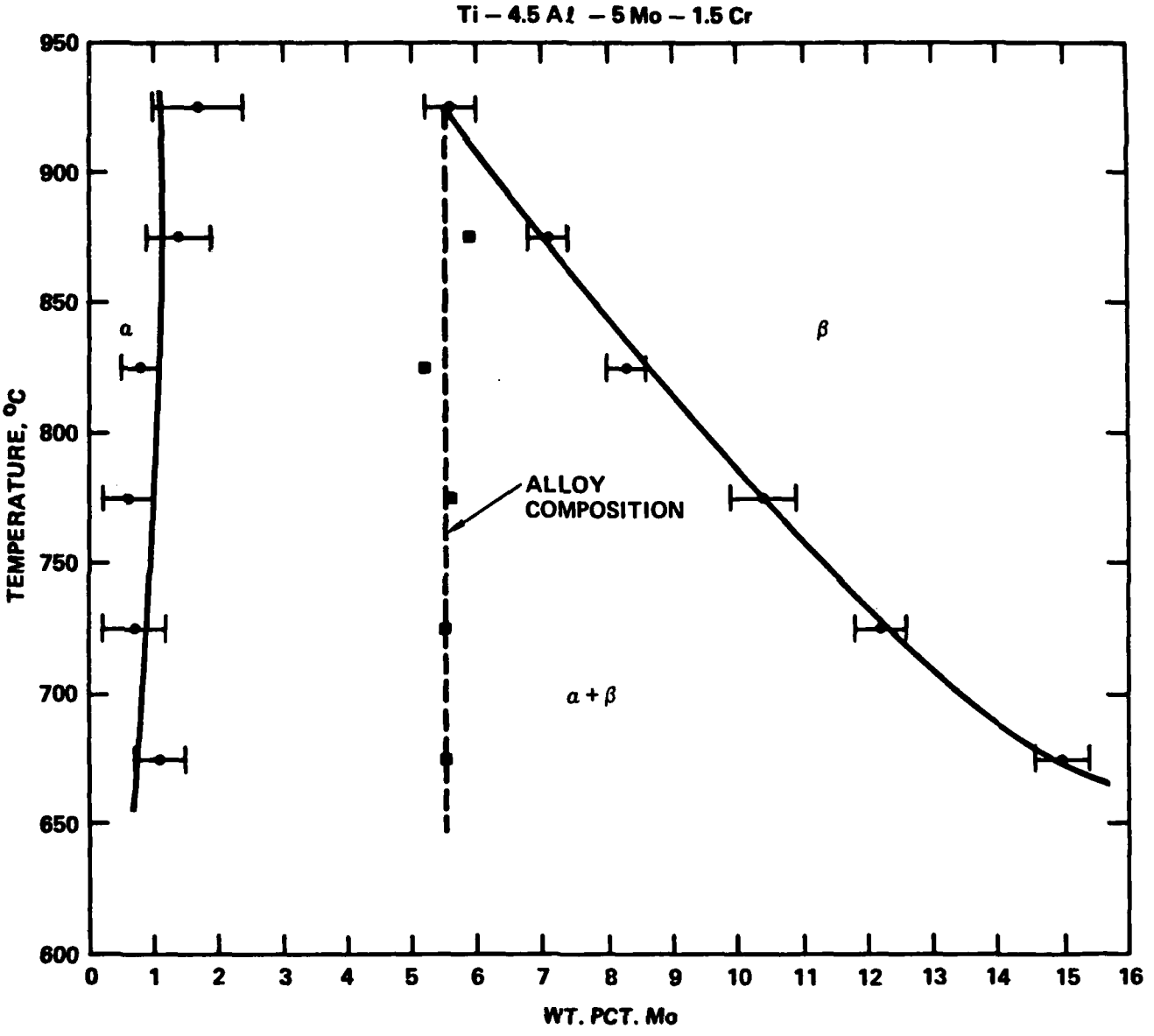

Fig. 14 Mo-(Ti-4.5Al-1.5Cr) phase diagram constructed from micro-analysis data from Ti-4.5Al-5Mo-1.5Cr.

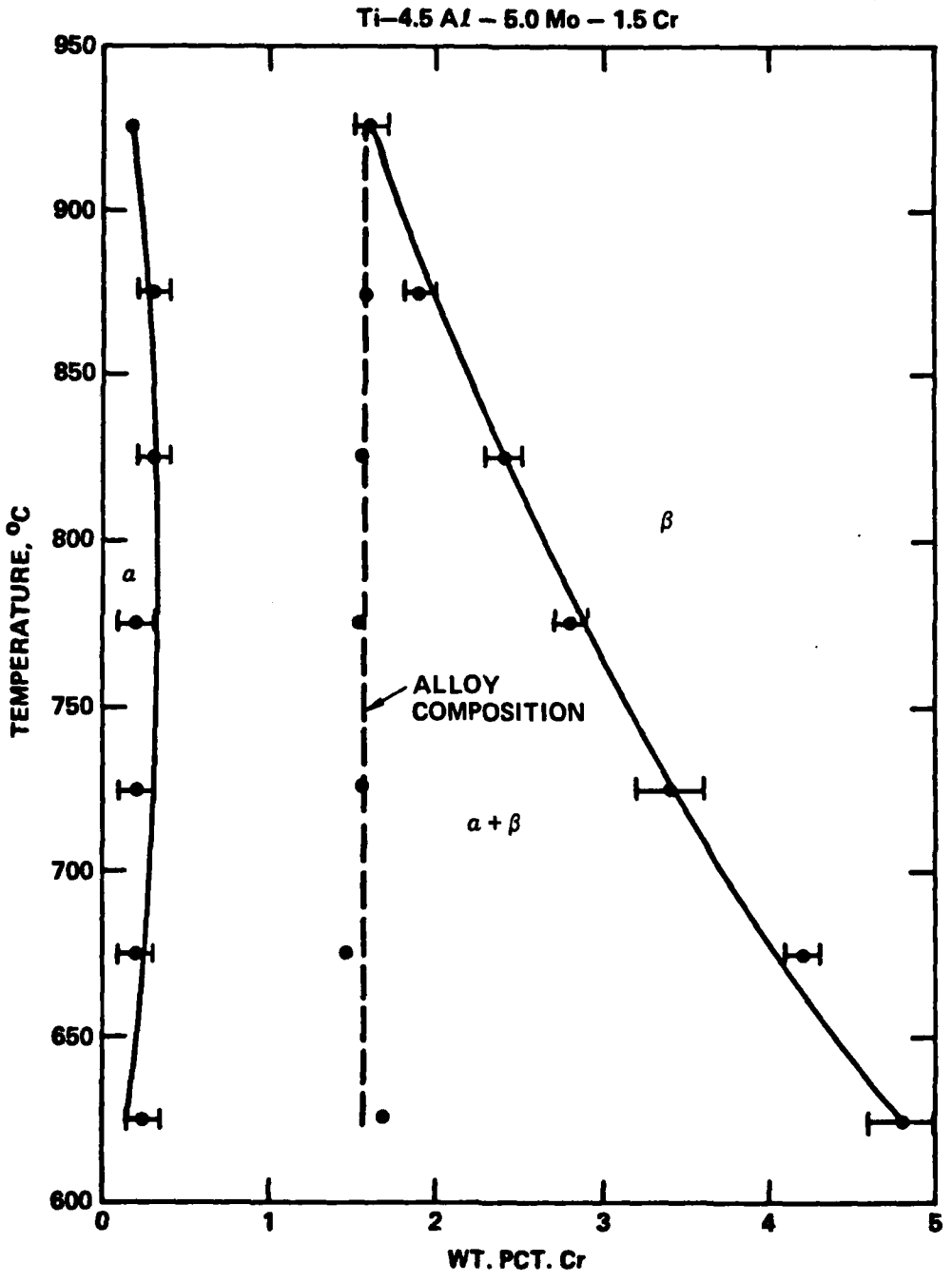

Fig. 15 Cr-(Ti-4.5Al-5Mo) phase diagram constructed from micro-analysis data from Ti-4.5Al-5Mo-1.5Cr.

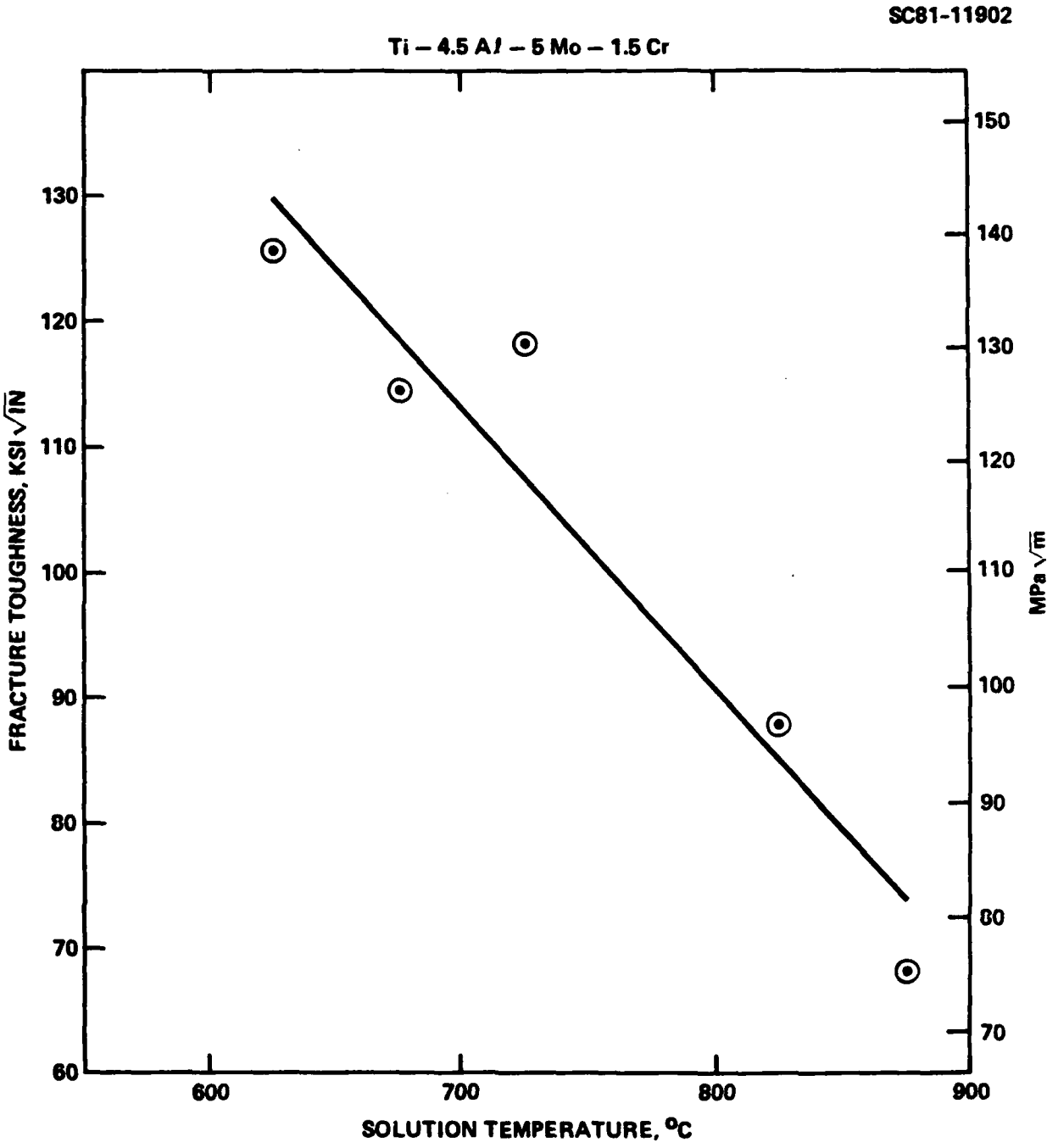

Fig. 16 Room temperature fracture toughness as a function of prior solution temperature for quenched Ti-4.5Al-5Mo-1.5Cr.

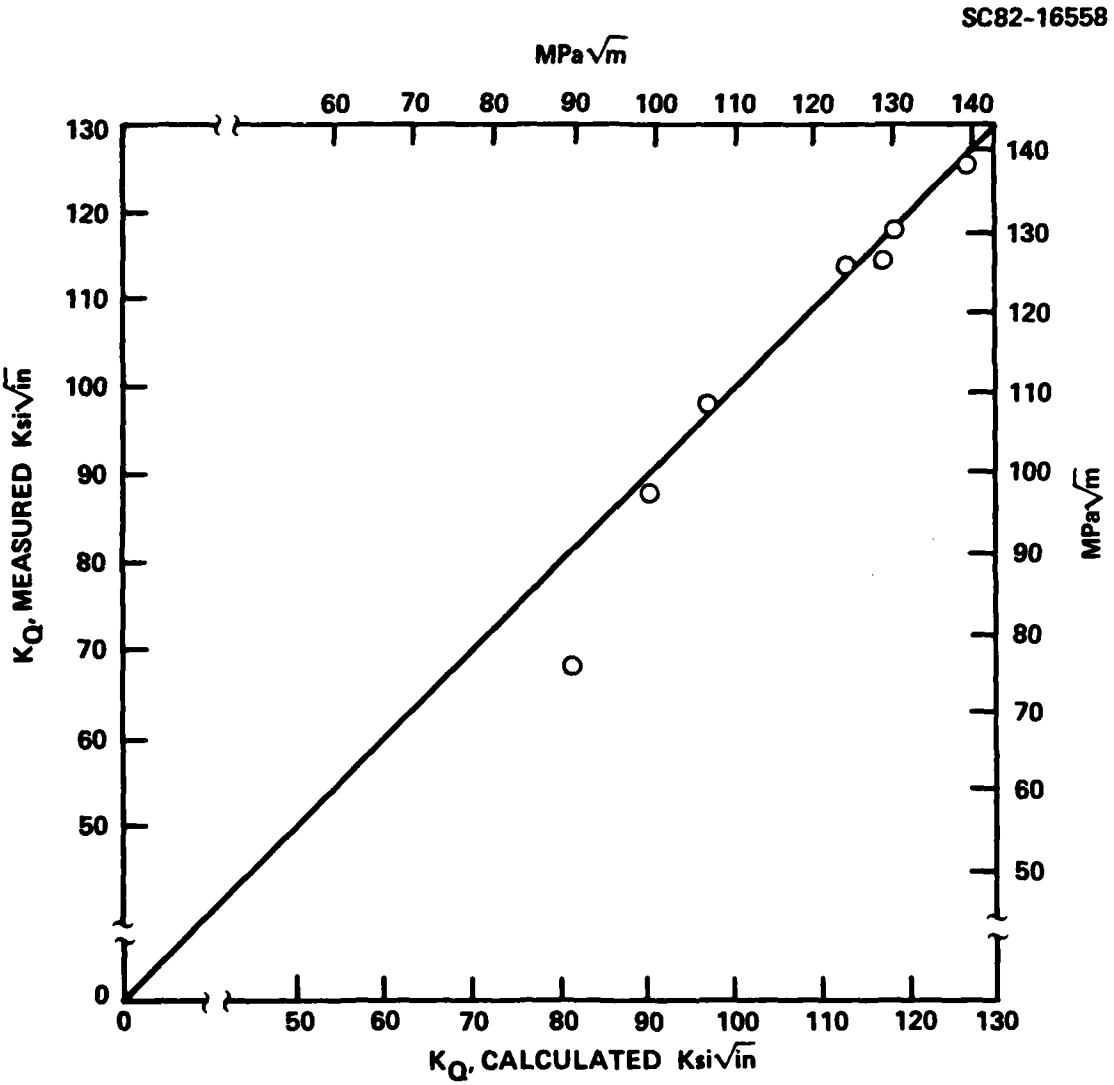

Fig. 17 Measured fracture toughness of solution treated Ti-4.5Al-5Mo-1.5Cr vs fracture toughness calculated using Eq. (3).

SC82-16557

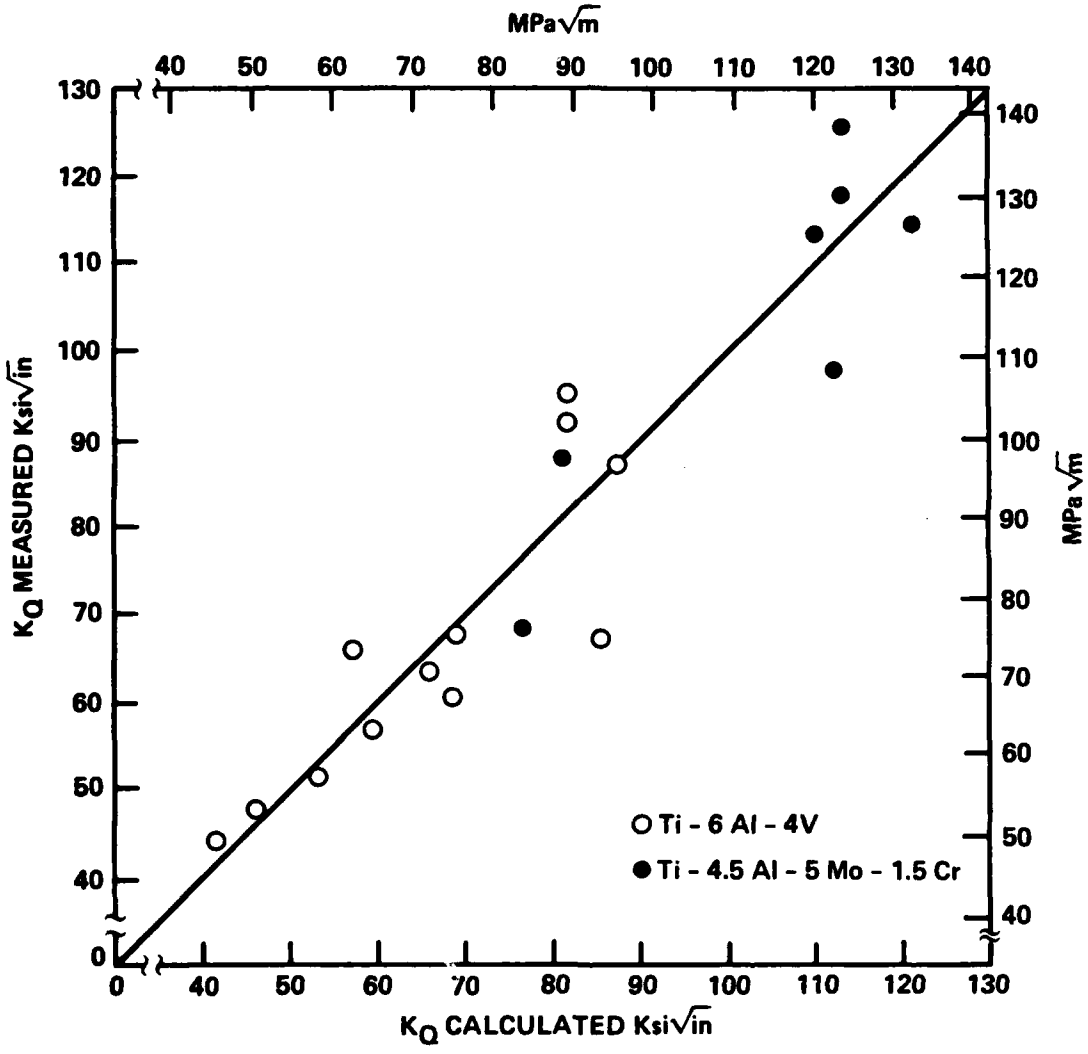

Fig. 18 Measured fracture toughness of solution treated Ti-6Al-4V and Ti-4.5Al-5Mo-1.5Cr vs fracture toughness calculated using Eq. (4).

SC82-18123

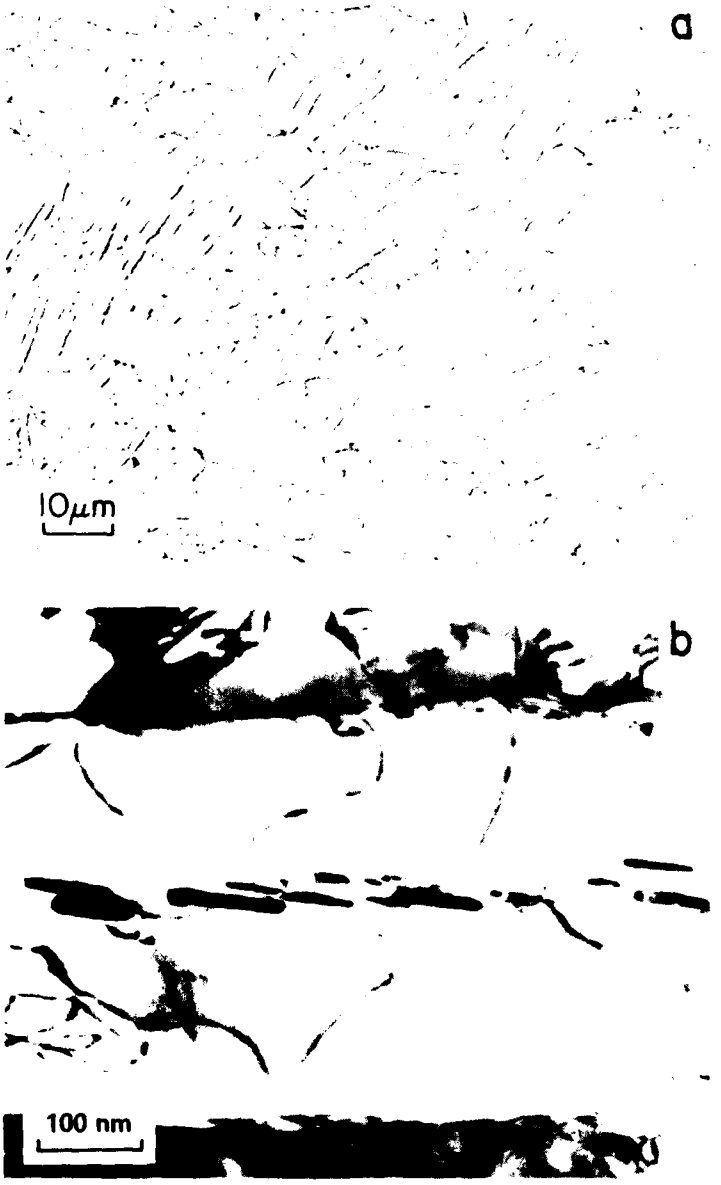

Fig. 19 Ti-6Al-4V solution treated at 954°C and aged six hours at 538°C. (a) Light micrograph, (b) transmission electron micrograph of transformed beta region.

SC82-18124

Fig. 20 Ti-6Al-4V solution treated at 954°C and aged 48 hours at 483°C. (a) Light micrograph, (b) transmission electron micrograph of transformed beta region.

SC82-18125

Fig. 21 Ti-6Al-4V solution treated at 954°C and aged 1 hour at 635°C. (a) Light micrograph, (b) transmission electron micrograph of transformed beta region.

AD-A117 155 ROCKWELL INTERNATIONAL THOUSAND OAKS CA SCIENCE CENTER F/G 11/6
FRACTURE & FATIGUE CHARACTERISTICS IN TITANIUM ALLOYS.(U)
JUN 82 C G RHODES, M R MITCHELL, J C CHESNUTT N00014-79-C-0567
UNCLASSIFIED SC5227-1FR NL

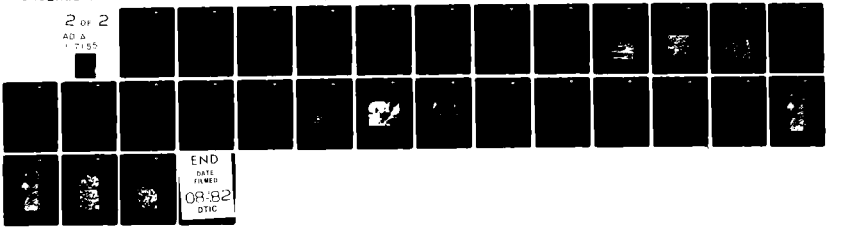

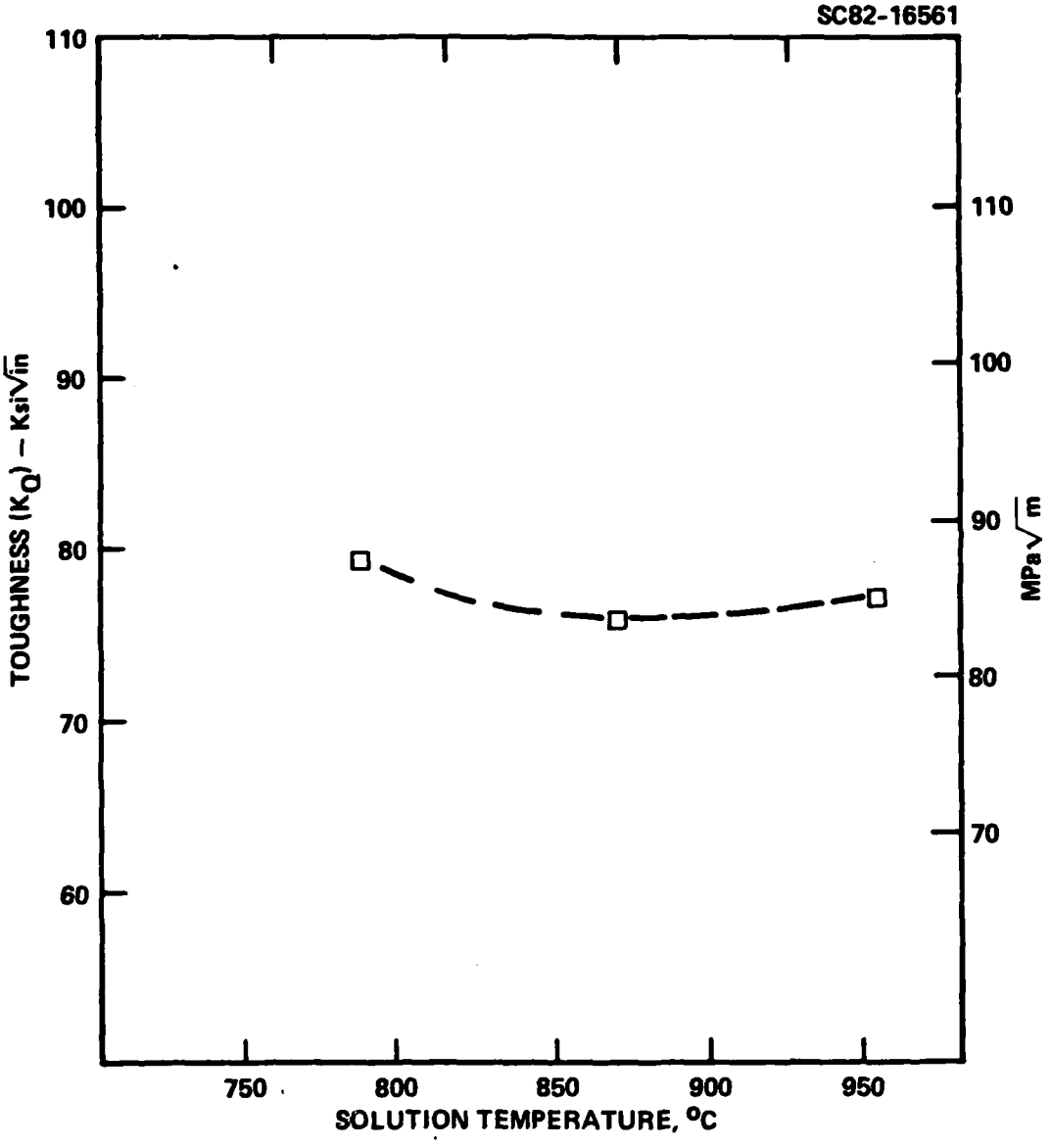

Fig. 22 Room temperature fracture toughness vs prior solution temperature for Ti-6Al-4V aged 6 hours at 538°C.

SC82-16559

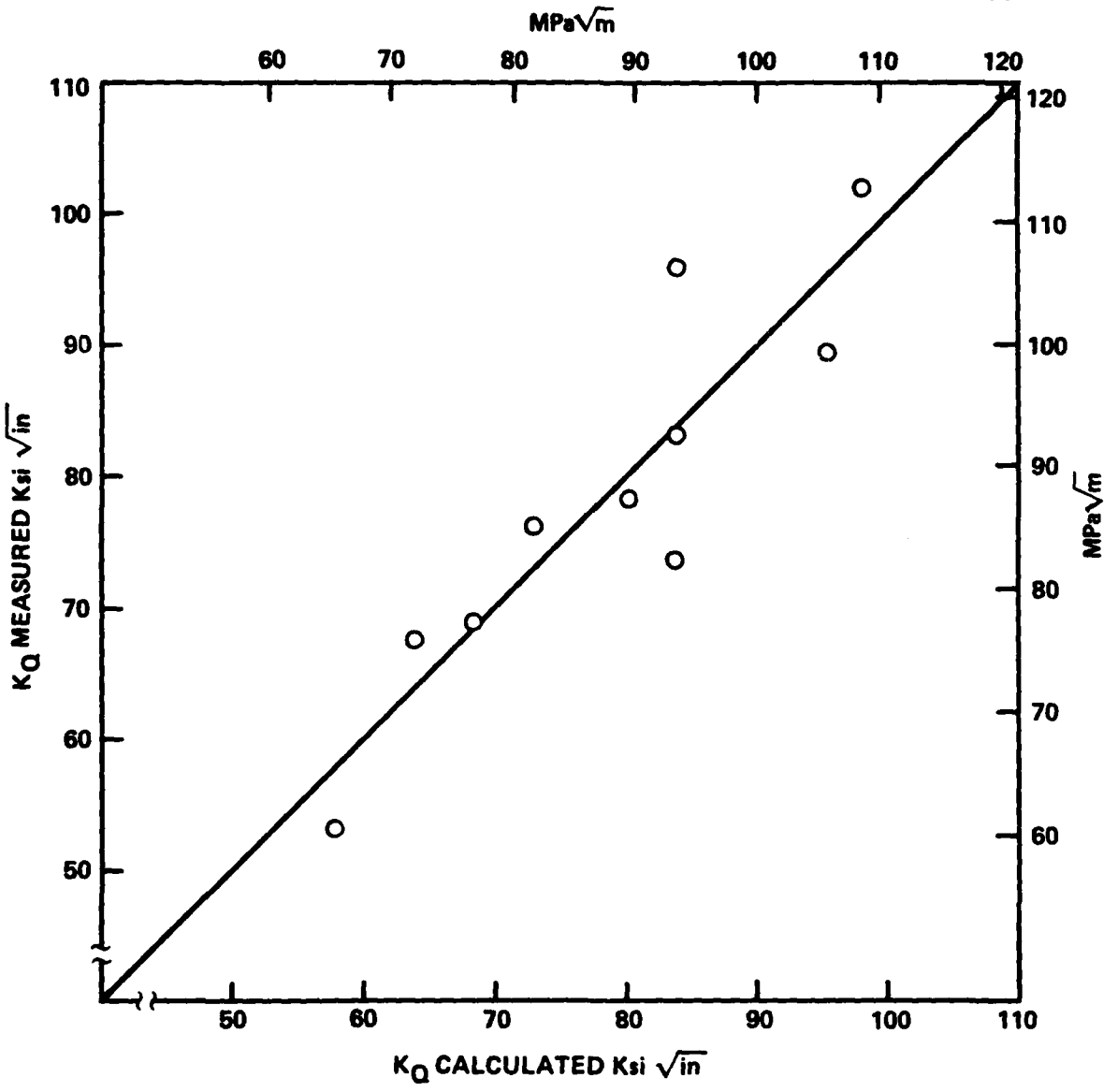

Fig. 23 Measured fracture toughness of STA Ti-6Al-4V vs fracture toughness calculated using Eq. (5).

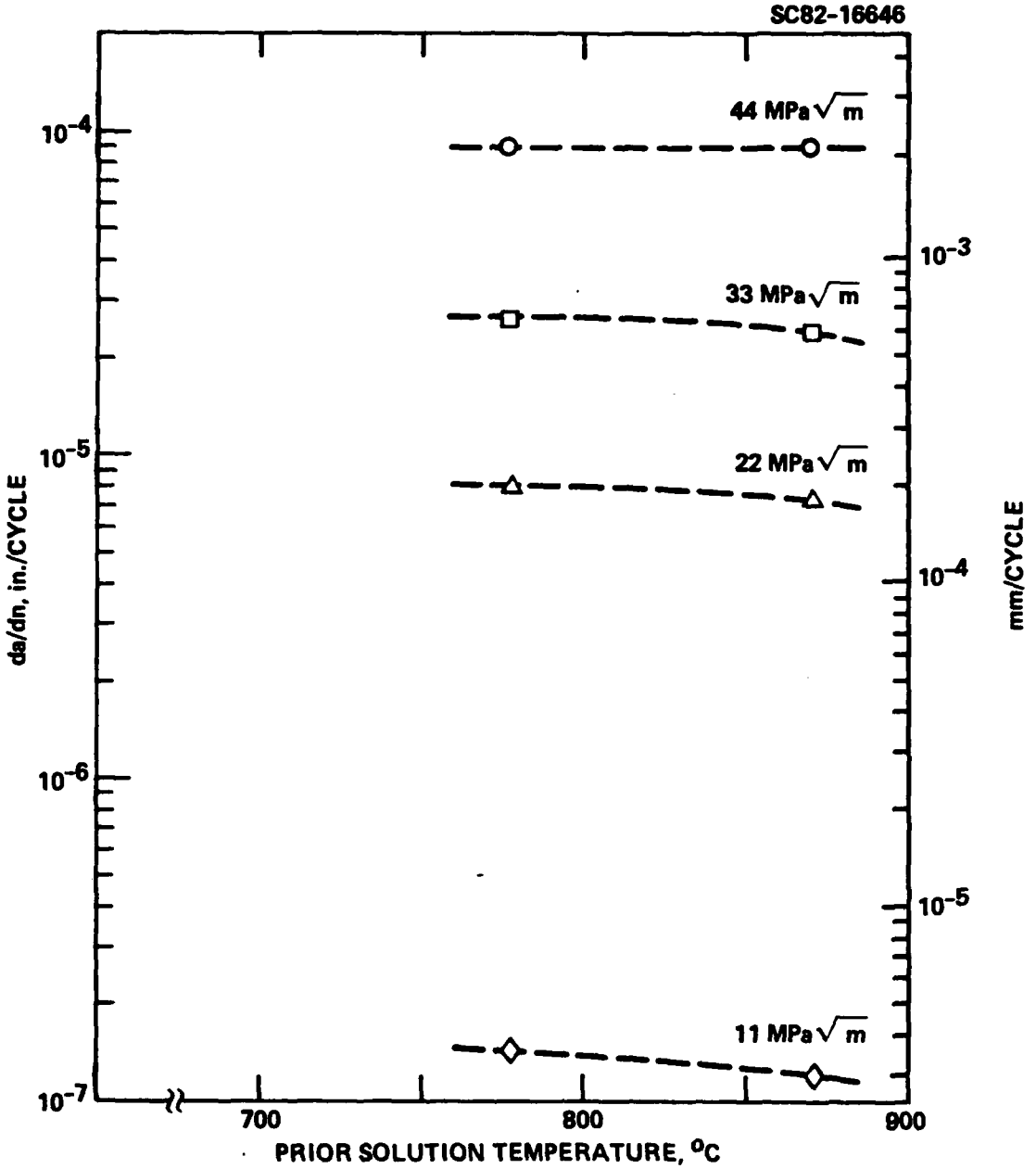

Fig. 24 Fatigue crack growth rate vs prior solution temperature at four stress intensity levels for Ti-6Al-4V aged six hours at 538°C.

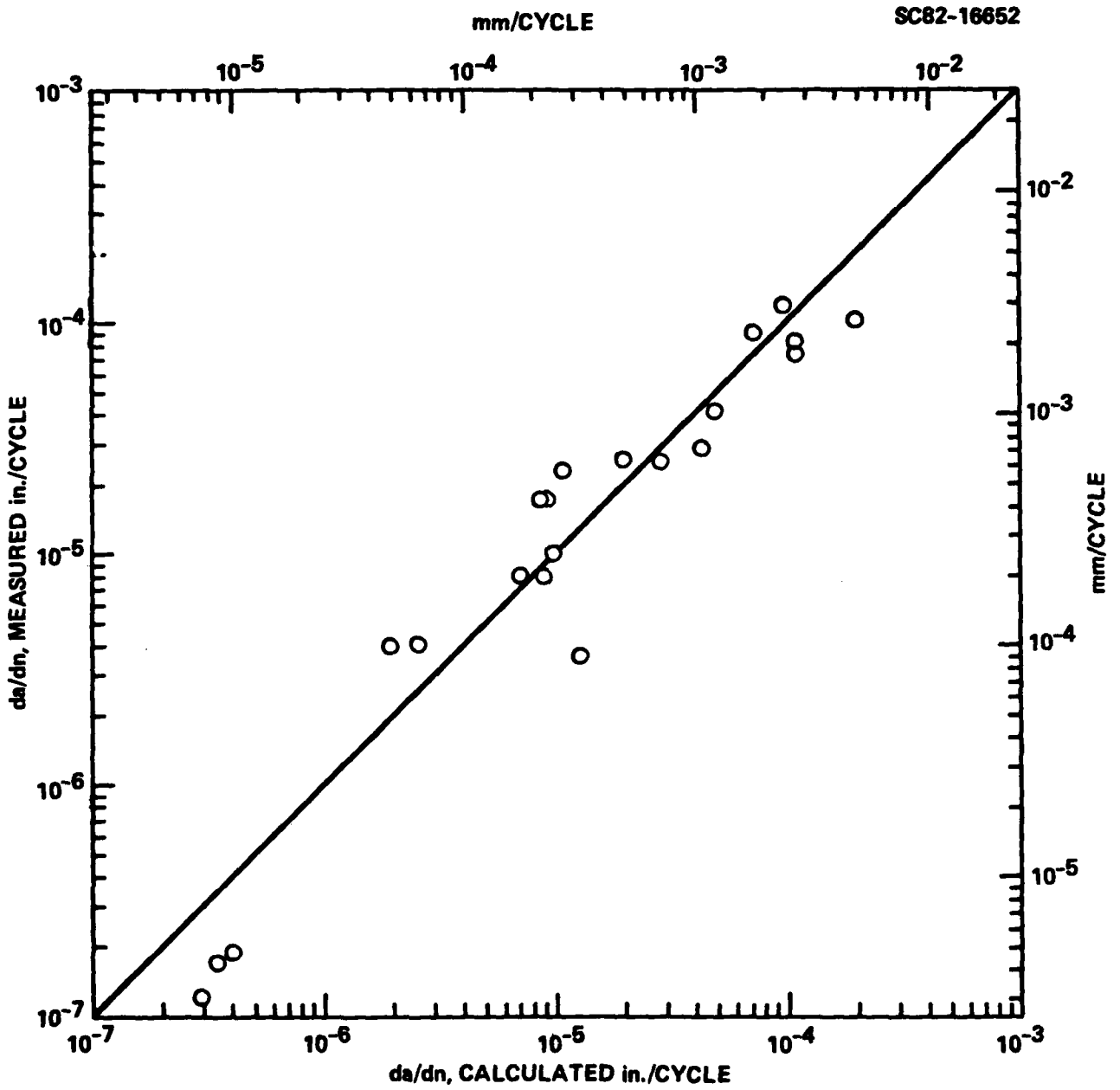

Fig. 25 Measured fatigue crack growth rate of STA Ti-6Al-4V vs fatigue crack growth rate calculated using Eq. (6).

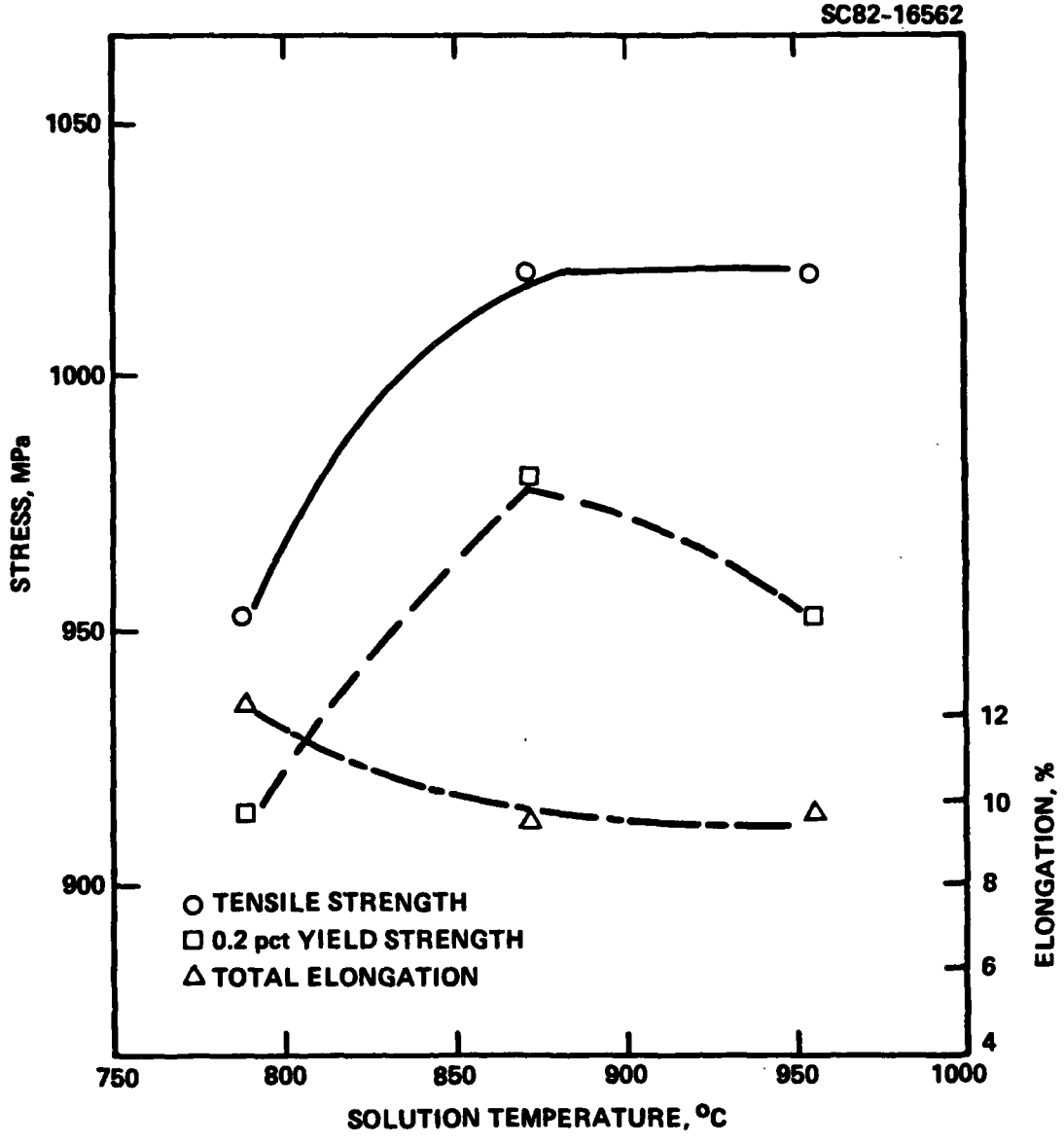

Fig. 26 Room temperature tensile properties as a function of prior solution temperature for Ti-6Al-4V aged six hours at 538°C.

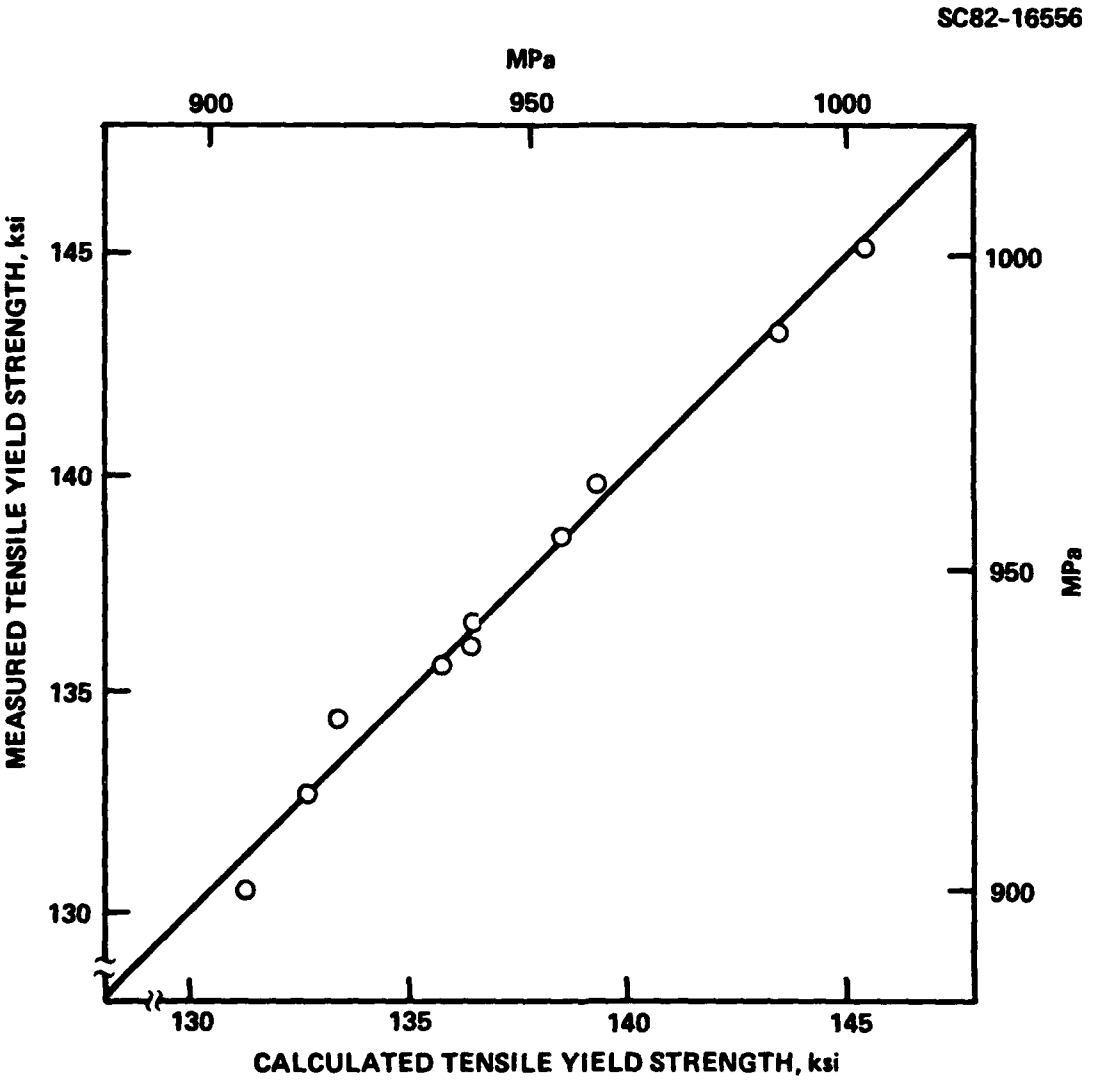

Fig. 27 Measured yield strength of STA Ti-6Al-4V vs yield strength calculated using Eq. (7).

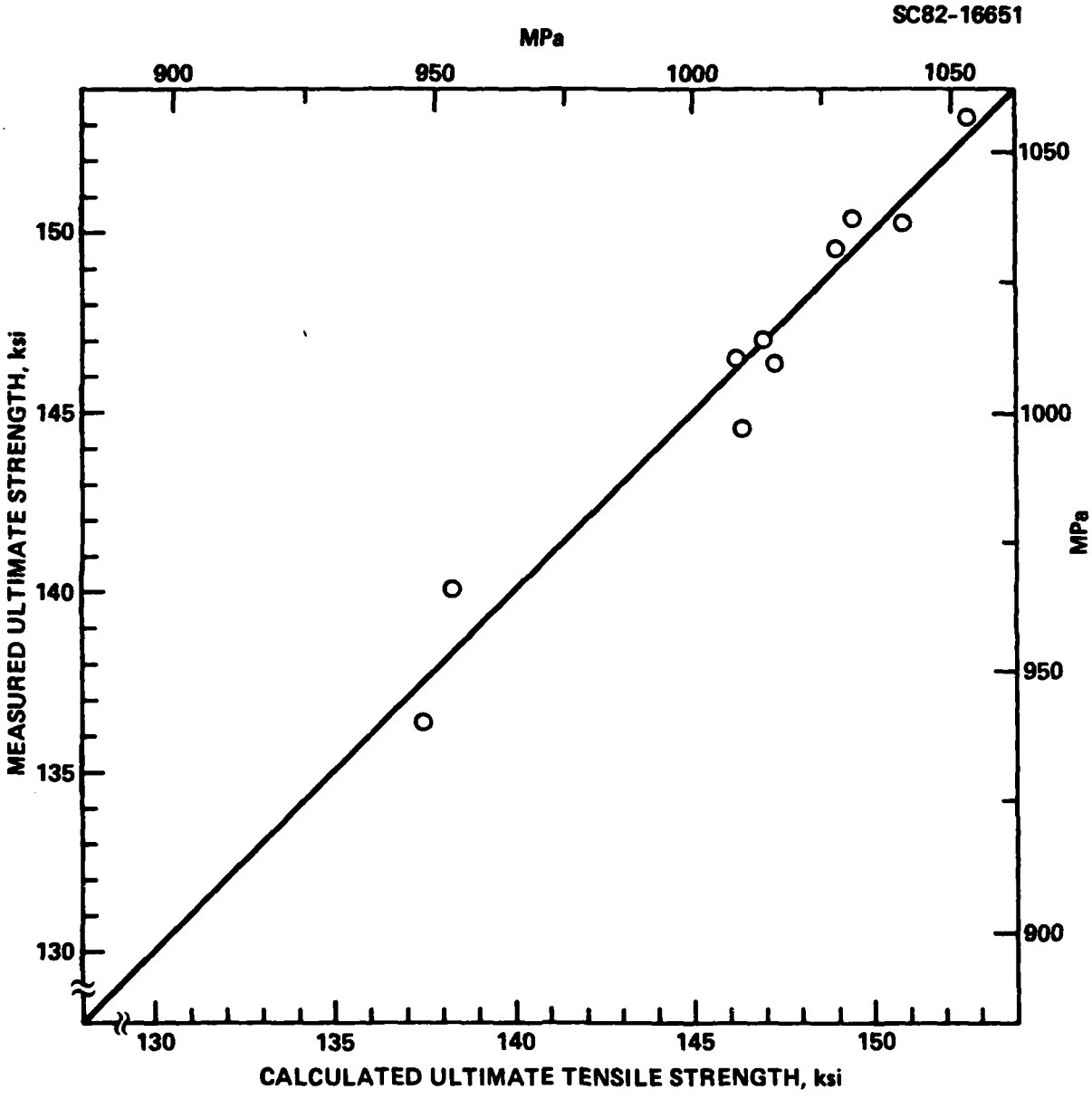

Fig. 28 Measured ultimate strength of STA Ti-6Al-4V vs ultimate strength calculated using Eq. (8).

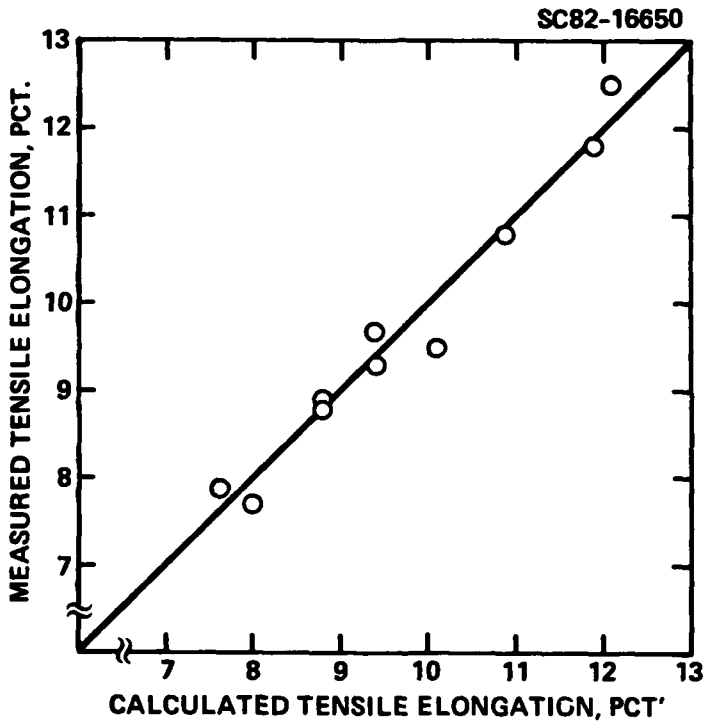

Fig. 29 Measured elongation of STA Ti-6Al-4V vs elongation calculated using Eq. (9).

SC82-18126

Fig. 30 Ti-4.5Al-5Mo-1.5Cr solution treated at 830°C and aged four hours at 593°C. (a) Light micrograph, (b) transmission electron micrograph of transformed beta region.

SC82-18127

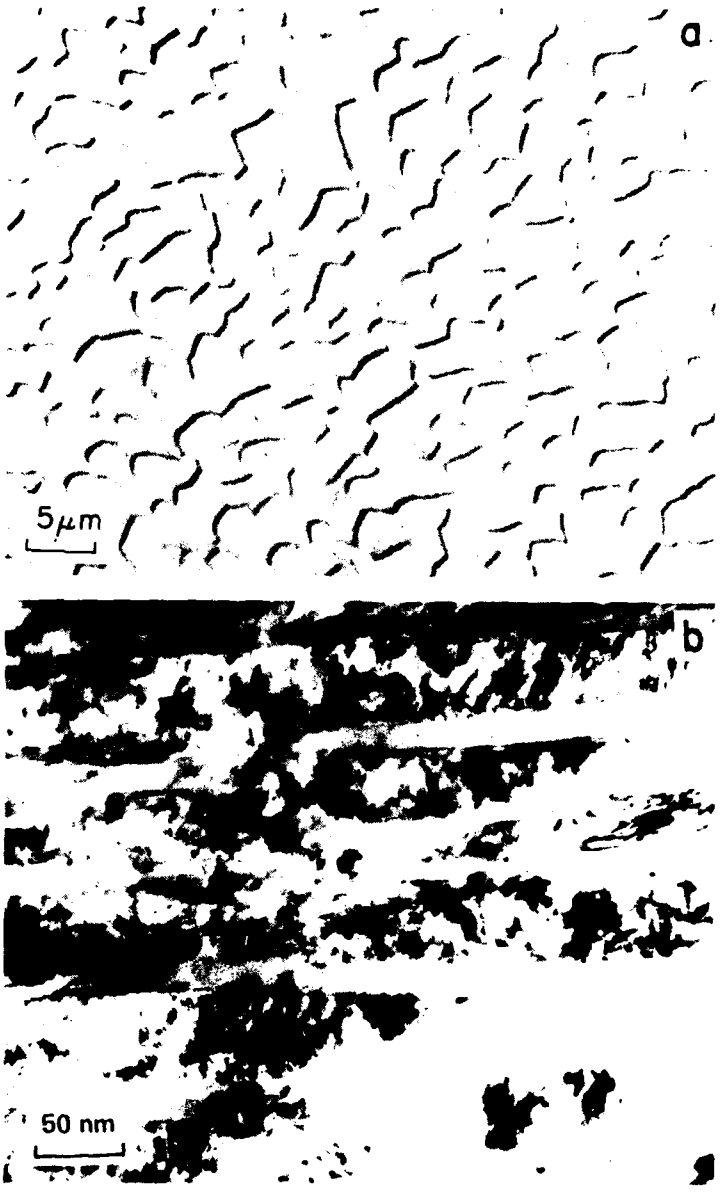

Fig. 31 Ti-4.5Al-5Mo-1.5Cr solution treated at 830°C and aged 24 hours at 510°C. (a) Light micrograph, (b) transmission electron micrograph of transformed beta region.

SC82-18128

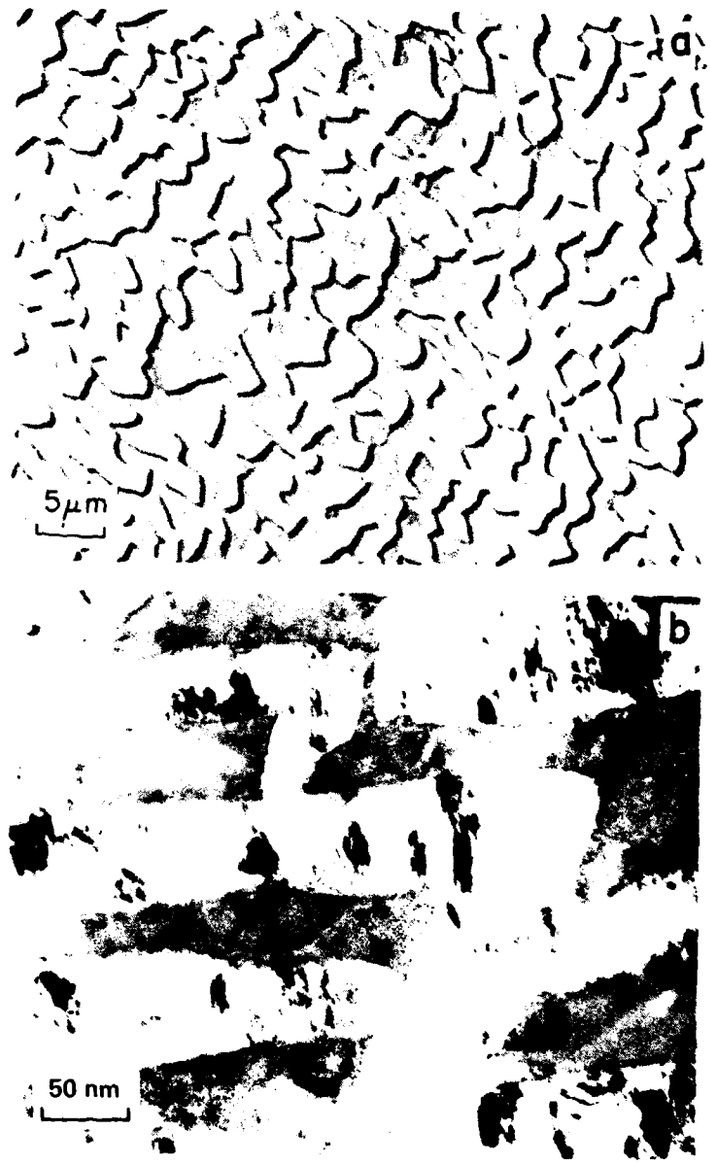

Fig. 32 Ti-4.5Al-5Mo-1.5Cr solution treated at 830°C and aged 20 minutes at 677°C. (a) Light micrograph, (b) transmission electron micrograph of transformed beta region.

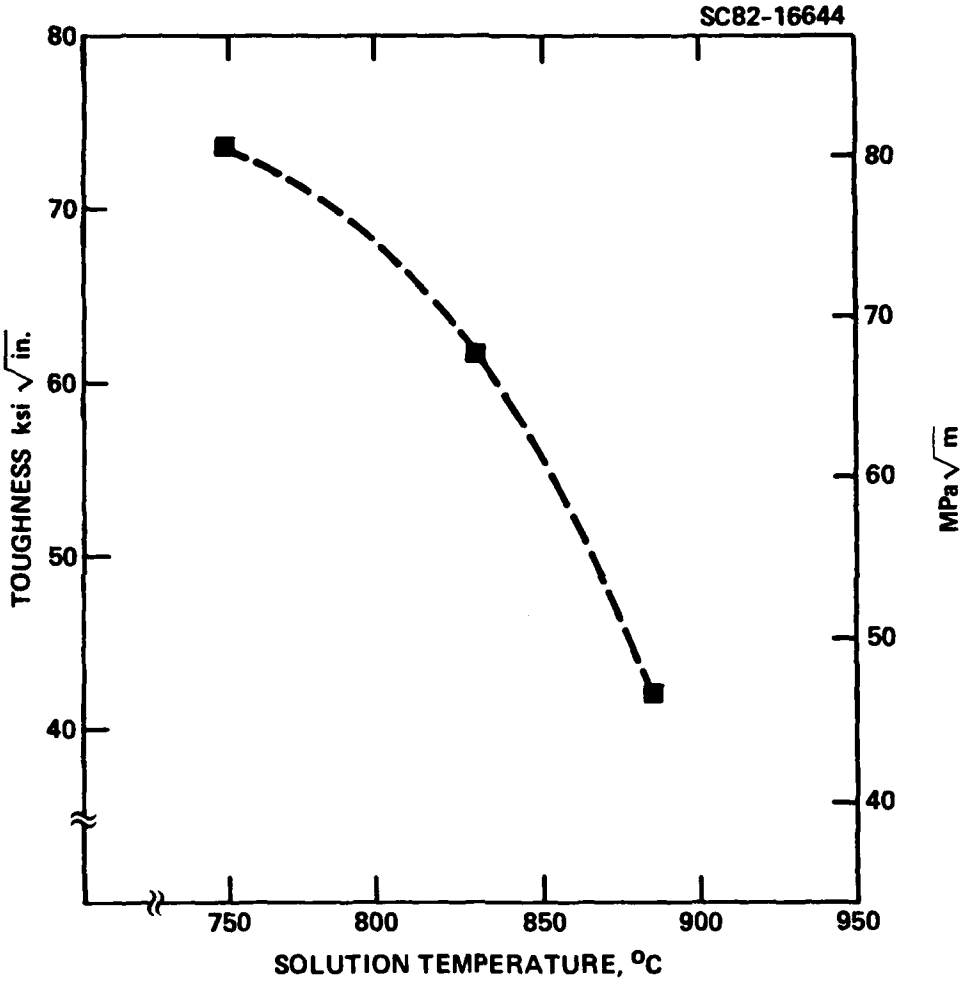

Fig. 33 Room temperature fracture toughness as a function of prior solution temperature for Ti-4.5Al-5Mo-1.5Cr aged four hours at 593°C.

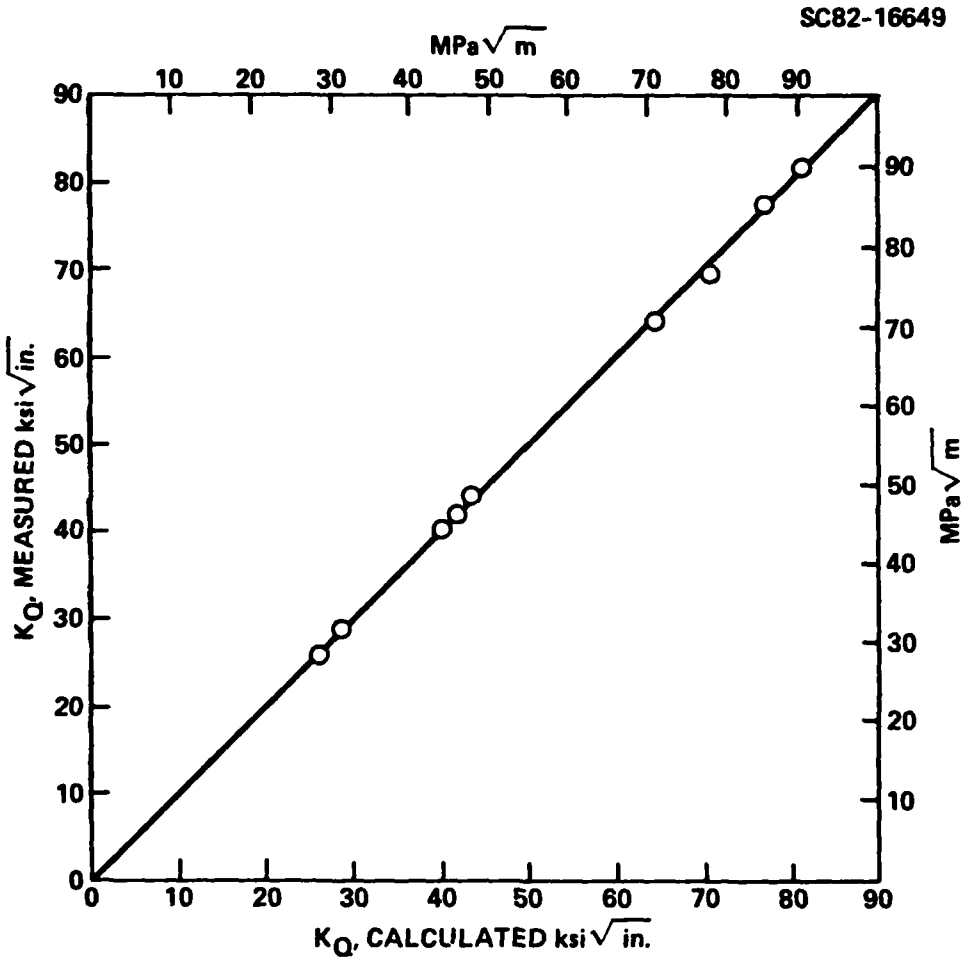

Fig. 34 Measured fracture toughness of STA Ti-4.5Al-5Mo-1.5Cr vs fracture toughness calculated using Eq. (10).

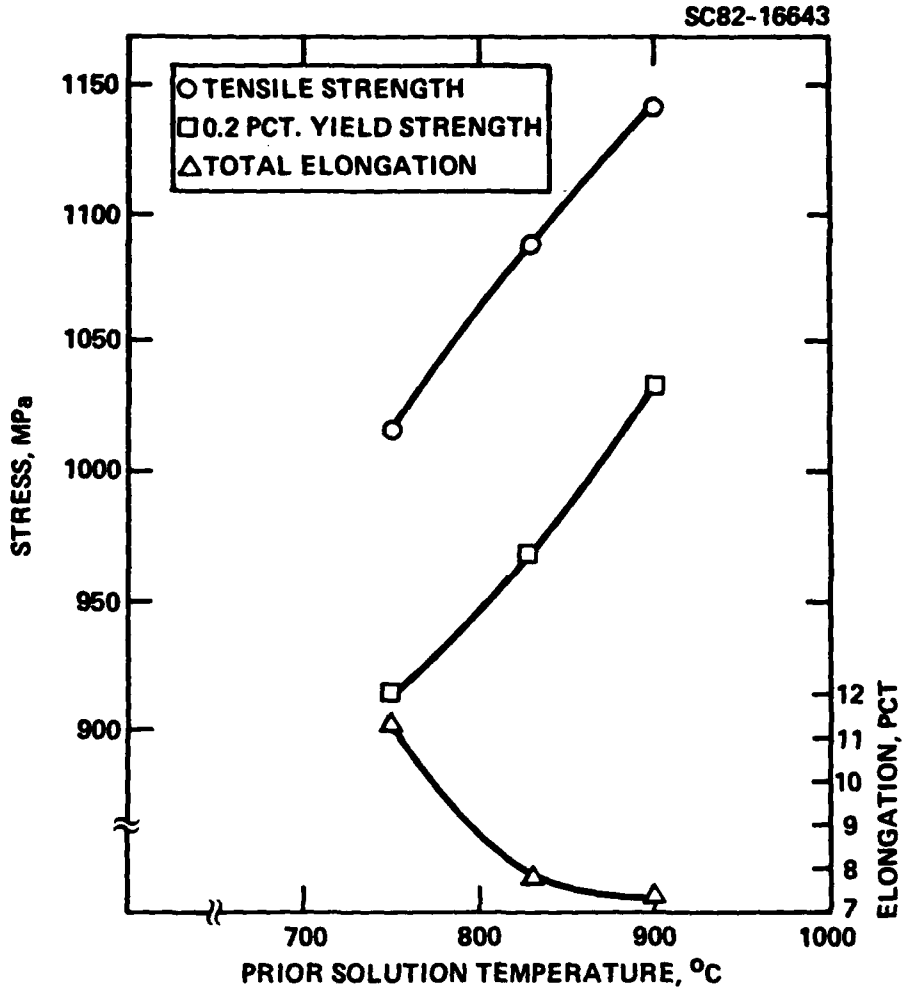

Fig. 35 Room temperature tensile properties as a function of prior solution temperature for Ti-4Al-5Mo-1.5Cr aged four hours at 593°C.

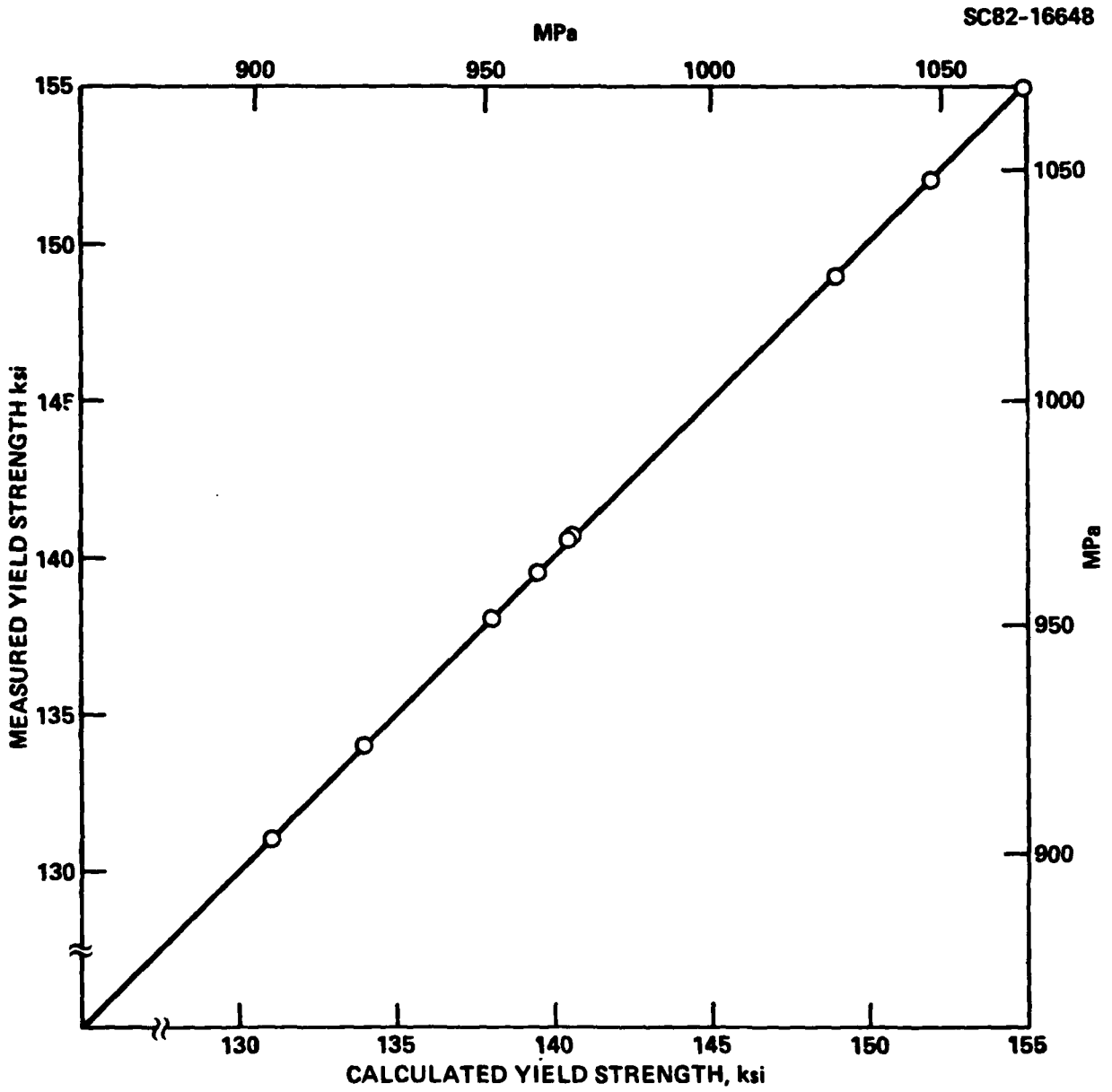

Fig. 36 Measured yield strength of STA Ti-4.5Al-5Mo-1.5Cr vs yield strength calculated using Eq. (11).

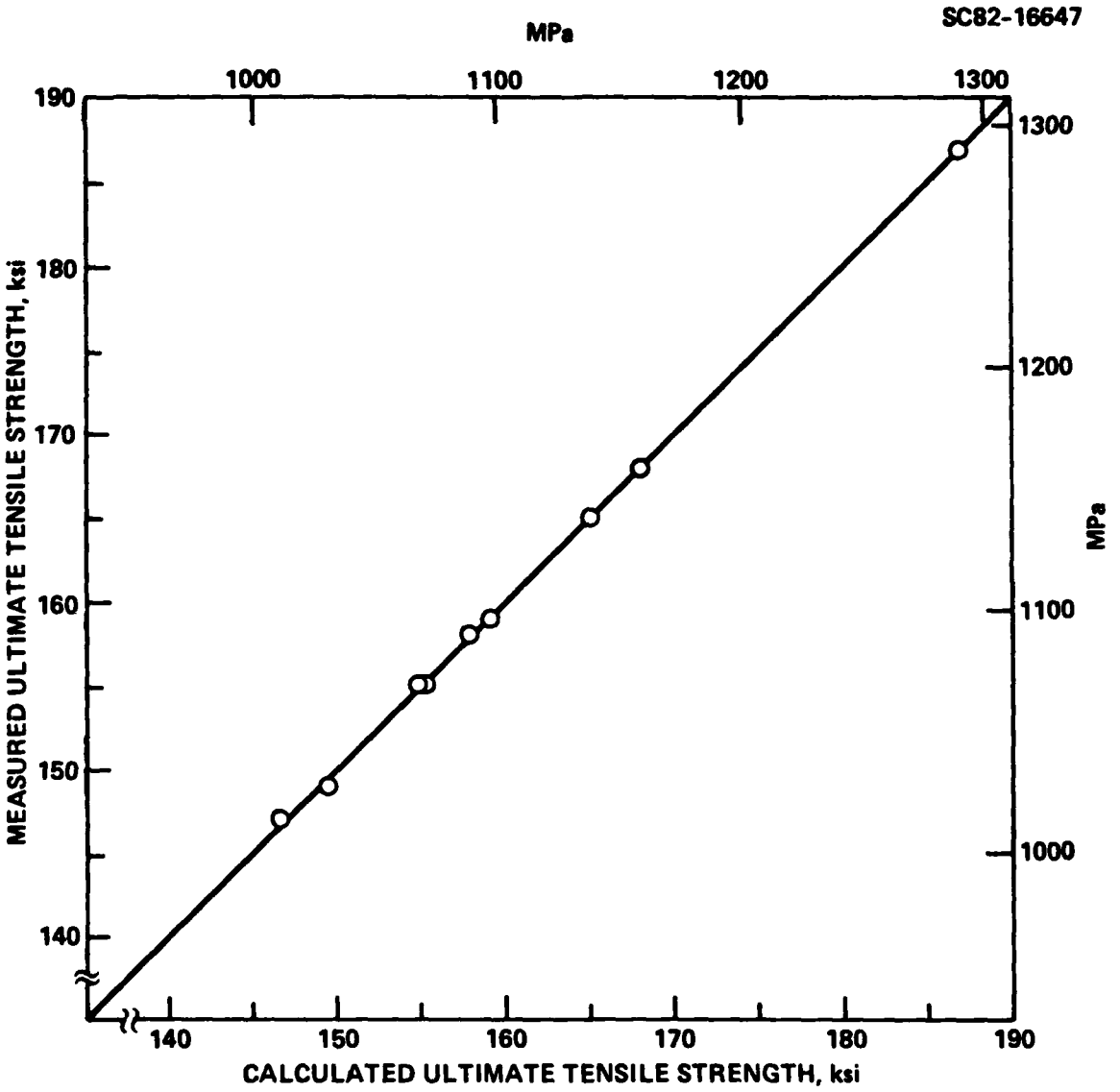

Fig. 37 Measured ultimate strength of STA Ti-4.5Al-5Mo-1.5Cr vs ultimate strength calculated using Eq. (12).

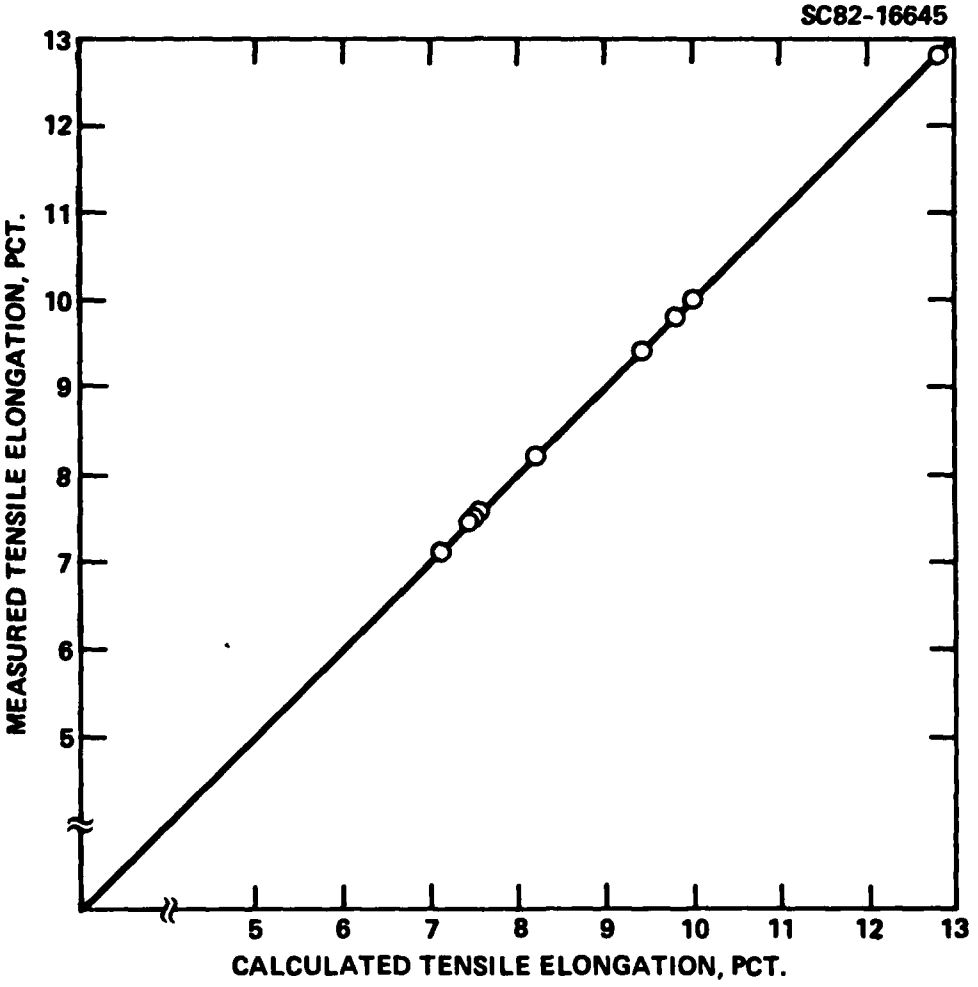

Fig. 38 Measured elongation of STA Ti-4.5Al-5Mo-1.5Cr vs elongation calculated using Eq. (13).

SC82-18129

Fig. 39 Light micrograph of powder processed Ti-6Al-4V. Pre-alloyed powder hot isostatically pressed at 900°C for 2 hours at 15 ksi. Large voids and inclusions are present in microstructure.

SC82-18130

Fig. 40 Transmission electron micrograph of pre-alloyed Ti-6Al-4V hot isostatically pressed at 900°C. Voids have planar surfaces, bubbles are spherical.

SC82-18131

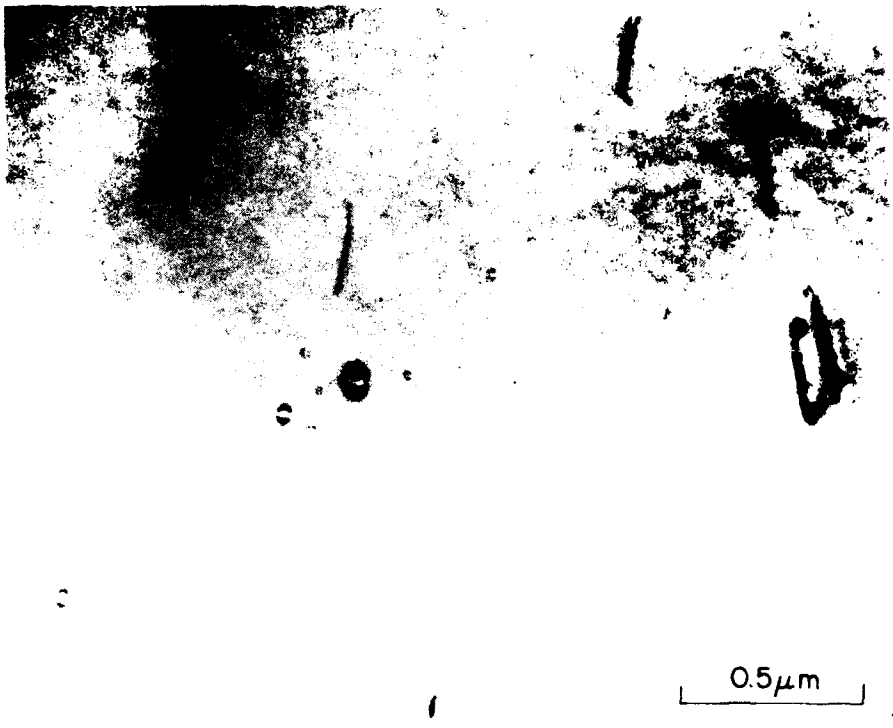

Fig. 41 Transmission electron micrograph of pre-alloyed Ti-6Al-4V hot isostatically pressed at 900°C showing coherent particles (exhibiting line of no contrast).

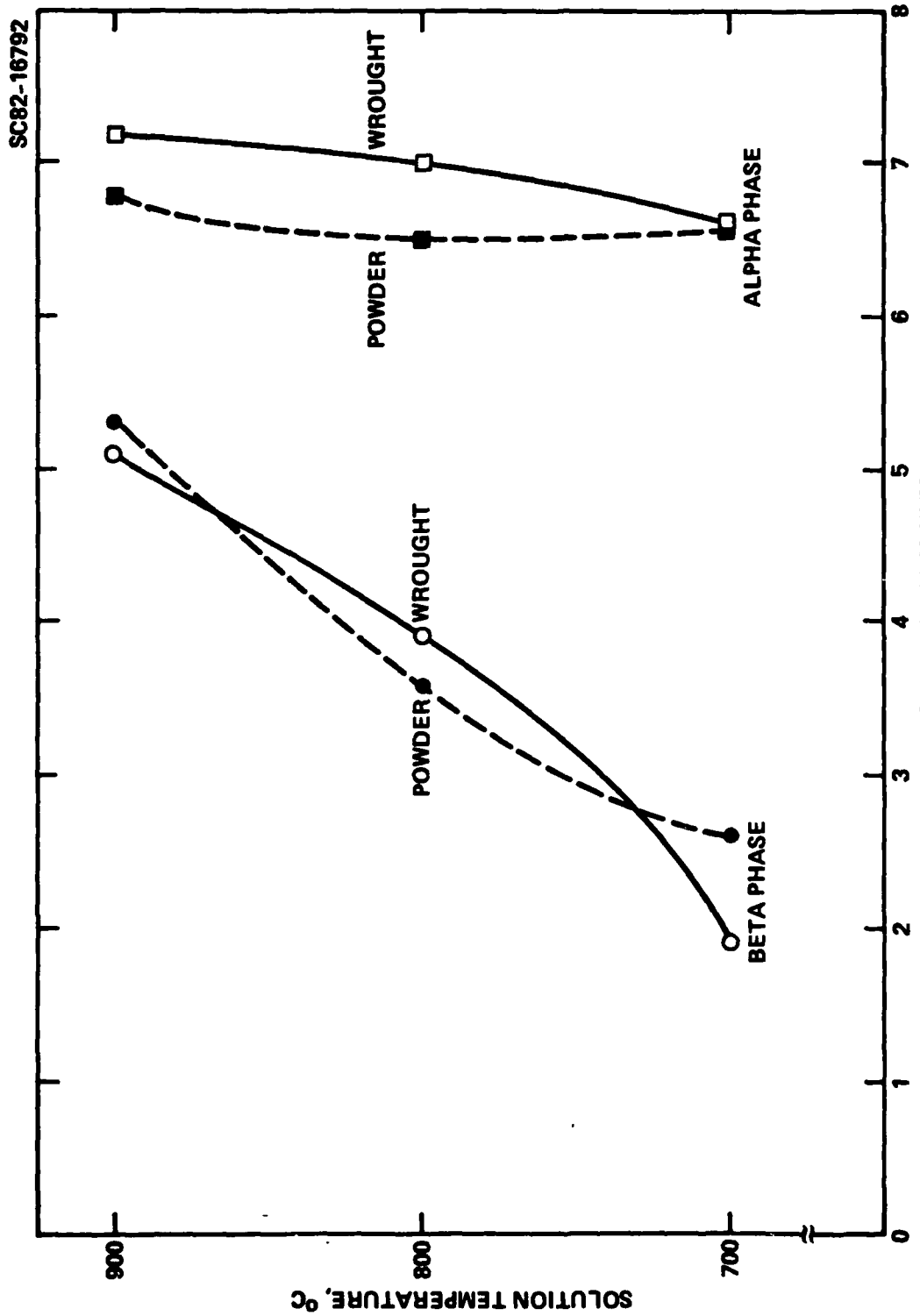

Fig. 42 Aluminum concentration in alpha and beta phases of wrought and powder processed Ti-6Al-4V quenched from solution temperature.

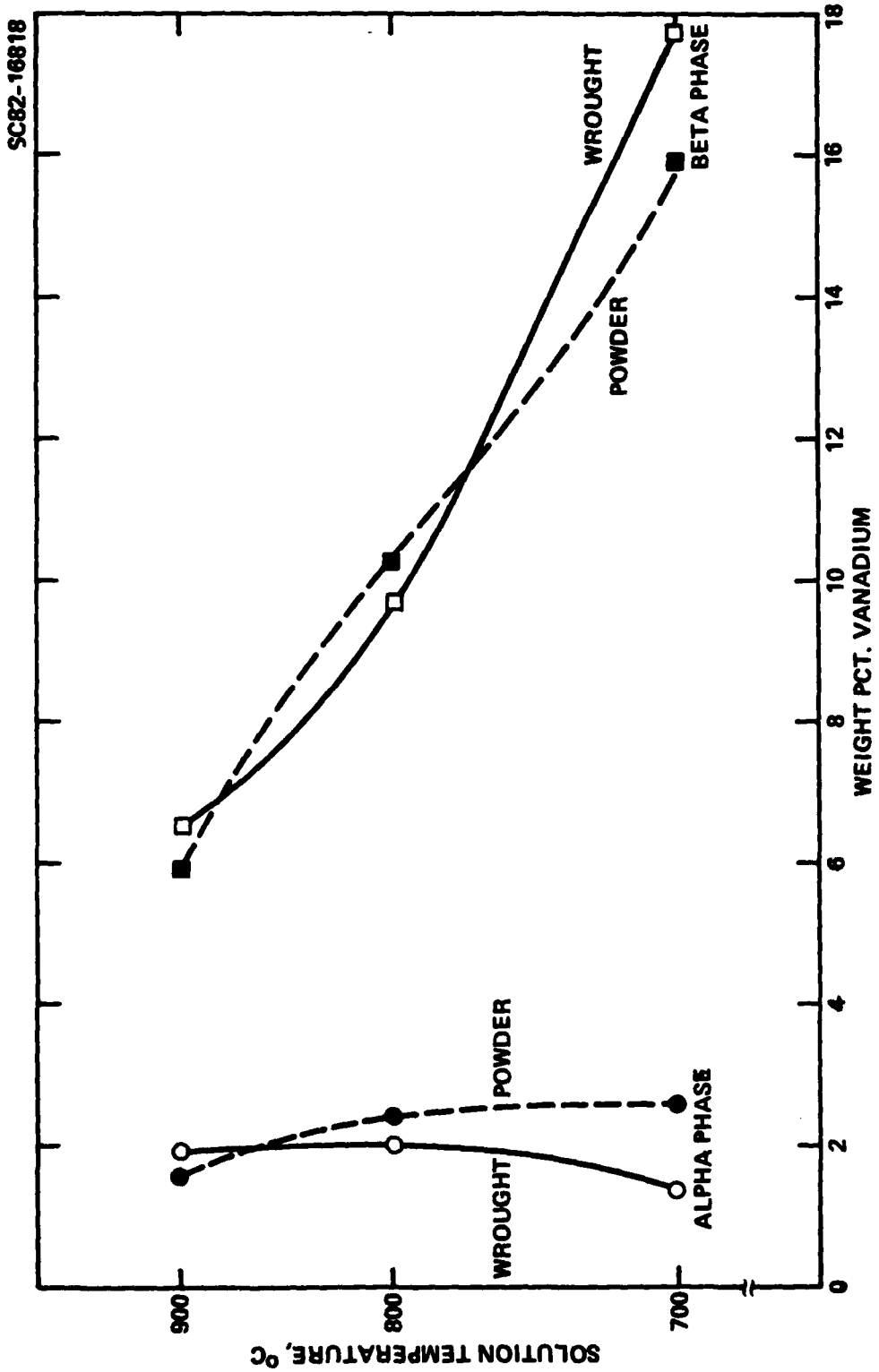

Fig. 43 Vanadium concentration in alpha and beta phases of wrought and powder processed Ti-6Al-4V quenched from solution temperature.

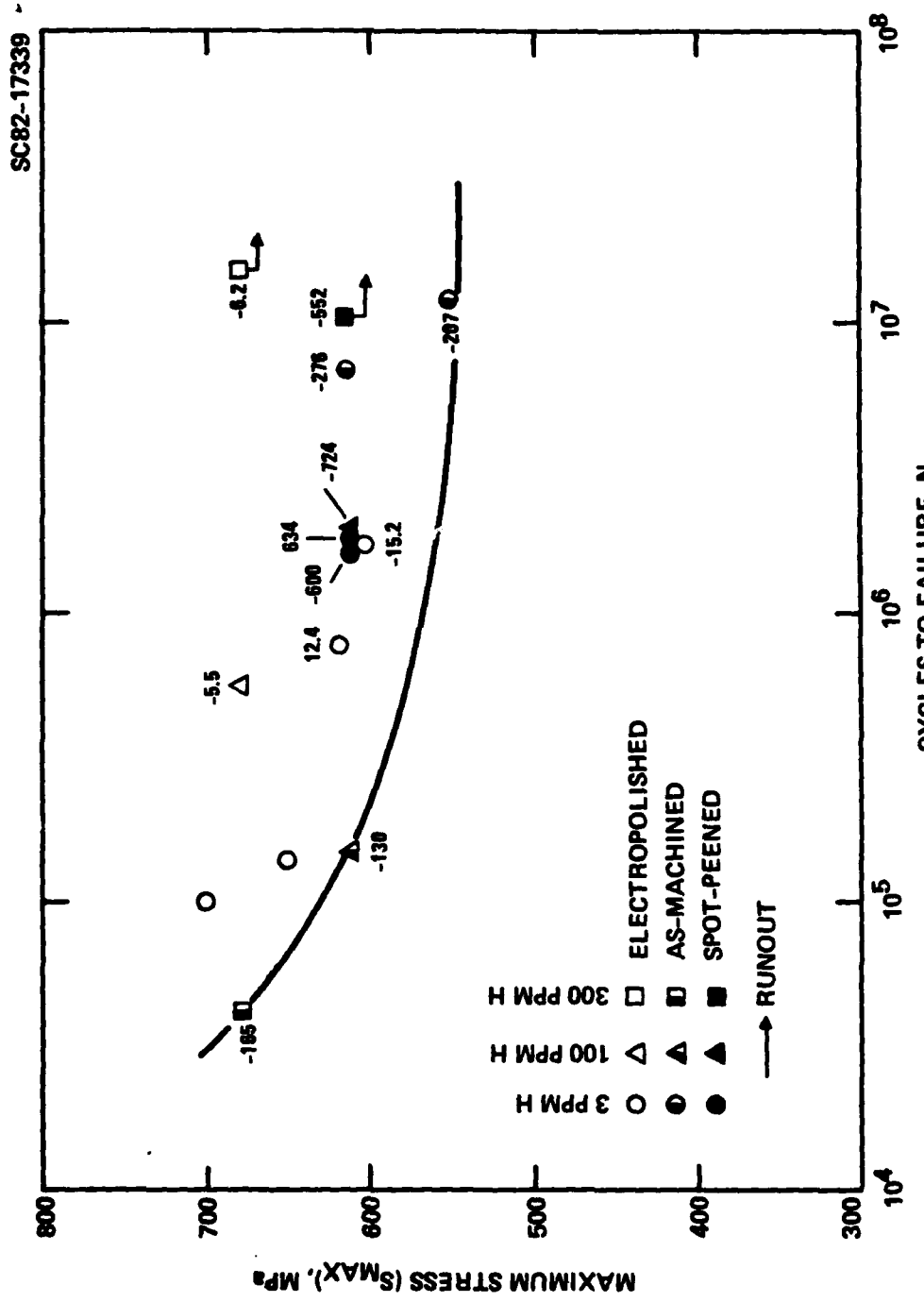

Fig. 44 S/N data for Ti-6Al-4V in STOA condition. 0.2% yield strength = 980 MPa.

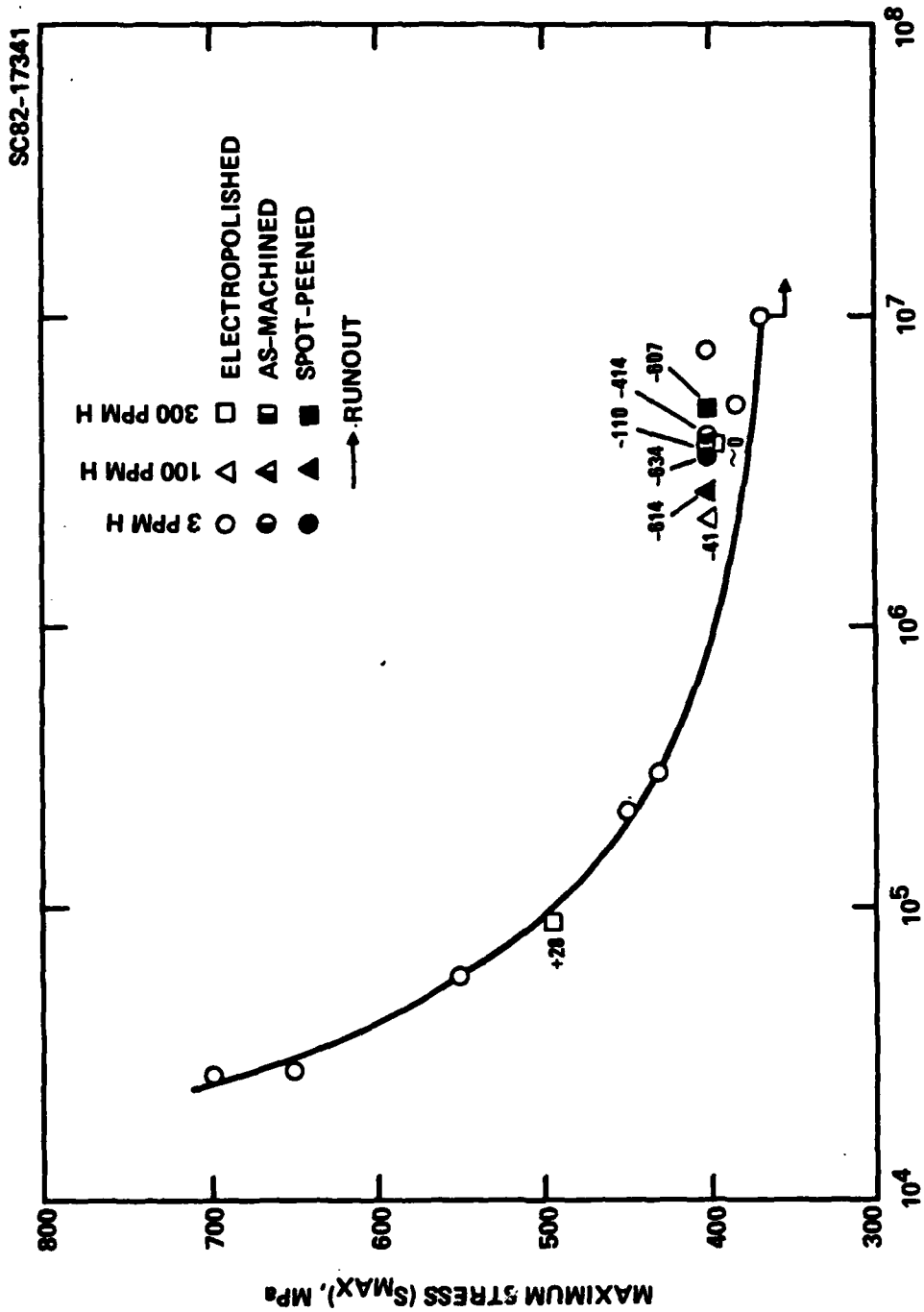

Fig. 45 S/N data for Ti-6Al-4V in RA condition. 0.2% yield strength = 876 MPa.

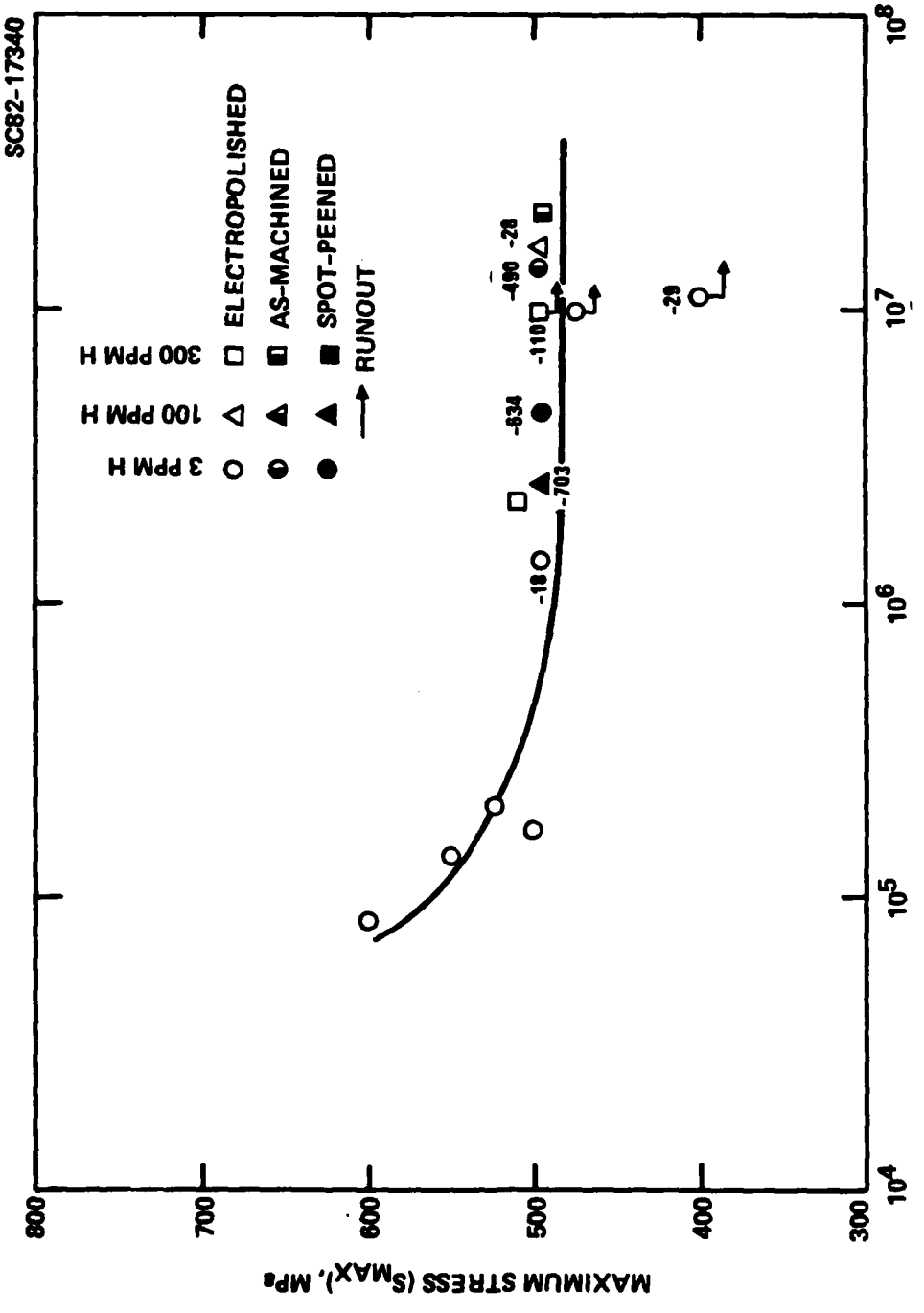

Fig. 46 S/N data for Ti-6Al-4V in βF condition. 0.2% yield strength = 855 MPa.

SC82-18132

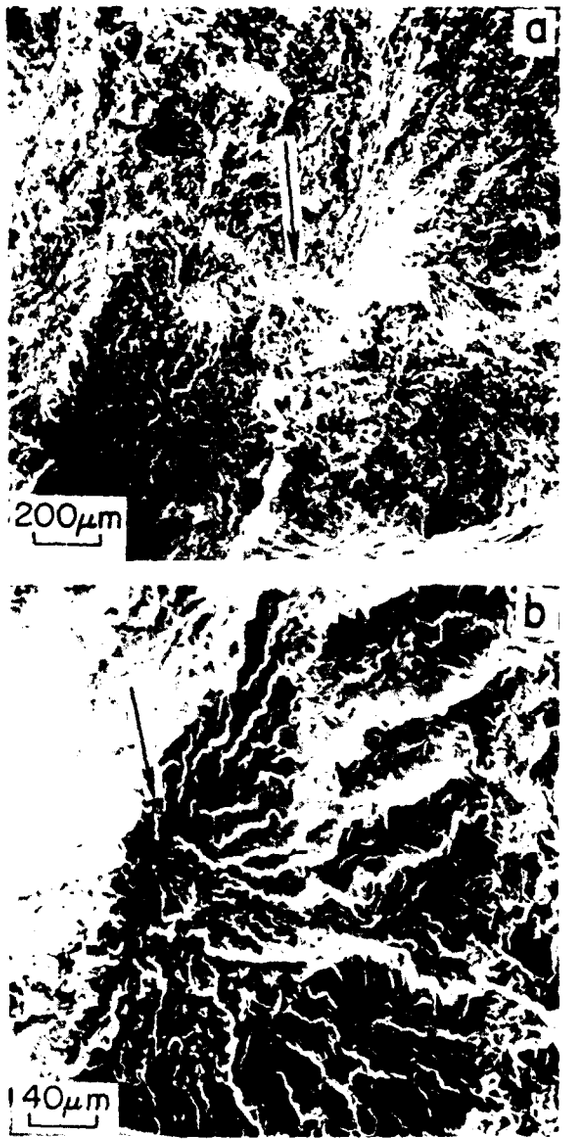

Fig. 47 SEM fractographs of RA Ti-6Al-4V showing sub-surface fatigue crack initiation sites (arrows). (a) 3 ppm hydrogen, shot-peened and (b), 100 ppm hydrogen, electropolished.

SC82-18132

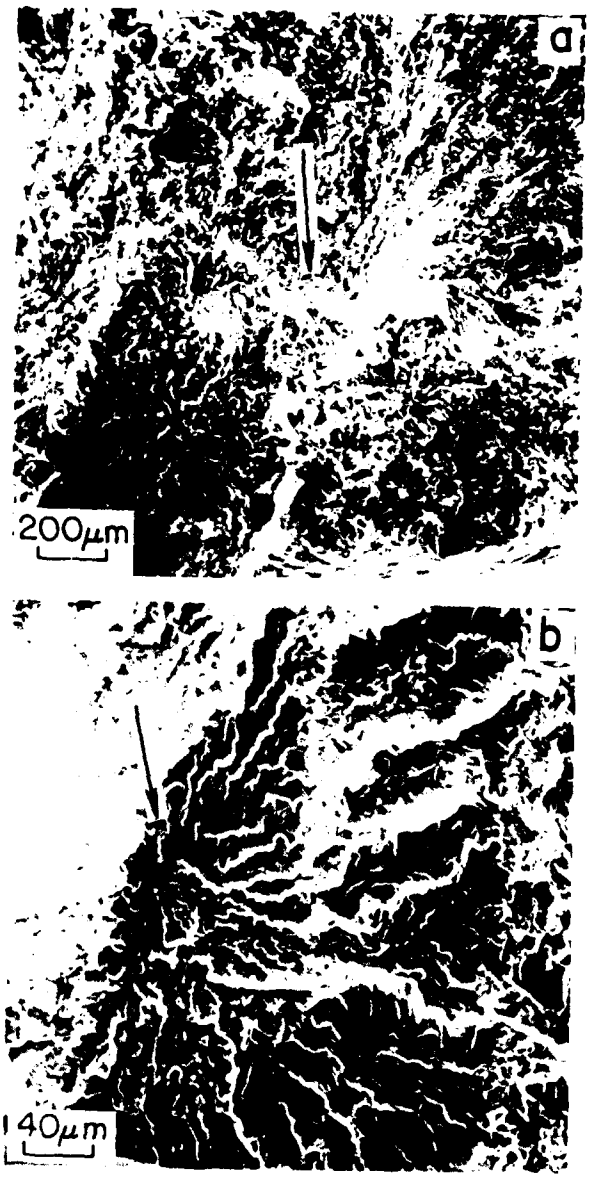

Fig. 47 SEM fractographs of RA Ti-6Al-4V showing sub-surface fatigue crack initiation sites (arrows). (a) 3 ppm hydrogen, shot-peened and (b), 100 ppm hydrogen, electropolished.

SC82-18133

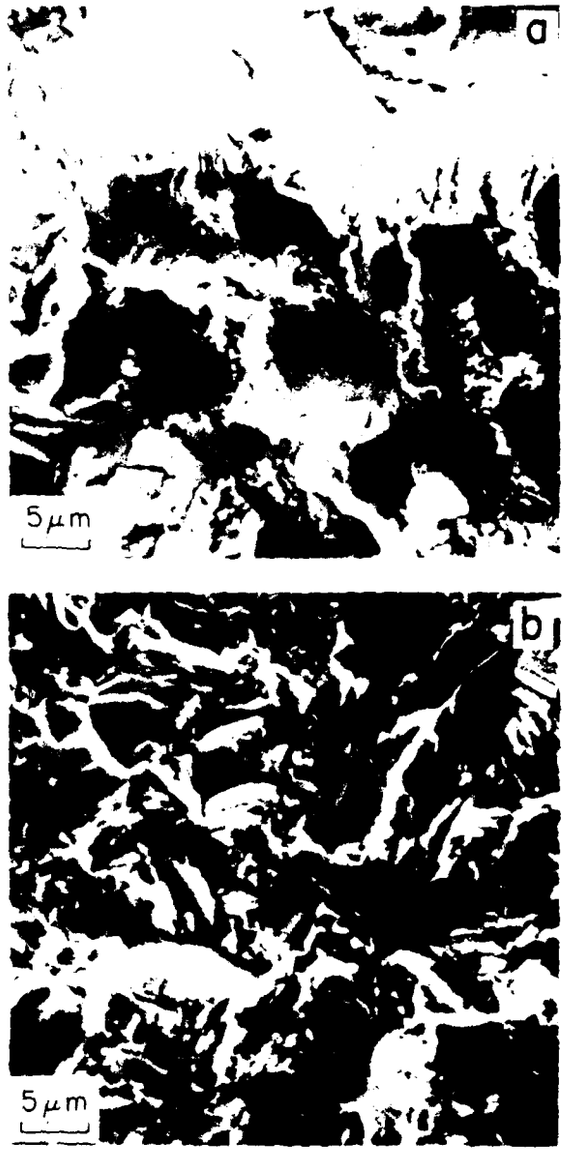

Fig. 48 SEM fractographs of STOA Ti-6Al-4V showing the change in amount of cyclic cleavage with hydrogen (a) 3 ppm hydrogen, as machined, (b) 100 ppm hydrogen, electropolished

SC82-18134

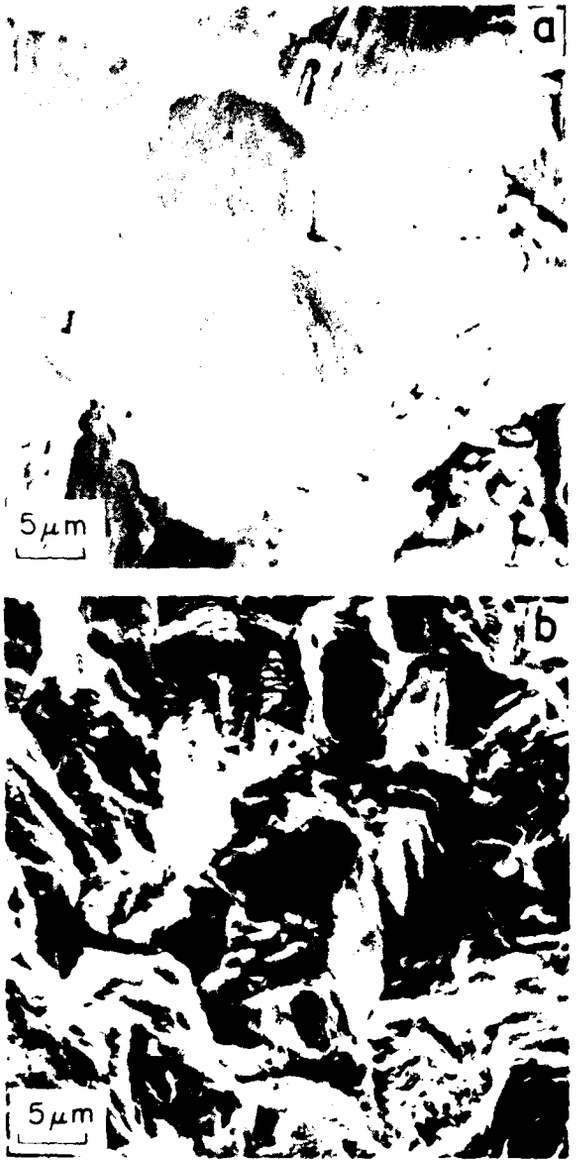

Fig. 49 SEM fractographs of RA Ti-6Al-4V showing change in amount of cyclic cleavage with hydrogen. (a) 3 ppm hydrogen, shot peened; (b) 300 ppm hydrogen, shot peened.

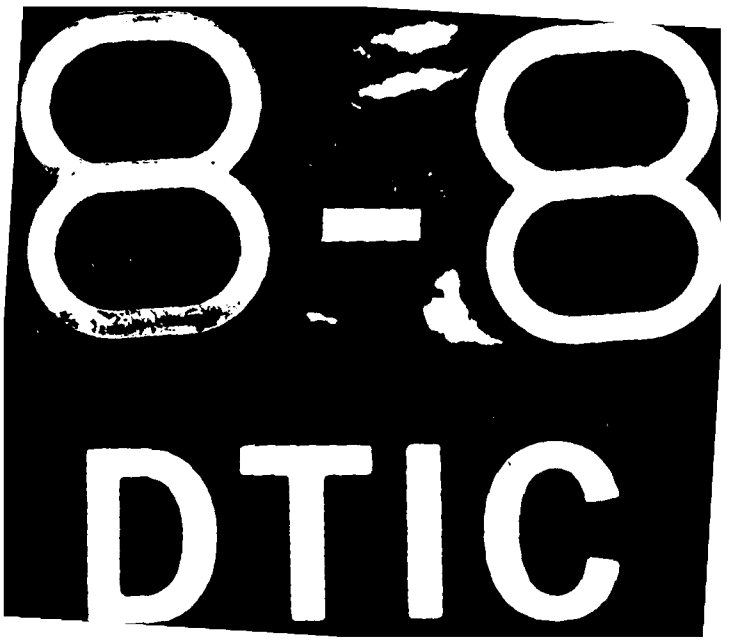
8-8
DTIC